

SANDIA REPORT

SAND88-2839 • UC-71

Unlimited Release

Printed January 1989

Thermal Measurements in the Nuclear Winter Fire Test

M. E. Schneider, N. R. Keltner, L. A. Kent

Prepared by
Sandia National Laboratories
Albuquerque, New Mexico 87185 and Livermore, California 94550
for the United States Department of Energy
under Contract DE-AC04-76DP00789

Issued by Sandia National Laboratories, operated for the United States Department of Energy by Sandia Corporation.

NOTICE: This report was prepared as an account of work sponsored by an agency of the United States Government. Neither the United States Government nor any agency thereof, nor any of their employees, nor any of their contractors, subcontractors, or their employees, makes any warranty, express or implied, or assumes any legal liability or responsibility for the accuracy, completeness, or usefulness of any information, apparatus, product, or process disclosed, or represents that its use would not infringe privately owned rights. Reference herein to any specific commercial product, process, or service by trade name, trademark, manufacturer, or otherwise, does not necessarily constitute or imply its endorsement, recommendation, or favoring by the United States Government, any agency thereof or any of their contractors or subcontractors. The views and opinions expressed herein do not necessarily state or reflect those of the United States Government, any agency thereof or any of their contractors or subcontractors.

Printed in the United States of America
Available from
National Technical Information Service
U.S. Department of Commerce
5285 Port Royal Road
Springfield, VA 22161

NTIS price codes
Printed copy: A07
Microfiche copy: A01

SAND88-2839
Unlimited Release
Printed January 1989

**THERMAL MEASUREMENTS IN THE
NUCLEAR WINTER FIRE TEST**

M. E. Schneider, N. R. Keltner, L. A. Kent
Sandia National Laboratories
Albuquerque, New Mexico 87185

Abstract

In March, 1987, a large open pool fire test was performed to provide test measurements to help define the thermal characteristics of large open pool fires and estimates of the smoke source term for the nuclear winter (global effects) scenario. This report will present the results of the thermal measurements as well as comparisons with previous test results. These measurements included flame temperatures, heat fluxes to a variety of calorimeters, and gas velocities in the lower flame regions.

ACKNOWLEDGEMENTS

The authors would like to acknowledge the help of Bill Jacoby, Dan Luna, Jerry Meloche, Prospero Toledo, Joe Jaramillo and the technical and millwright support. In addition we thank the test engineer, R. Mata, Jr.

TABLE OF CONTENTS

I.	Introduction	9
II.	Overview of Instrumentation	11
III.	Temperatures on Towers	21
IV.	Gas Velocities	41
V.	Heat Flux to the Plate Calorimeter	49
VI.	Heat Flux to the Large Cylindrical Calorimeter	75
VII.	Heat Flux to the Ten Cm Cylindrical Calorimeters	95
VIII.	Fuel Levels and Burning Rates	103
IX.	Weather Conditions during the Test	113
	References	119
	Appendix A	120
	Appendix B	122

LIST OF TABLES

2.1	Overview of instrumentation	13
3.1	Average temperatures and velocities	23
3.2	Comparison on conditionally averaged tower temperatures from three tests	24
4.1	Effects of conditional sampling of the velocities	43
5.1	Average temperatures near calorimeters	53
5.2	Average cold wall heat fluxes	54
6.1	Integrated heat flux at 30 minutes	78

LIST OF FIGURES

2.1	Instrumentation on the Test	14
2.2	10 cm Calorimeter Construction	15
2.3	Center Tower Instrumentation Scheme	16
2.4	Cutaway of the Plate Calorimeter	17
2.5	Large Calorimeter Construction	18
2.6	Pool Surface Calorimeter	19
3.1	Flame Temperatures - Lower Part of Center Tower	25
3.2	Flame Temperatures - Upper Part of Center Tower	26
3.3	Flame Temperatures - North Tower	27
3.4	Flame Temperatures - East Tower	28
3.5	Flame Temperatures - South Tower	29
3.6	Flame Temperatures - West Tower	30
3.7	Average Temperatures vs Height	31
3.8	Average Temperatures (Trupact-I-Test 1)	32
3.9	Average Temperatures (Trupact-I-Test 0)	33
3.10	Standard Deviations in Temperatures	34
3.11	Standard Deviations (Trupact-I-Test 1)	35
3.12	Standard Deviations (Trupact-I-Test 0)	36
3.13	Comparison of Different Conditioning Signals	37
3.14	Conditionally Averaged Tower Temperatures	38
3.15	Flame Present Temperatures (Trupact-I-Test 1)	39
3.16	Flame Present Temperatures (Trupact-I-Test 0)	40
4.1	Center Tower Velocity Histories	44
4.2	Center Tower Velocity Histories	45
4.3	Average Velocity vs Elevation	46

4.4	Comparison to the Literature	47
5.1	Backface Temperature on West 6.35 mm Plate Calorimeter	56
5.2	Backface Temperature on West 19 mm Plate Calorimeter	57
5.3	Flame Temperatures on West Side of Plate Calorimeter	58
5.4	Net Heat Flux and Temperature Relationships	59
5.5	Cold Wall Heat Flux to West 6.35 mm Plate Calorimeter	60
5.6	Cold Wall Heat Flux to West 19 mm Plate Calorimeter	61
5.7	Average Cold Wall Flux vs Average Flame Temperature	62
5.8	Blackbody Fluxes Calculated From Flame Temperatures	63
5.9	Flux vs Surface Temperature West 6.35 mm Plate	64
5.10	Flux vs Surface Temperature West 19 mm Plate	65
5.11	Backface Temperature of East 6.35 mm Plate Calorimeter	66
5.12	Temperature of East Shroud	67
5.13	Flame Temperature on East Side of Plate Calorimeter	68
5.14	Comparison Between Three Heat Flux Calculations - 4.11 m Station	69
5.15	Comparison Between Three Heat Flux Calculations - 3.30 m Station	70
5.16	Comparison Between Three Heat Flux Calculations - 2.49 m Station	71
5.17	Comparison Between Three Heat Flux Calculations - 1.68 m Station	72
5.18	Cold Wall Heat Flux to shroud	73
6.1	Large Cylinder - North Intrinsic	79
6.2	Large Cylinder - North Externals	80
6.3	Large Cylinder - North Nanmacs	81
6.4	Large Cylinder - Insulation Temperatures	82
6.5	Large Cylinder - South Intrinsic	83
6.6	Large Cylinder - South Shroud Temperature	84
6.7	Large Cylinder - North Flux vs Surface Temperature	85
6.8	Large Cylinder - North Cold Wall Heat Flux	86
6.9	Nanmacs vs SODDIT Surface Temperature Estimates (Top Station)	87
6.10	Nanmacs vs SODDIT Surface Temperature Estimates (East Station)	88
6.11	Nanmacs vs SODDIT Surface Temperature Estimates (Bottom Station)	89
6.12	Nanmacs vs SODDIT Surface Temperature Estimates (West Station)	90
6.13	Comparison Between Two Heat Flux Calculations (Top Station)	91
6.14	Comparison Between Two Heat Flux Calculations (East Station)	92
6.15	Comparison Between Two Heat Flux Calculations (West Station)	93
7.1	East 10 cm Calorimeter Backface Temperatures	96
7.2	West 10 cm Calorimeter Backface Temperatures	97
7.3	East 10 cm Calorimeter Cold Wall Heat Flux	98
7.4	West 10 cm Calorimeter Cold Wall Heat Flux	99
7.5	East 10 cm Calorimeter Heat Flux vs Surface Temps	100
7.6	West 10 cm Calorimeter Heat Flux vs Surface Temps	101
8.1	Fuel Level	105
8.2	Fuel Recession Rate	106
8.3	Backface Temperature Histories for Slug Calorimeters at Fuel Surface	107
8.4	Smoothed Temperature Histories for Slug Calorimeters	108
8.5	Heat Flux to Pool Surface From Slug Calorimeters	109
8.6	Fuel Surface Radiometer Output	110
8.7	Fuel Surface Radiometer Temperature	111
9.1	Wind Speed During Test	114
9.2	Wind Direction During Test	115
9.3	East Wind Velocity Component	116
9.4	North Wind Velocity Component	117
9.5	Ambient Temperature	118
A.1	Radiation Enhancement Due to Intermittency	121

NOMENCLATURE

c_p	Specific Heat
dx	Thickness
dT	Change in temperature
$d\tau$	Change in time
F	Radiation shape factor
h	Convective heat transfer coefficient
Q	Heat flux per unit area
T	Temperature

Greeks

α	Radiation enhancement cf. Eqn. A.3.
ϵ	Emissivity
ρ	Density
σ	Stefan-Boltzmann constant ($5.66 \times 10^{-8} \text{ W/m}^2\text{K}^4$)
σ_t	Standard deviation in temperature
ψ	Defined in appendix A
ζ	Defined in appendix A

Subscripts

ave	Average flame temperature
bf	Flame to boiling fuel
bp	Boiling point
cw	Cold wall
f	Flame
ff	Front face
fs	Flame smoothed
f→p	Net from flame to plate
f→s	Flame to shroud
net	Net
o	Constant
p	Plate
p→r	Thick plate to ring
r	Ring on cylinder
s	Shroud
sto	Stored in shroud
s→p	From shroud to plate
s→r	Shroud to ribs (on cylinder)
s→s	Shroud to itself

I. INTRODUCTION

A large, open pool fire test was performed in March, 1987 to define the thermal characteristics of large open pool fires and to provide information about the smoke source term for nuclear winter (global effects) scenario studies. This test report describes the measurements which were made to help evaluate the parameters that define an open pool fire, examine the repeatability between open pool fire tests, and determine typical thermal input to massive test articles. All of these measurements were made in the lower flaming region of the fire. Results from the airborne sampling in the plume region are reported by Einfeld, et al. [1].

Definition of the characteristics of large open pool fires is required to improve predictions of the response of shipping containers when such fires are used to simulate severe transportation accidents. Parameters which are important in establishing this definition include:

- Temperature
- Thermal transport in the fire
- Fire dimensions
- Velocities in the fire
- Chemistry

To try to provide part of this definition, a wide variety of diagnostic instrumentation was fielded in the large pool fire test. The types of instrumentation and their use are outlined below.

INSTRUMENTATION	INFORMATION
Thermocouples mounted on towers	- Fire temperatures at elevations up to 15 meters - Amplitude and frequency of temperature fluctuations
Thick wall cylindrical calorimeters mounted on towers	- Transient hot wall heat flux and surface temperature data from inverse heat conduction codes - Heat flux data for comparison to similar measurements in other fires
Large thick and thin wall plate calorimeters	- Transient hot wall heat flux and surface temperature data for plates - Amplitude and frequency of temperature fluctuations
Large half-shielded cylindrical calorimeter	- Heat flux to large cylinders
Bidirectional velocity probes	- Gas velocity measurement from a pitot type device designed for low Reynolds number flows

Infrared imaging cameras (3-5 & 8-12 micron range)	- Mapping of temperature contours in the lower part of the fire
Pressure static head in the pool	- Fuel recession rate
Plate calorimeter at fuel surface	- Total heat flux to fuel surface
Radiometer at the fuel surface	- Radiant flux to fuel surface
Wood smoke generators	- Flow visualization and air entrainment in the lower part of the fire
Video records from four directions with closeup and distant stations	- Velocity of large turbulent structures around the outside of the fire - Plume shape for comparison with plume models
Airplane @ ~500 meters	- Soot characterization and emission factors - Plume gas composition
Wind velocity and direction	- Compliance with test specifications - Correlation with thermal measurements

Measurements of temperature and heat flux are important in trying to define the fire environment and the response of a test item. Temperature measurements provide part of the primary definition of the fire environment. Calorimeter temperatures define the response of an item to the fire environment, and the potential for material failures that occur due to temperature. Heat transfer affects both the development of the fire and the response of a test item to the fire. The heat flux levels indicate how severely an item will be stressed by the fire and the integrated flux defines the total thermal insult. It is important to note that the size and design of a test item affects the the local fire environment which in turn affects the heat transfer to the test item.

The measurements of particular interest in determining the thermal input to items in fires are the temperatures and heat fluxes from the calorimeters and the temperature and velocity profiles obtained from the towers located throughout the fire.

II. OVERVIEW OF THE INSTRUMENTATION

The setup of the Nuclear Winter Fire Test instrumentation is shown in Figure 2.1. The fire test described here was performed in the 9 by 18 meter large fire test pool in Lurance canyon. For this test, there were four 6 meter high instrumentation towers located in a diamond shape around the 15 meter centrally located tower. Type K thermocouples with ungrounded junctions in 1.6 mm OD inconel sheaths were used on all five towers to measure flame temperatures.

Thermocouples were mounted on the 6 meter high towers at elevations of 1.37, 2.29, 3.51, 4.72 and 6.1 meters from the bottom of the pool. Two of these towers had 10.2 centimeter diameter, 20.3 cm long, 31.8 mm thick mild steel calorimeters mounted with their centerlines 2 meters from the bottom of the pool. The same type of calorimeter had been used in the TRUPACT pool fire tests and the DOT fire test series [2,3,4,5]. Thus, this instrument provided comparative hot wall heat flux data for the large pool fire tests. The construction of the 10 centimeter calorimeters is shown in Figure 2.2. These calorimeters were split into quadrants and isolated to provide a measure of circumferential variation of the heat flux. Thus, one quadrant preferentially viewed the top, bottom, north, or south side of the fire. A 15 meter tall tower was located in the exact geometrical center of the pool.

The center tower had thermocouples and velocity probes mounted as shown in Figure 2.3. Thermocouples and glass coated, stainless steel, bidirectional velocity probes [6] were at heights of 2.21 meters, 3.40 meters, 4.78 meters, 6.1 meters, 9.14 meters, 12.19 meters and 15.24 meters from the bottom of the pool.

A plate calorimeter was used to investigate the heat flux to vertical surfaces in fires. It was placed due east of the central tower, still on the long pool axis. The east facing side was designed to simulate a radiation shielded wall situation; the outer surface was a 1.02 mm steel sheet with a 6.35 mm plate mounted 9.5 mm behind it. The west facing side of the calorimeter was used to look at the effects of wall thickness on the heat transfer. The north half of the west side was a 19 mm mild steel plate; the south half was a 6.35 mm mild steel plate. The steel plates were mounted such that the outer surfaces were in the same plane. Intrinsic junction thermocouples were mounted on the backface of all of the plates. Sheathed thermocouples, like those used on the towers, protruded from the exterior surface of each side 10 centimeters into the flames. Figure 2.4 shows a cutaway view of the plate calorimeter.

In order to examine the heat flux to large cylindrical objects, a 10 ton cylindrical calorimeter was instrumented and placed in the pool. The calorimeter was very similar to those examined in the DOT test series [2,3]. The axis of the cylinder was placed 4.6 meters from the west side of the pool in a north/south orientation as sketched in Figure 2.1. Figure 2.5 gives more details regarding the construction of the calorimeter and the instrumentation stations. The south half of the calorimeter was shrouded with a thin mild steel shield. Basically two instrumentation stations existed. One on the unshrouded north end, and one on the shrouded south end. On each end duplicate instrumentation was placed at 90 degree intervals facing up, down, to the east, and to the west.

On the bare North end, the following temperatures were monitored at the four angular positions: steel backface temperature, temperature 2.54 cm into the insulation, surface temperature (using Nanmac TCs), and external flame temperatures. In addition, a transpiration

radiometer was mounted in the wall at each angular location. On the shrouded (south) end only the thick steel backface and the shroud temperatures were recorded.

Two types of measurements of heat flux to the pool surface were attempted in this test. Figure 2.6 shows a cutaway view of a pool surface slug calorimeter. Three of these devices were placed in the pool as indicated in Figure 2.1. A transpiration radiometer was placed near the center slug calorimeter, facing up.

Outside of the pool, located due west ~ 45 meters away was a propeller type wind anemometer. This was used to record wind speed and direction during the test. On the north, south, east, and west axes of the pool, located ~ 150 meters away from the edges of the pool, were video cameras which viewed the pool side plus three meters in either direction. In addition, a 16-mm movie camera was ~ 750 meters away viewing the fire plus the smoke plume. These cameras were used to record events within the fire. In close proximity to the south video camera were two infrared imaging cameras. One recorded radiation in the 3-5 micron wavelength range while the other recorded radiation in the 8-12 micron wavelength range. At six locations around the periphery of the pool, wooden posts were held in a vertical position. These posts had been soaked in water and produced a white smoke for approximately 15 minutes which helped in visualizing the flow field near the base of the fire.

Table 2.1 is a summary of the data which was acquired on the test items during the test. The table includes an indication of the acquisition system used to gather data from various transducers along with the type and placement of the transducers in the pool.

TABLE 2.1 Instrumentation Overview

Number of Channels	Location	Acquisition System	Scan Rate [Sec/Reading]
24	Large cyl Calorimeter	HP 1000	10
8	10 cm Calorimeters	HP 1000	10
5	N Tower	HP 1000	10
5	E Tower	HP 1000	10
5	S Tower	HP 1000	10
5	W Tower	HP 1000	10
1	Wind Speed	HP 1000	10
1	Wind Direction	HP 1000	10
2	Fuel Level	HP 1000	10
24	Plate Calorimeter	HP 3054	5
7	Center Tower TCs	HP 3054	5
3	Pool Surface Slugs	HP 3054	5
2	Trans Radiometer	HP 3054	5
7	Velocity Probes	HP 3054	5

Notes :

- HP 3054S - HP 9826 Computer and HP 3497A Data Acquisition/Control Unit
- HP 1000 - HP A600 Computer and HP 3852 Data Acquisition/Control Unit

WOOD POSTS
(TYP. OF 6)

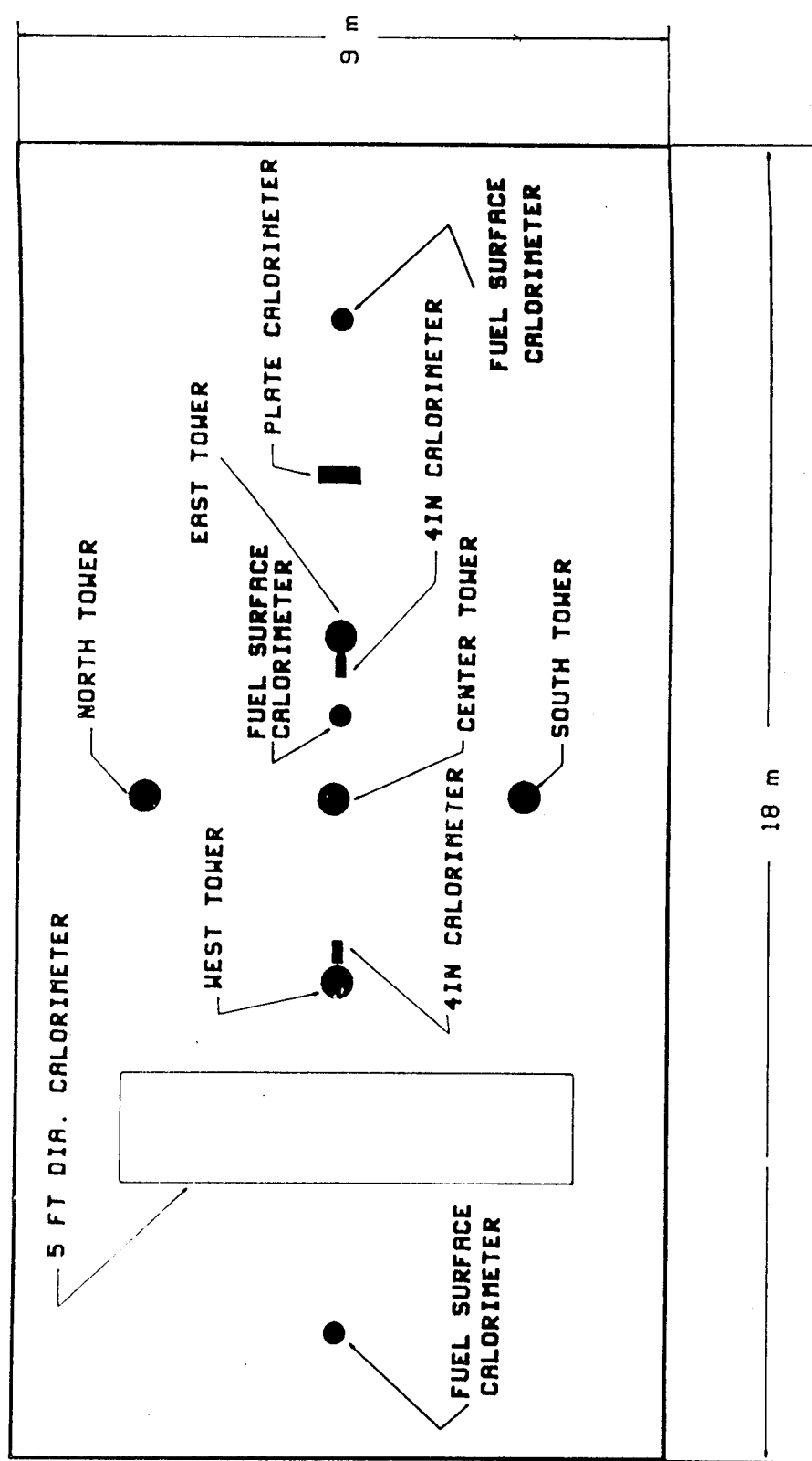
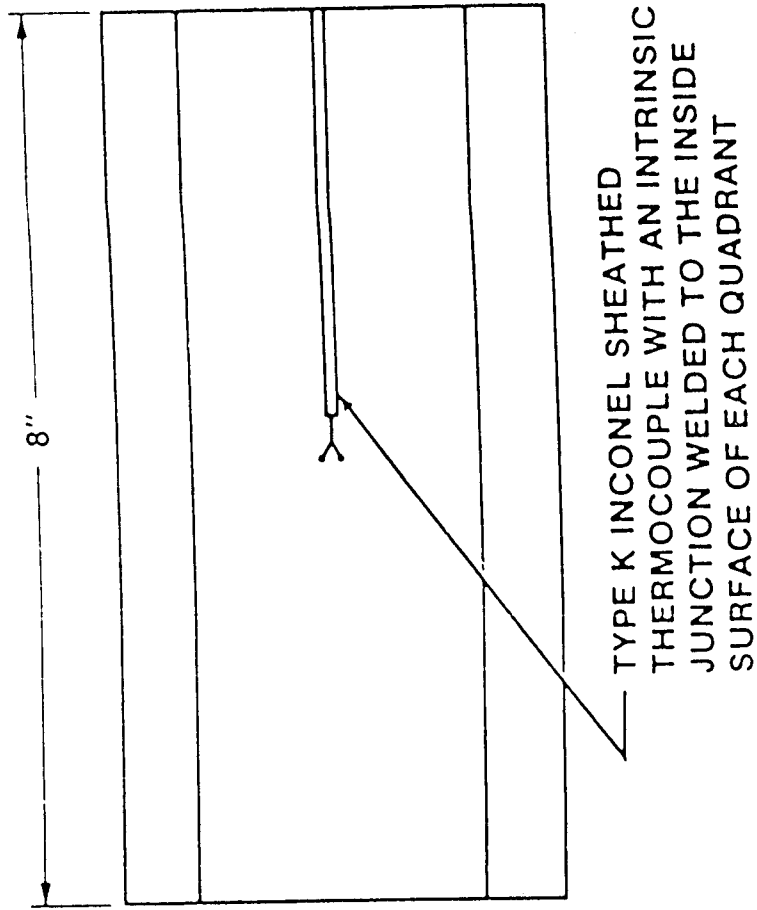
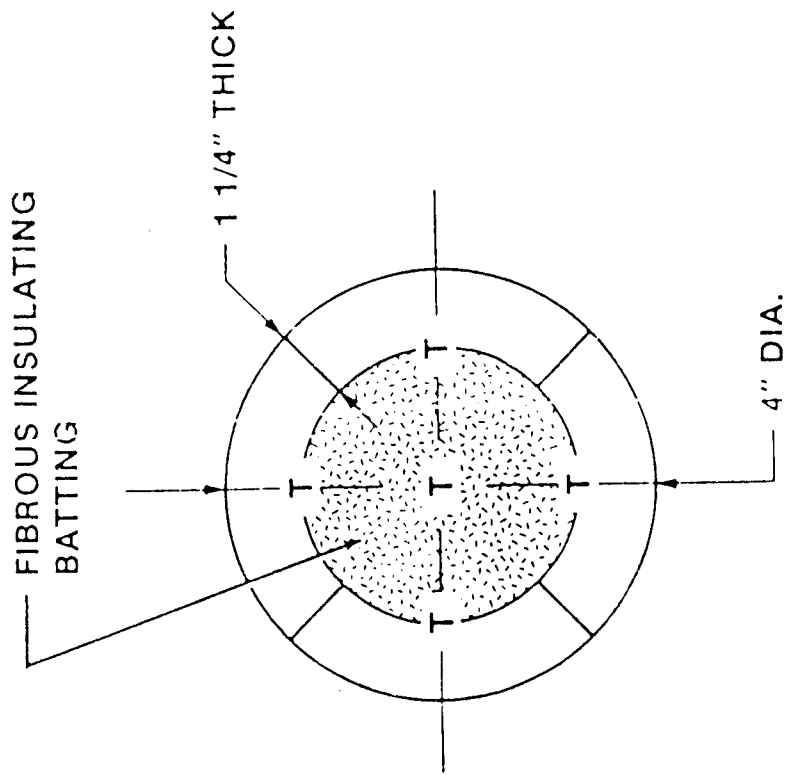


Figure 2.1 Instrumentation on the Test



NOTE:
T DESIGNATES A THERMOCOUPLE LOCATION

Figure 2.2 10 cm Calorimeter Construction

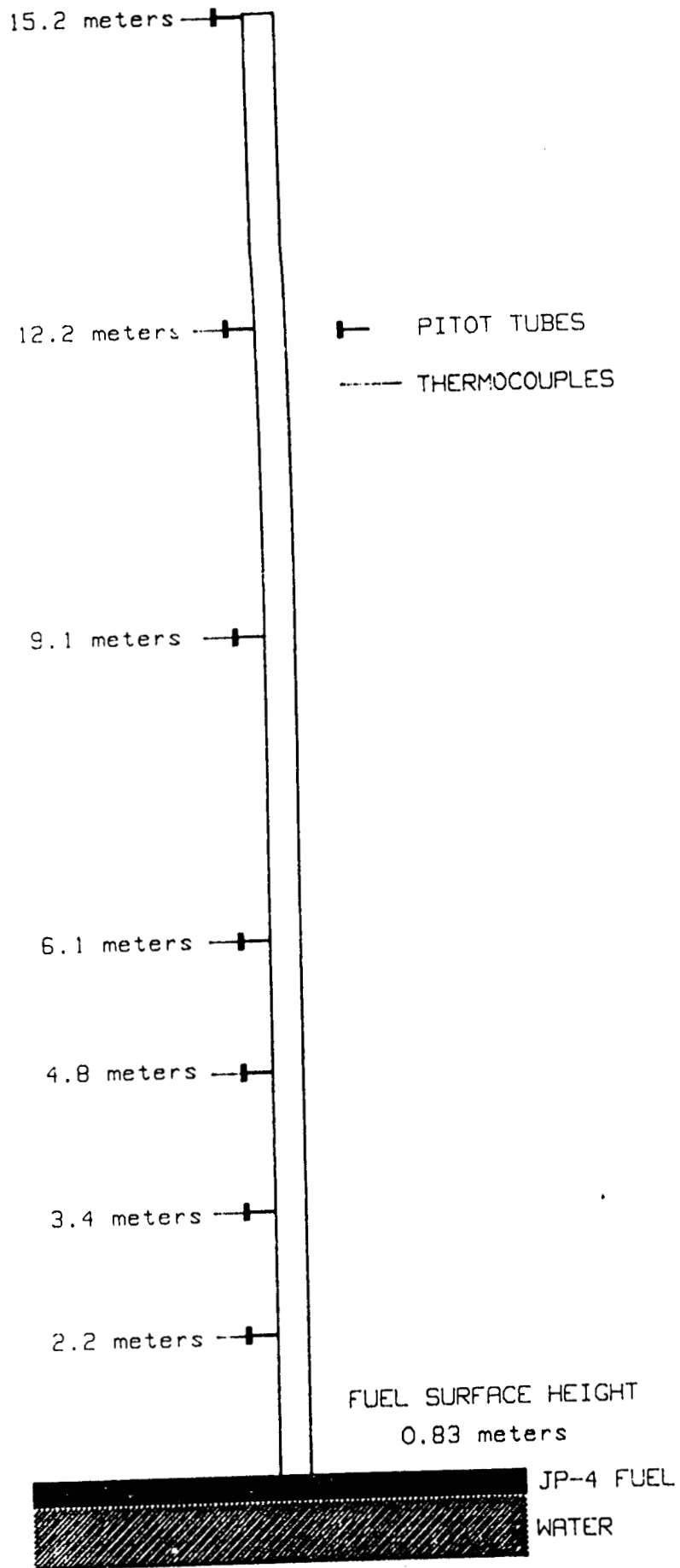


Figure 2.3 Center Tower Instrumentation Scheme

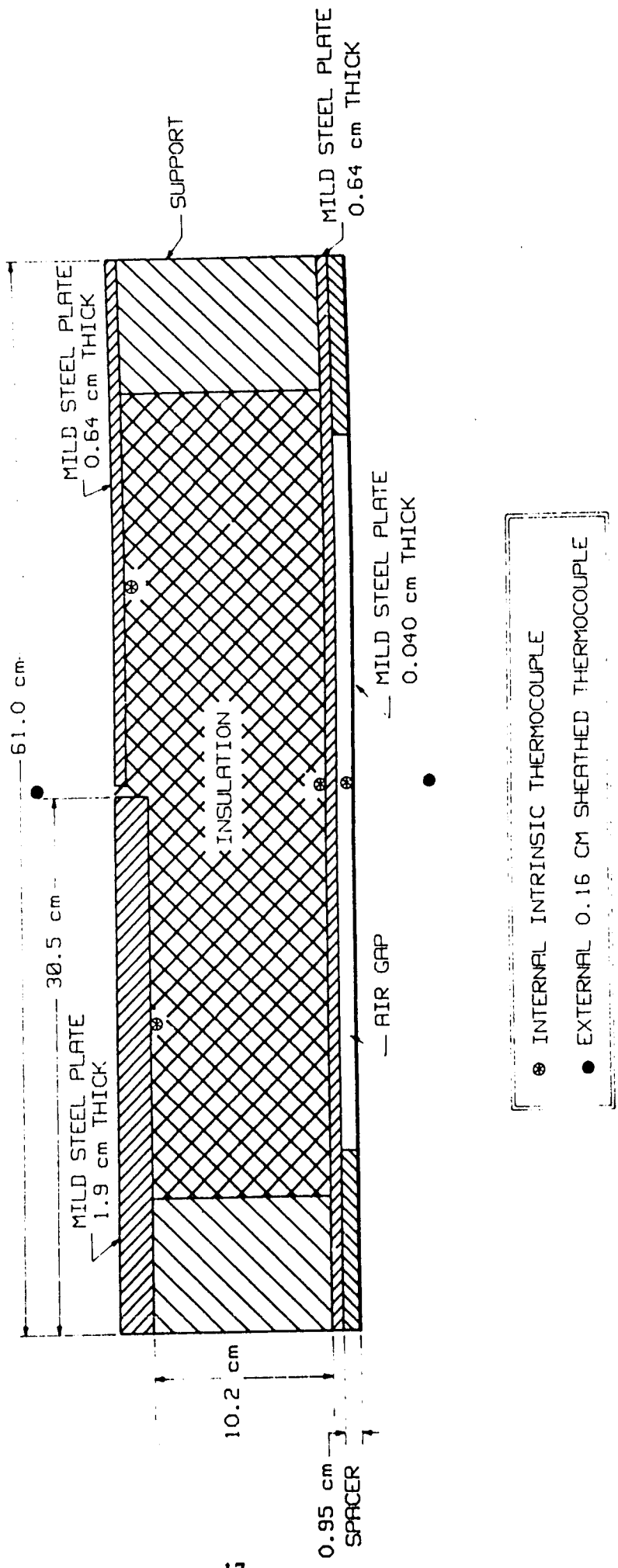


Figure 2.4 Cutaway of the Plate Calorimeter

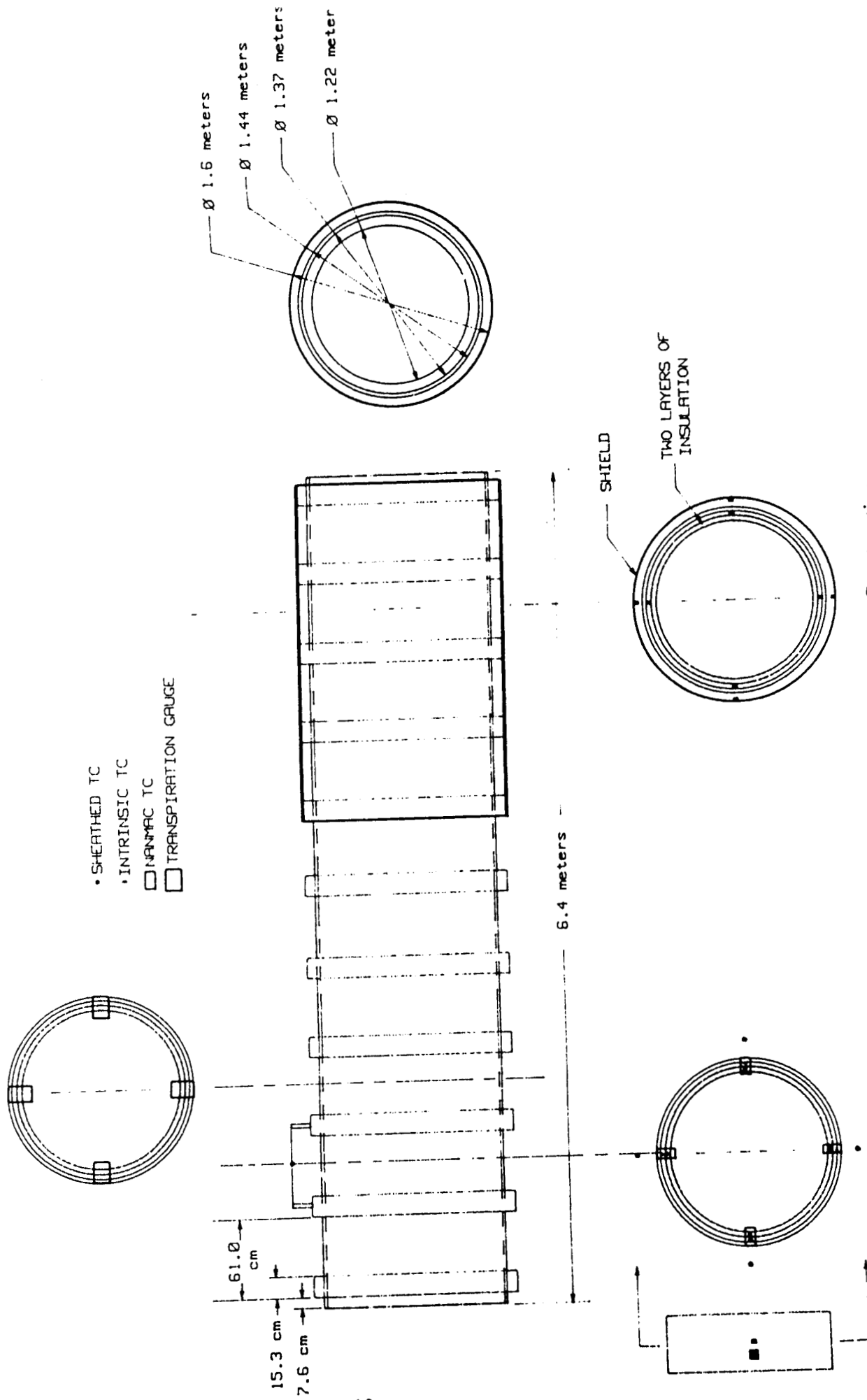


Figure 2.5 Large Calorimeter Construction

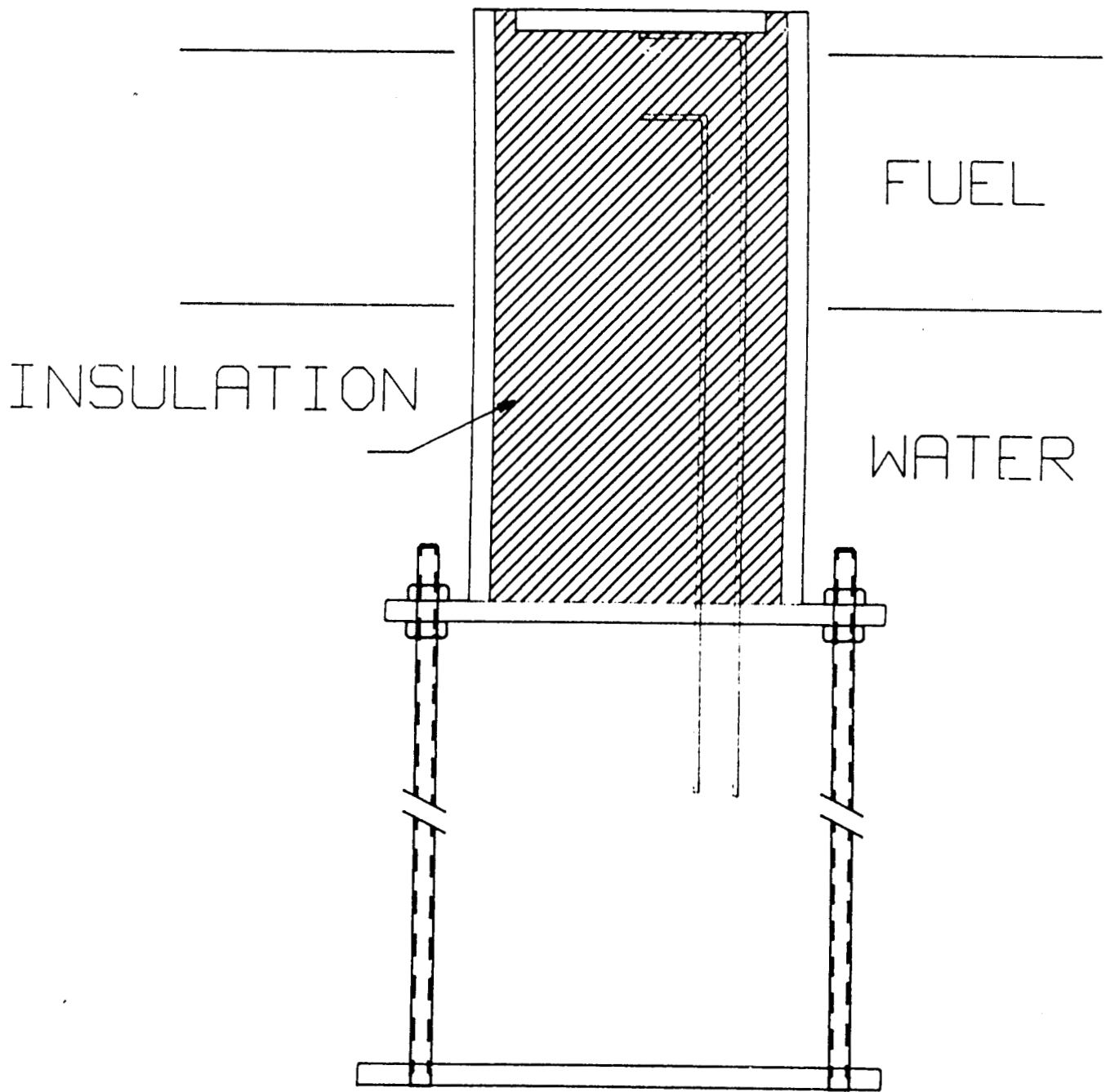


Figure 2.6 Pool Surface Calorimeter

III. TEMPERATURES ON TOWERS

Temperatures were measured at various locations near the base of the fire. The centrally located tower allowed measurements of flame temperatures at heights up to 15 meters. Figures 3.1 through 3.6 show the temperature histories for the five main instrumentation towers. The locations of the stations are included in the legends. Flame temperature measurements were also made near the calorimeters, but these results will be discussed in section 5 (Table 5.1 is a summary). The flame temperature histories look very similar to results from previous tests. Generally, the higher elevations show more extreme fluctuation due to the effects of winds. Average values of temperature are plotted in figure 3.7. Figures 3.8 and 3.9 show average temperature results from the two previous large open pool fire tests. The standard deviations in flame temperatures were calculated and are plotted in Figure 3.10. Again, for comparison, Figures 3.11 and 3.12 show previous results. The data from Trupact-I-Test 1 shows very good agreement from tower to tower. The agreement between towers is not nearly as good for either the current test or for Trupact-I-Test 0. The data from the current test is expected to be much more strongly affected by winds than Trupact-I-Test 1 (see section 9). Part of the difference between the measurements from Trupact-I-Test 0 may be due to the large size of the test unit and the effect on the placement of the instrumentation towers. Table 3.1 summarizes the results of the current test in tabular form.

The winds were strong enough during this test to cause the flames to be blown away from the highest stations for significant time periods, see for example Figure 3.2. In past tests it was helpful to try to estimate time periods during which the flames were not strongly affected by local wind conditions. Averages taken during these periods often were in better agreement than averages over the entire test. Three methods of estimating the importance of winds were used in this test.

First, wind speed data were input into a flame tilt equation [7] in order to determine the expected tilt of the flames with time. Then, using geometrical considerations and the wind direction, the vertical location at which the edge of the flames were expected to cross the pool centerline was calculated. If this height was less than 15 meters the flames were said to be "absent" from some stations. If the flame cylinder crosses the pool centerline at a vertical height greater than 15 meters the "flame present" condition was assumed.

A second method involved looking at the temperature measurements themselves and trying to determine if the flames were present at particular stations. This is basically the method detailed in [4,5].

The third method involved the tedious and careful examination of the video recordings of the flame region which were made from four different viewing directions. For each direction of viewing, the periods during which the uppermost station appeared to be obscured by flames were recorded. It was then assumed that if the 15 meter station could not be seen from any of the four views, it was indeed engulfed in flame. The conditioning signals generated from the three methods are shown in Figure 3.13.

The third method was eventually used to calculate the "flame present" averages listed in Table 3.1 and plotted in Figure 3.14. The same signal was used to condition the velocity measurements discussed in the next section.

The flame present conditional average temperatures for two earlier tests have been plotted as figures 3.15 and 3.16 for comparison. Again, as in the case of the average temperatures, the Trupact-I-Test 1 results show much better agreement, tower to tower, than the current test, or the Trupact-I-Test 0 results. The application of conditional sampling in previous tests seemed to give results which were in better agreement, both tower to tower and test to test, with the exception being the strongly wind effected southeast tower in the Trupact-I-Test 0. The current test results are disappointing in this sense. The most likely problem is that the total time of the "flame present" signal is very short; there are only 1.5 minutes of temperature readings to average. With less than 20 readings, this is probably not a statistically significant sample.

The conditional analysis of the data from Trupact-I-Test 0 and Test 1 used the temperature based second method. In these tests, the winds were lower and the conditioning signal could be developed from measurements at a lower station (6.1 meters). A better comparison of the average "flame present" temperatures, at elevations up to 6.1 meters above the pool floor, from three tests; Trupact-I-Test 0, Trupact-I-Test 1, and Nuclear Winter is shown in Table 3.2. For this comparison the towers for each test were conditioned in the same manner as described in [4.5]. There is good agreement at like tower locations from one test to another. On the center tower, the temperature consistently rises from the lowest station (1.37 meters), reaches a plateau at about 1000°C and then drops above the 6.1 meter station.

TABLE 3.1 Nuclear Winter Fire Test Average Results

Measurement	Height From Floor	Average	Std Dev Present	Flame
Velocity [m/sec]	15.24	-2.55	7.40	16.5
	12.19	5.41	5.56	17.4
	9.14	1.86	6.34	12.1
	6.10	5.87	5.61	12.1
	4.77	5.65	5.06	10.7
	3.40	5.94	4.43	8.4
	2.11	4.10	3.25	4.5
Center Tower Temperatures [°C]	15.24	326	313	1059
	12.19	382	330	1058
	9.14	477	328	968
	6.10	692	293	913
	4.77	829	267	959
	3.40	887	265	1040
	2.11	881	196	1086
East Tower	6.10	731	358	765
	4.72	765	363	818
	3.51	769	324	888
	2.29	843	242	1016
	1.37	902	85	943
South Tower	6.10	534	280	656
	4.72	633	248	690
	3.51	801	196	922
	2.29	938	87	1055
	1.37	932	93	830
West Tower	6.10	479	295	1119
	4.72	674	268	1102
	3.51	985	191	1064
	2.29	1009	144	904
	1.37	914	151	623
North Tower	6.10	810	287	993
	4.72	919	225	1009
	3.51	973	169	1071
	2.29	1040	116	1131
	1.37	933	112	873

TABLE 3.2

Comparison Of Conditionally Averaged Tower Temperatures From Three Tests

Height Above Floor [meters]	TRUPACT-1-TEST 0 Temperature °C Tower Location				TRUPACT-1-TEST 1 Temperature °C Tower Location				NUCLEAR WINTER Temperature °C Tower Location			
	<u>SW</u>	<u>NW</u>	<u>SE</u>	<u>NE</u>	<u>SW</u>	<u>NW</u>	<u>SE</u>	<u>NE</u>	<u>S</u>	<u>N</u>	<u>E</u>	<u>W</u>
6.10	986	934	810	888	782	897	927	977	939	976	987	906
4.72	986	974	***	***	914	998	1021	988	953	1038	1018	1013
3.51	942	1024	1046	1020	1069	1037	989	1051	1001	1029	976	1048
2.90	955	1065	1038	1002	***	***	***	***	***	***	***	***
2.29	964	1055	974	1039	1085	1029	981	964	971	1057	984	941
1.37	774	913	***	***	784	800	754	744	840	914	917	742

	TRUPACT-1-TEST 1 Temperature °C <u>CENTER TOWER</u>	NUCLEAR WINTER Temperature °C <u>CENTER TOWER</u>
6.10	974	927
5.44	1013	***
4.78	1025	1007
4.09	1036	***
3.40	1022	1014
2.79	1005	***
2.21	949	997
1.50	788	***

*** No thermocouple at this location.

NUCLEAR WINTER FIRE TEST FLAME TEMPS - CENTER TOWER

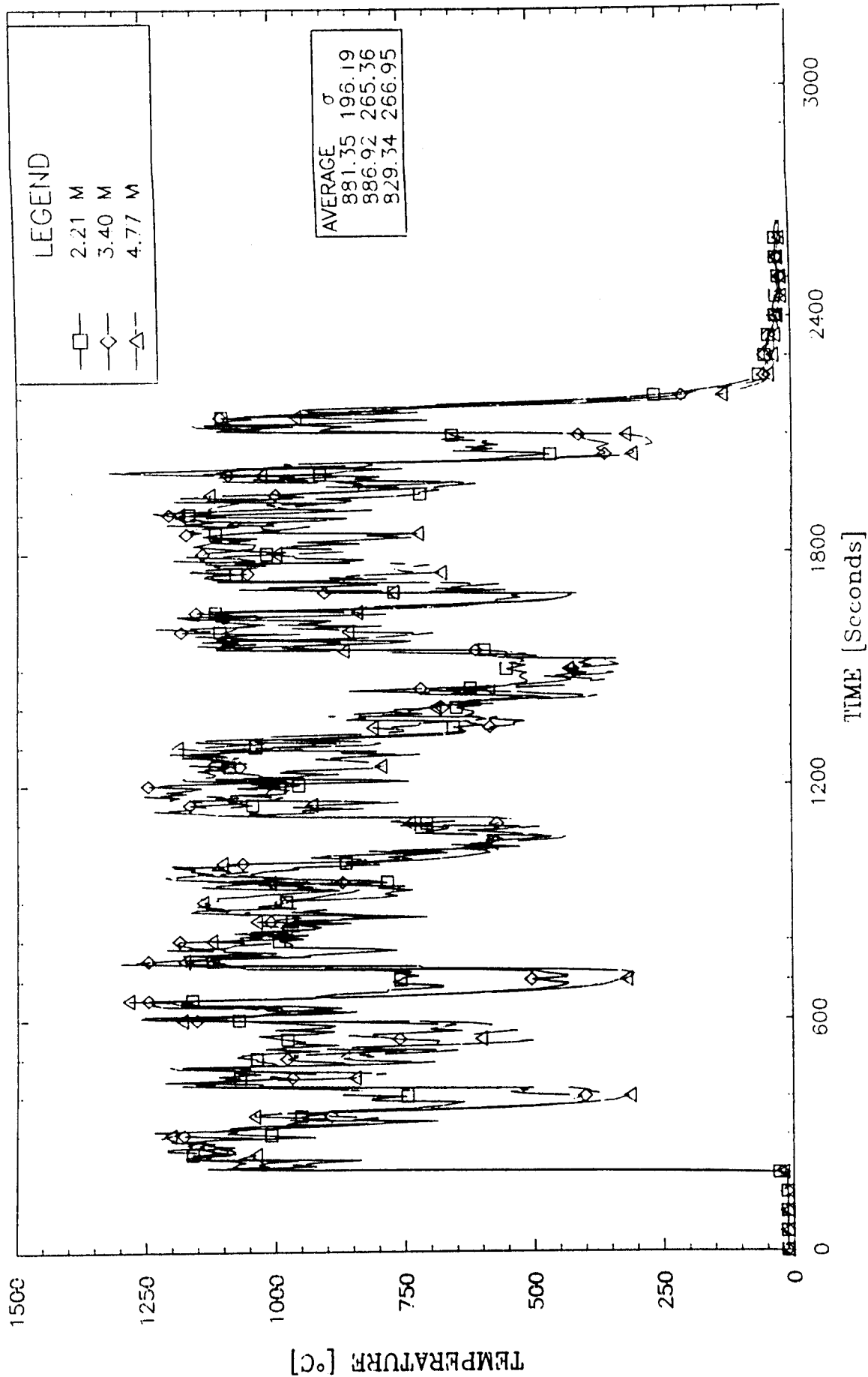


Figure 3.1 Flame Temperatures - Lower Part of Center Tower

NUCLEAR WINTER FIRE TEST FLAME TEMPS - CENTER TOWER

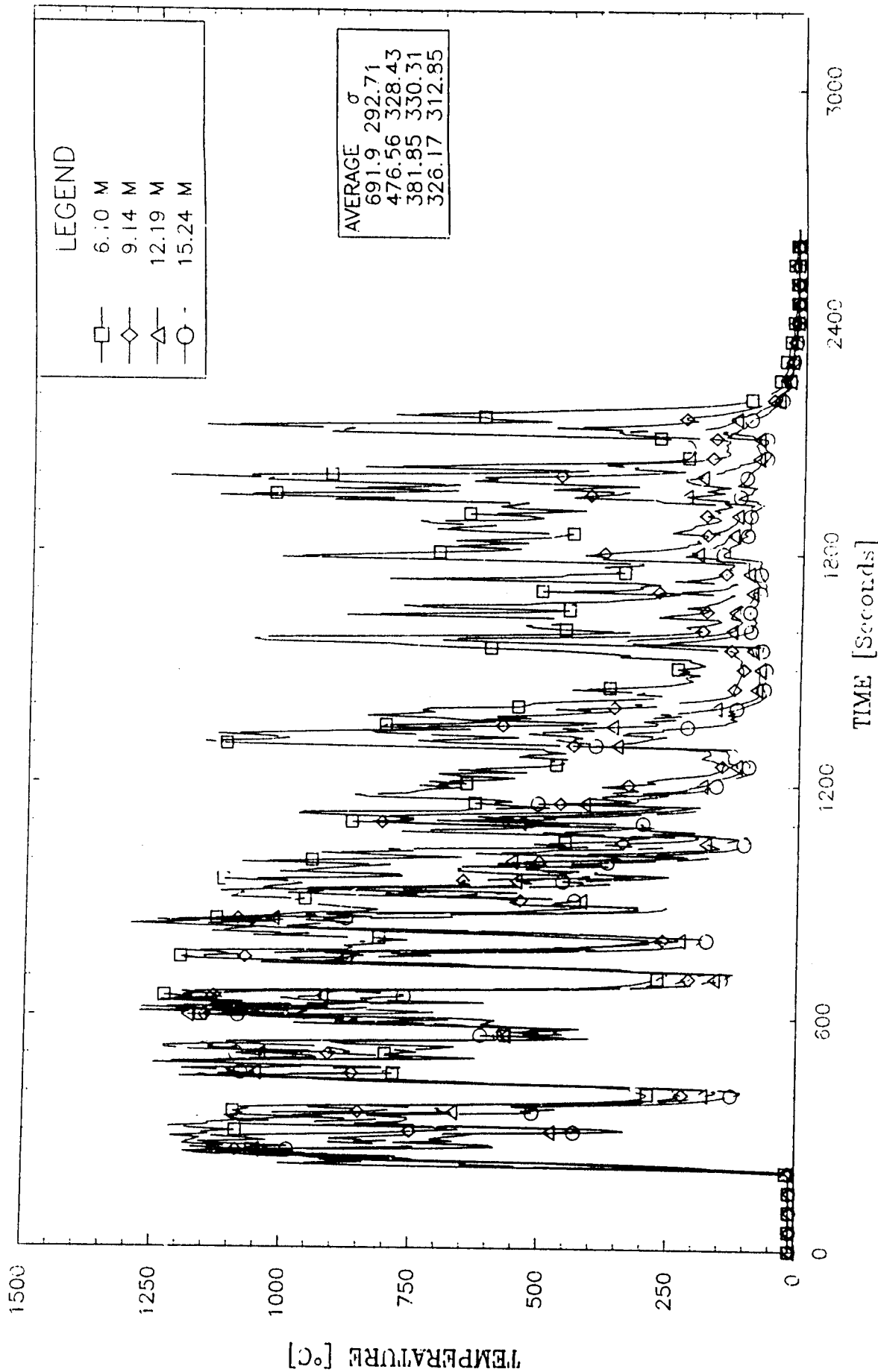


Figure 3.2 Flame Temperatures - Upper Part of Center Tower

NUCLEAR WINTER FIRE TEST FLAME TEMPS - NORTH TOWER

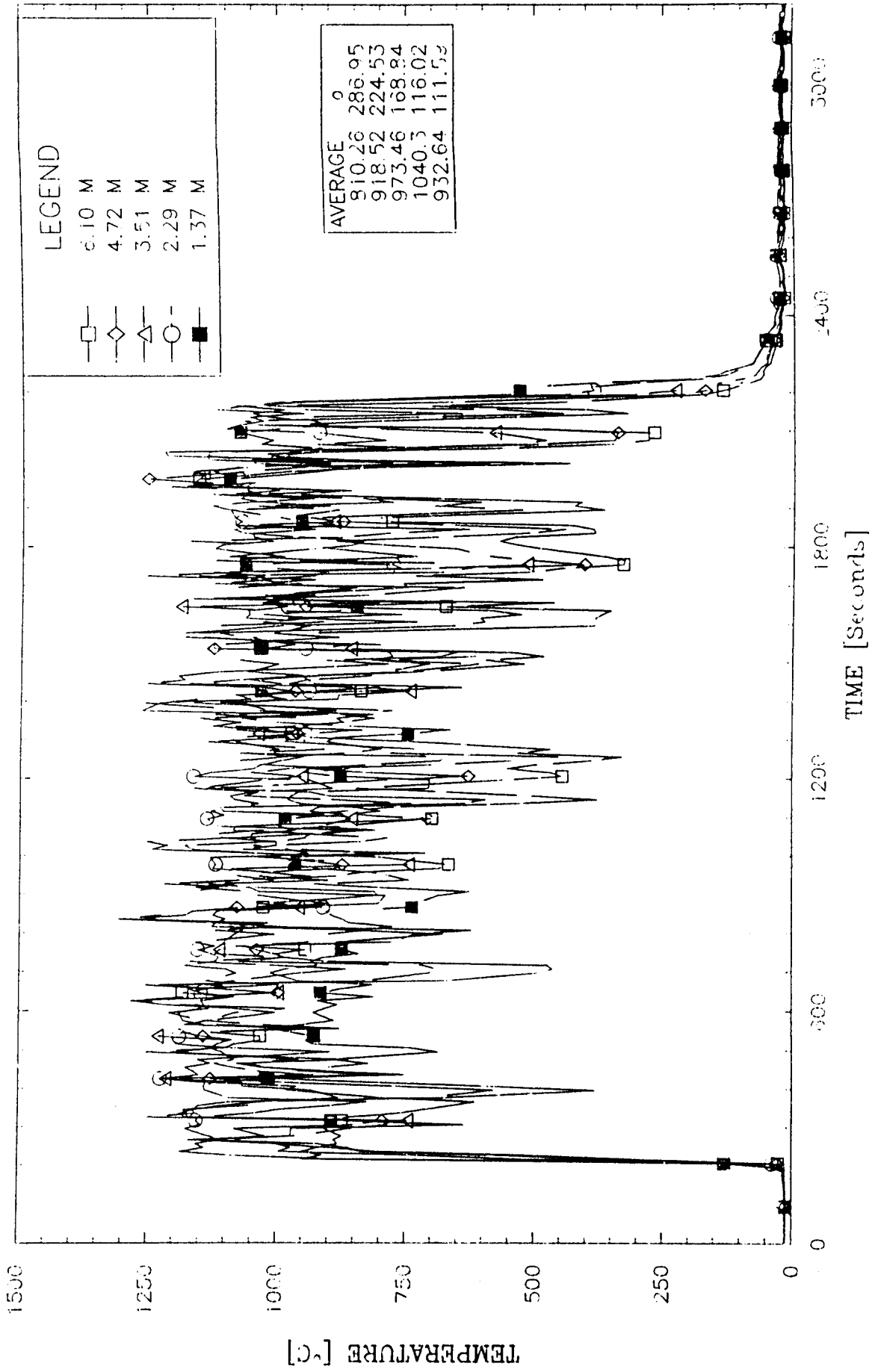


Figure 3.3 Flame Temperatures - North Tower

NUCLEAR WINTER FIRE TEST FLAME TEMPS - EAST TOWER

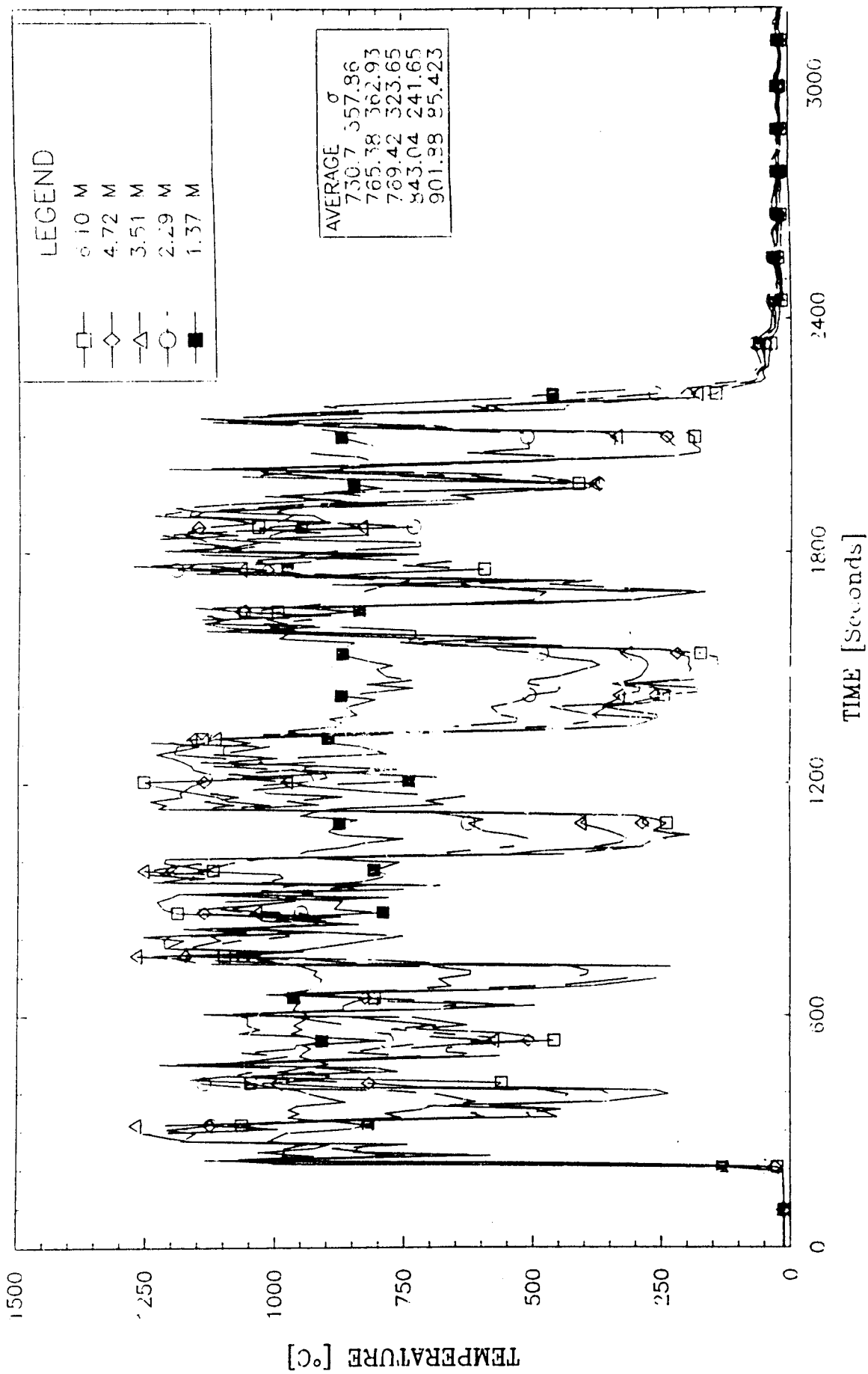


Figure 3.4 Flame Temperatures - East Tower

NUCLEAR WINTER FIRE TEST FLAME TEMPS - SOUTH TOWER

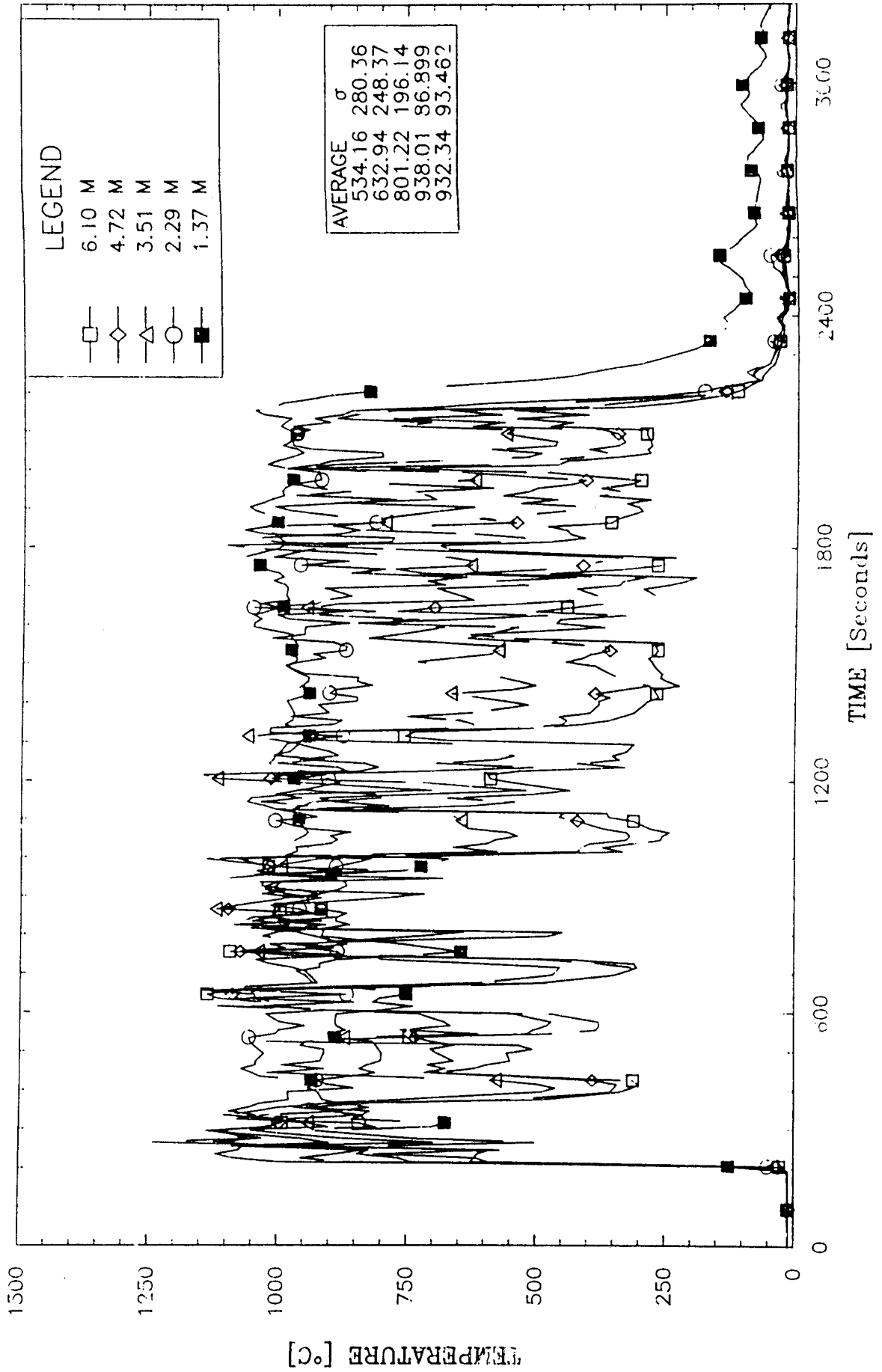


Figure 3.5 Flame Temperatures - South Tower

NUCLEAR WINTER FIRE TEST FLAME TEMPS - WEST TOWER

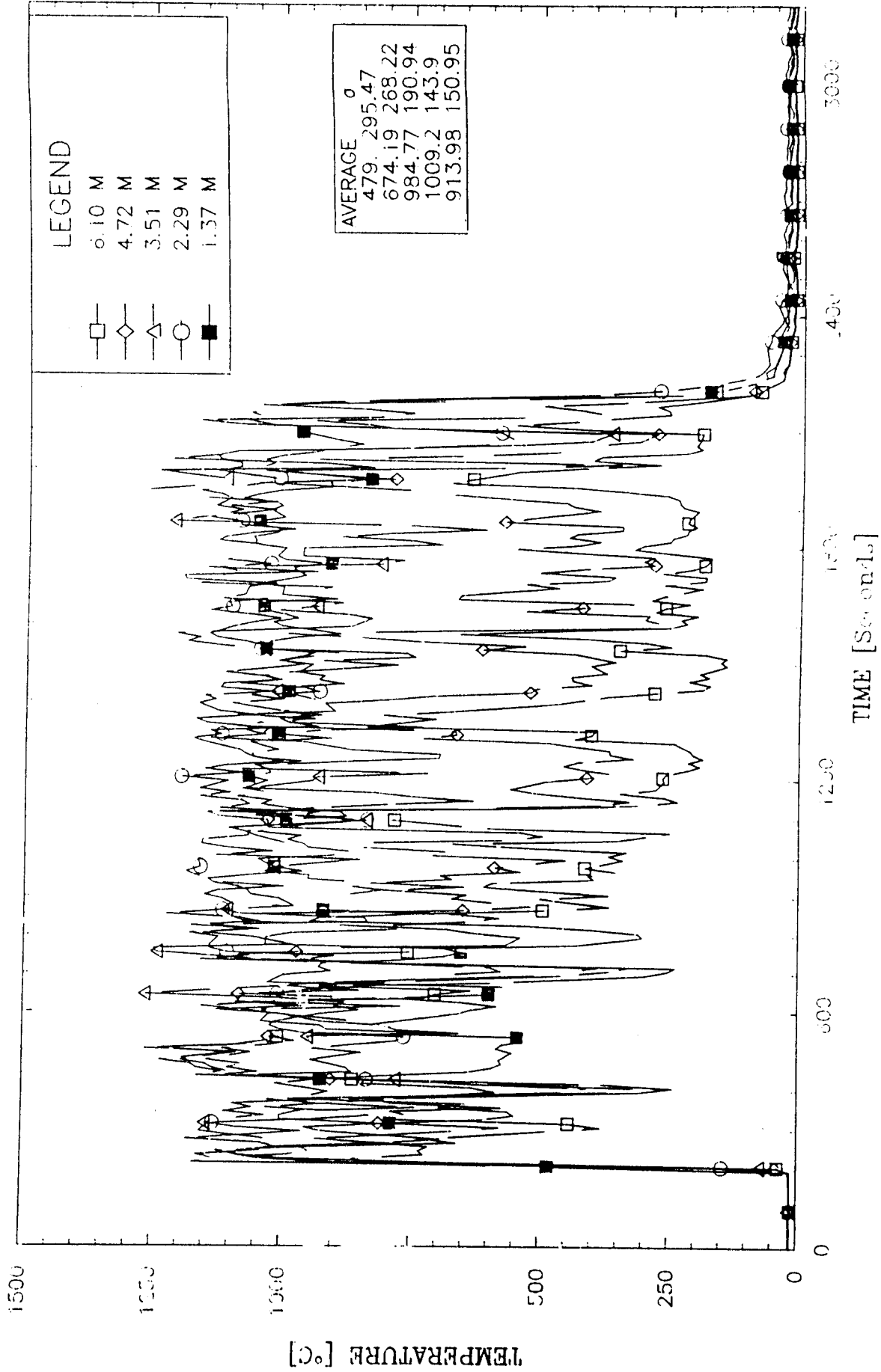


Figure 3.6 Flame Temperatures - West Tower

NUCLEAR WINTER FIRE TEST
AVERAGE TEMPERATURES

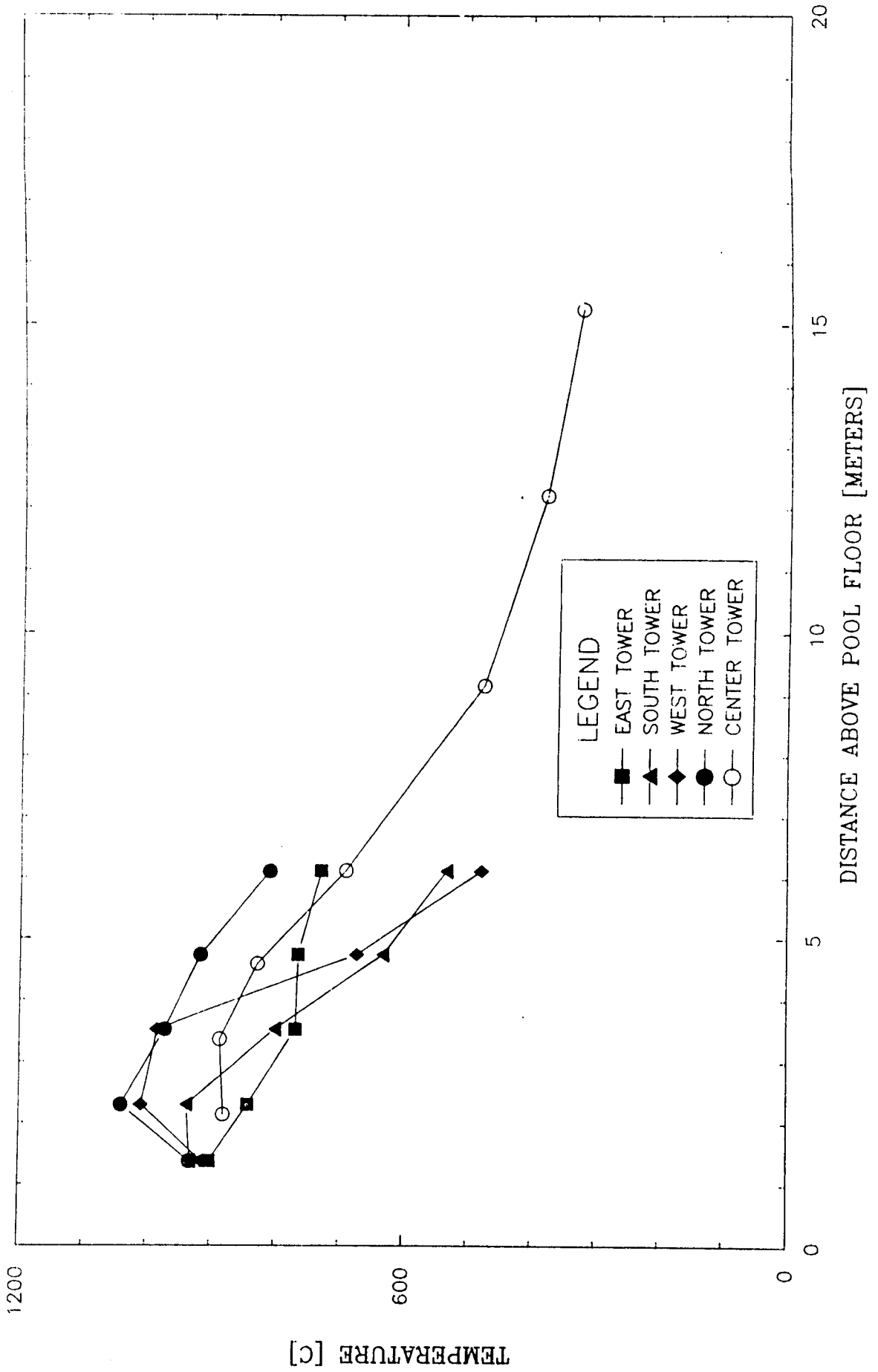


Figure 3.7 Average Temperatures vs Height

TRUPACT I FIRE TEST AVERAGE TEMPERATURES

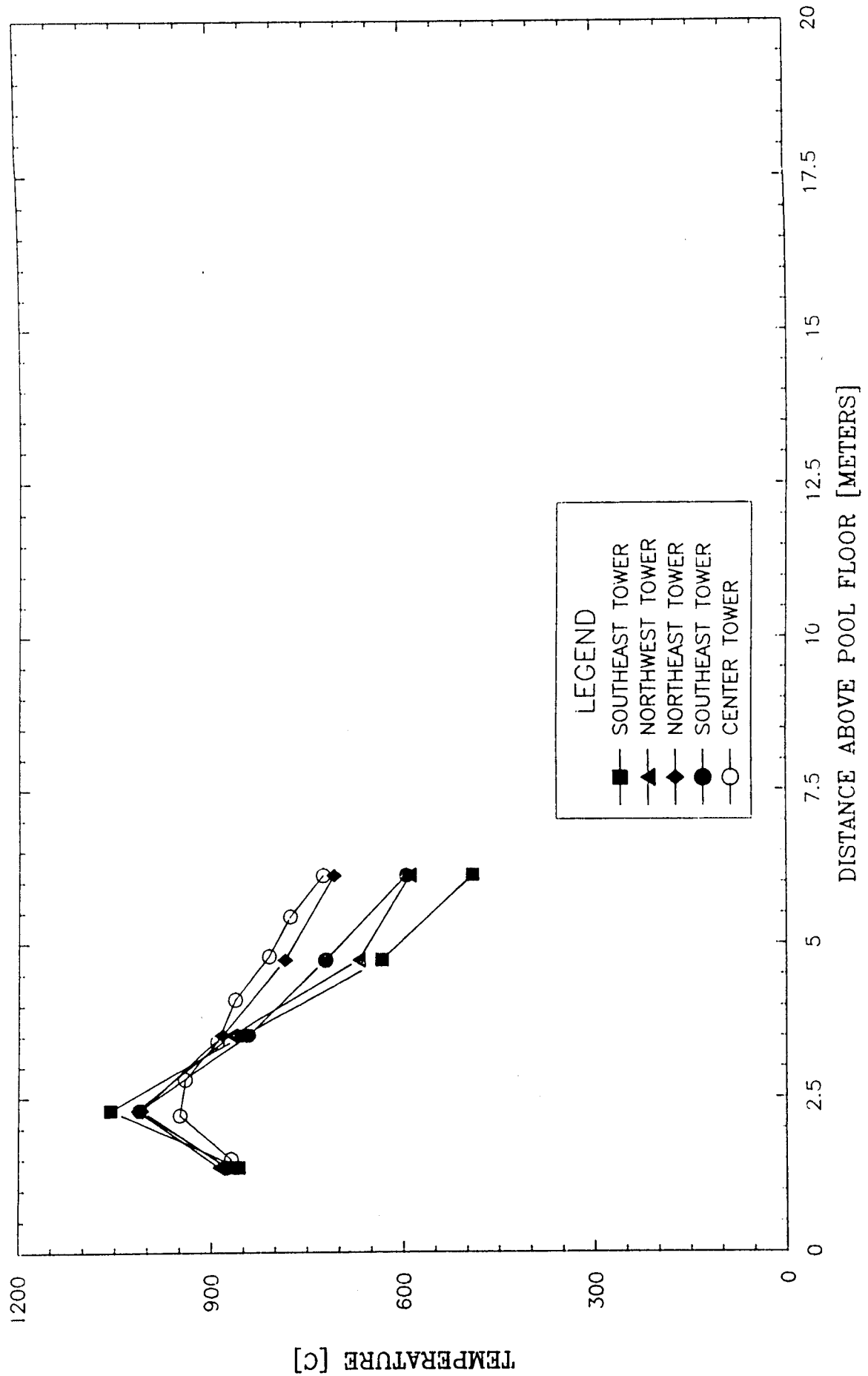


Figure 3.8 Average Temperatures (Trupact-I-Test 1)

TRUPACT 0 FIRE TEST
AVERAGE TEMPERATURES

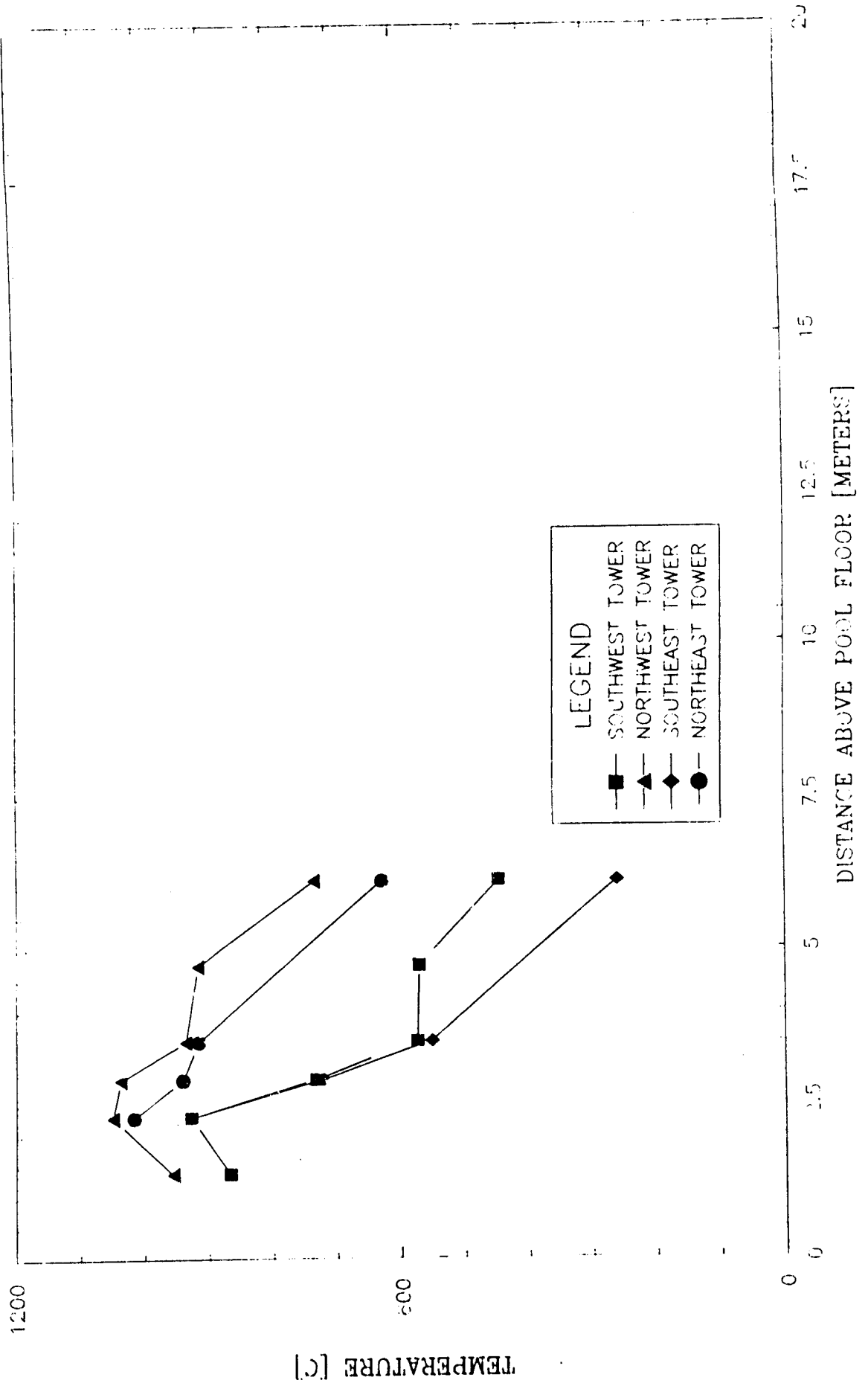


Figure 3.9 Average Temperatures (Trupact-I-Test 0)

NUCLEAR WINTER FIRE TEST STANDARD DEVIATIONS

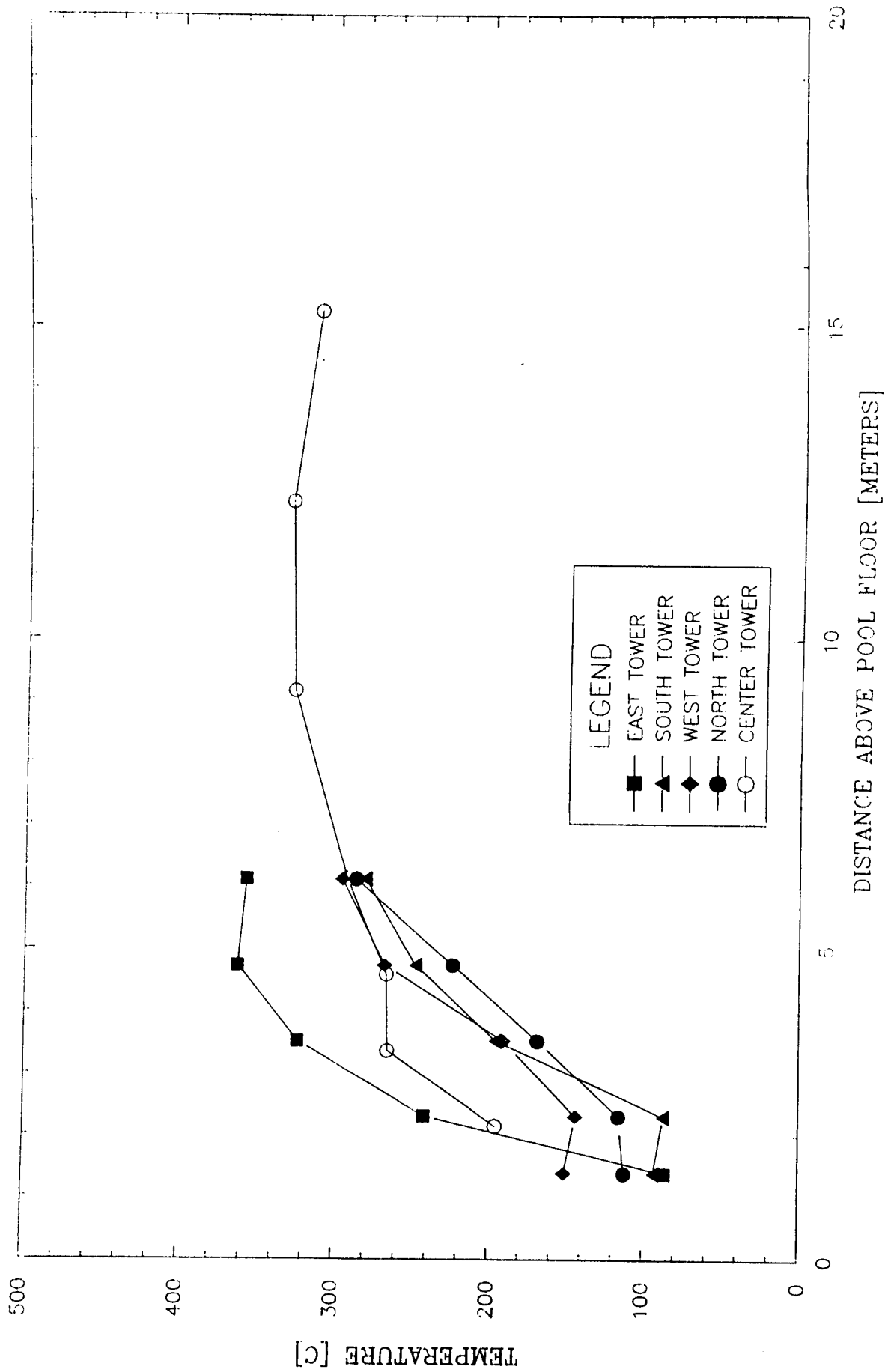


Figure 3.10 Standard Deviations in Temperatures

TRUPACT I FIRE TEST
STANDARD DEVIATIONS

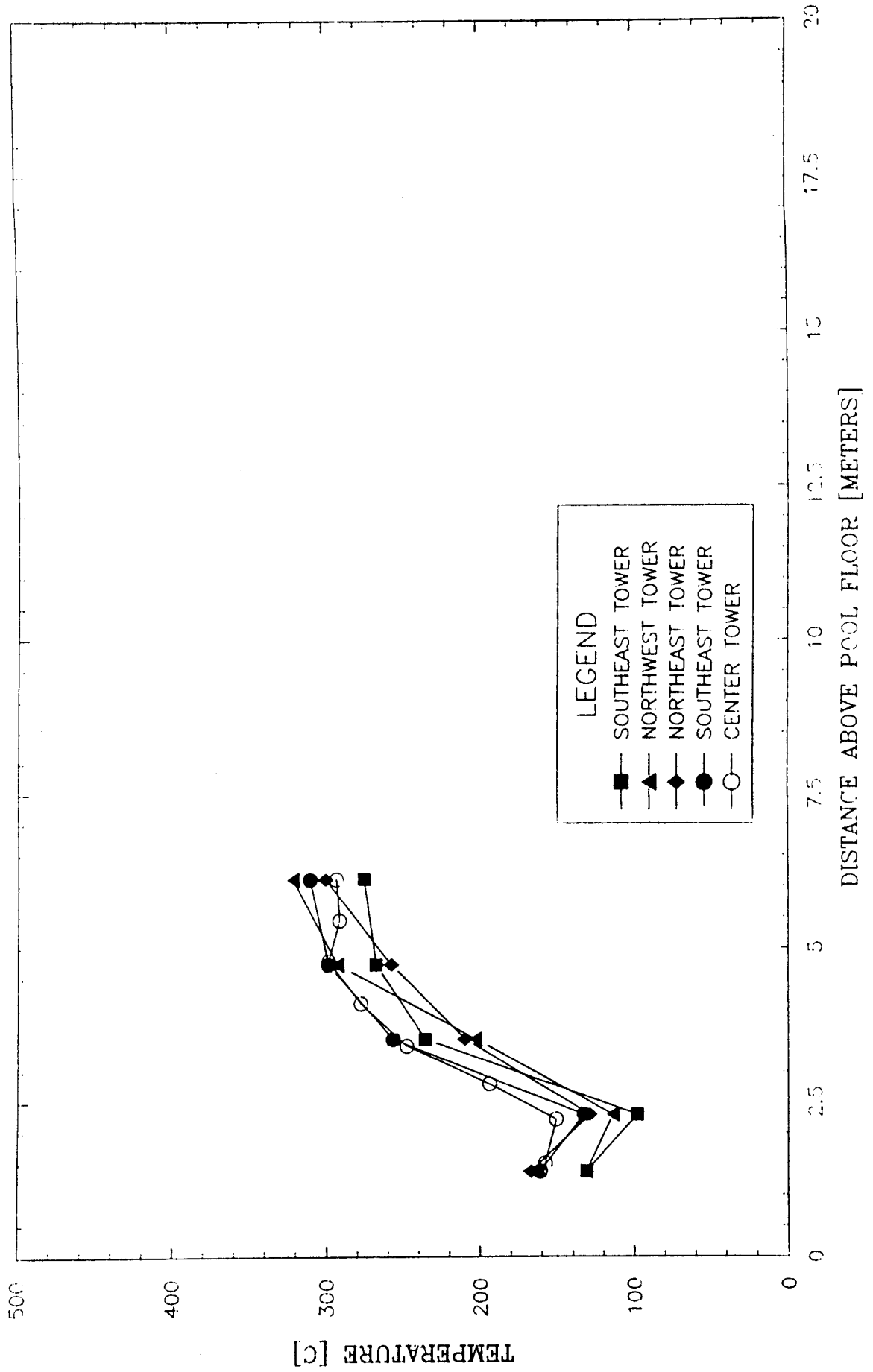


Figure 3.11 Standard Deviations (Trupact-I-Test 1)

TRUPACT 0 FIRE TEST
STANDARD DEVIATIONS

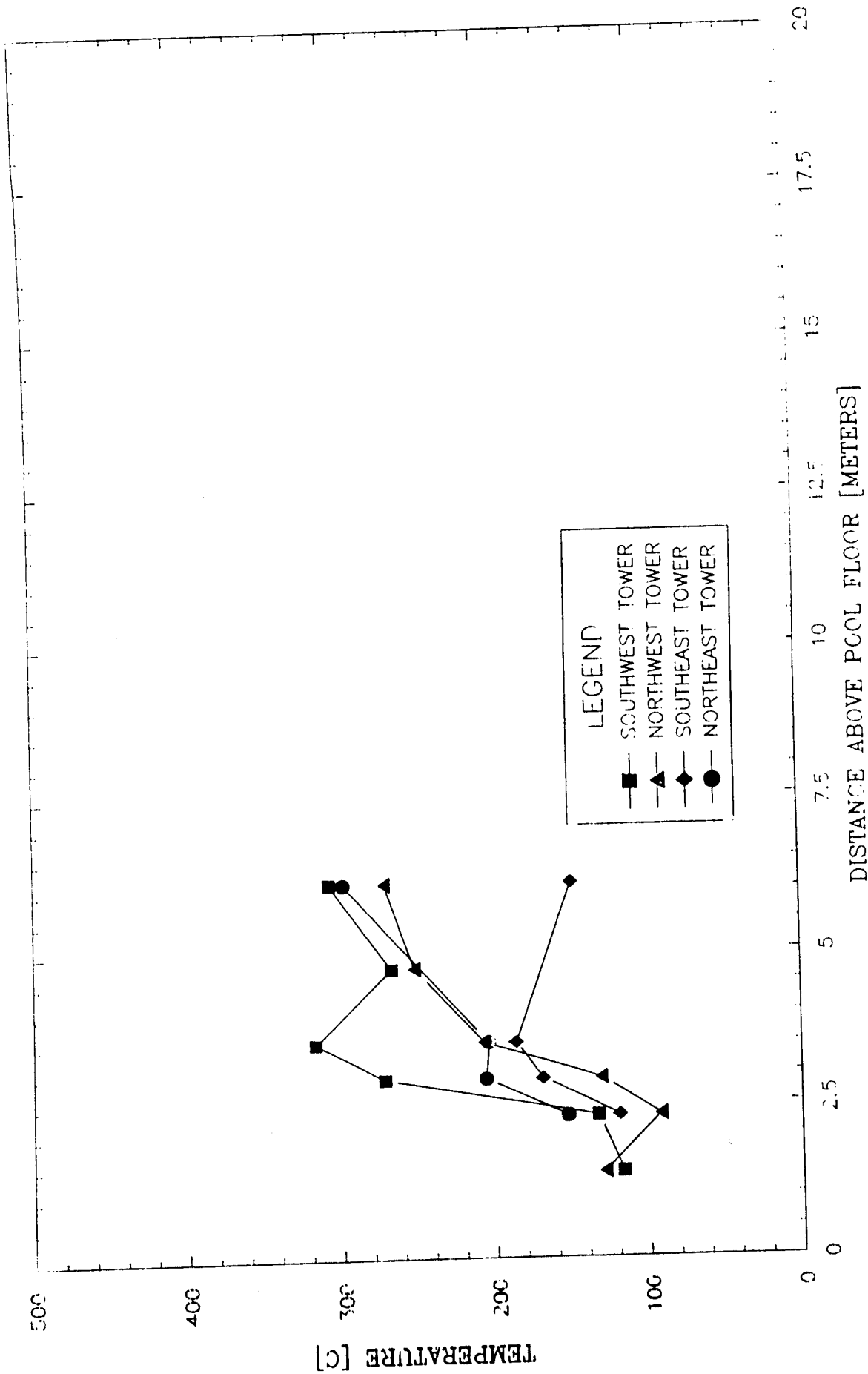
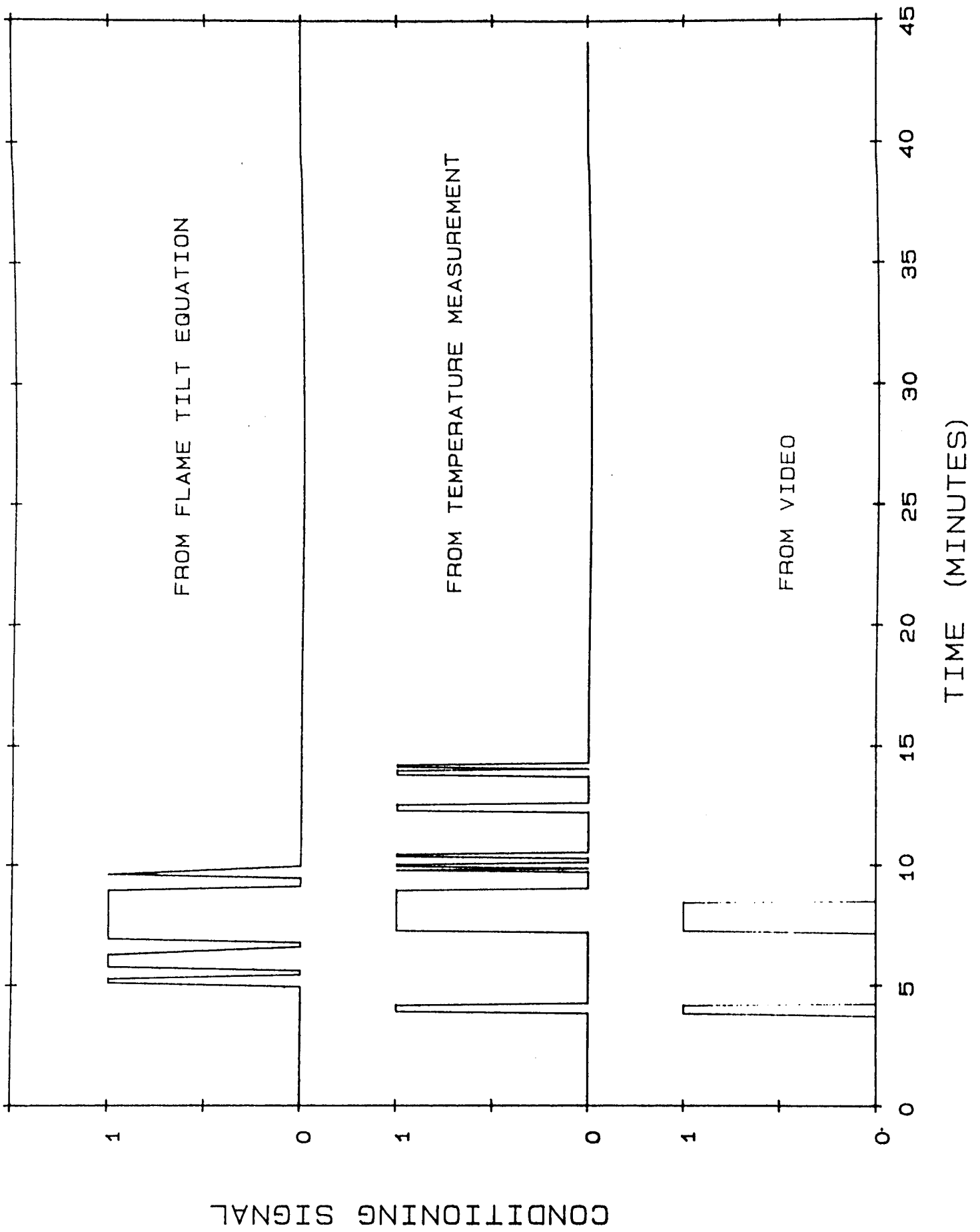


Figure 3.12 Standard Deviations (Trupact-I-Test 0)



NUCLEAR WINTER FIRE TEST
 FLAME PRESENT AVERAGES

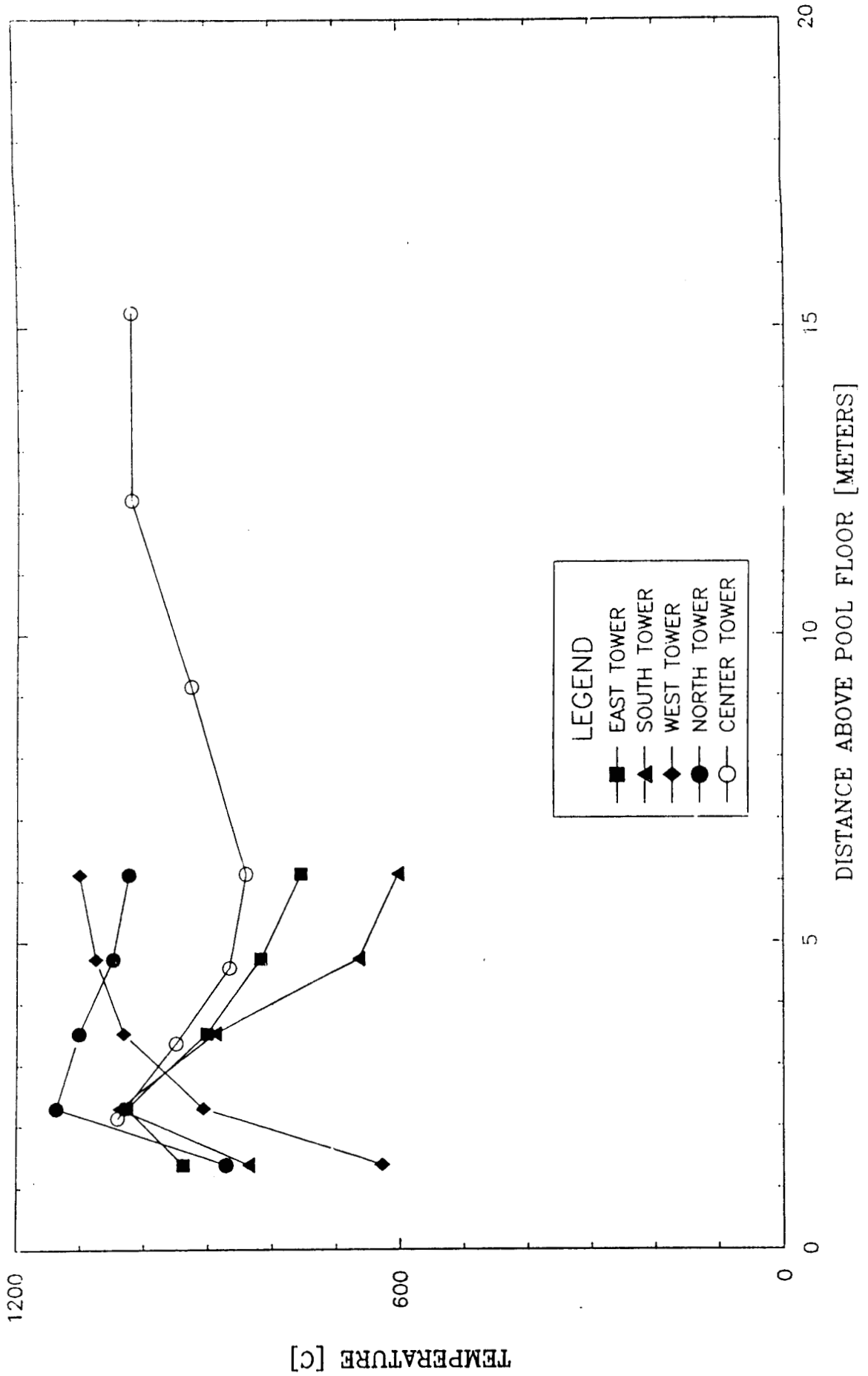


Figure 3.14 Conditionally Averaged Tower Temperatures

TRUPACT I FIRE TEST
 FLAME PRESENT AVERAGES

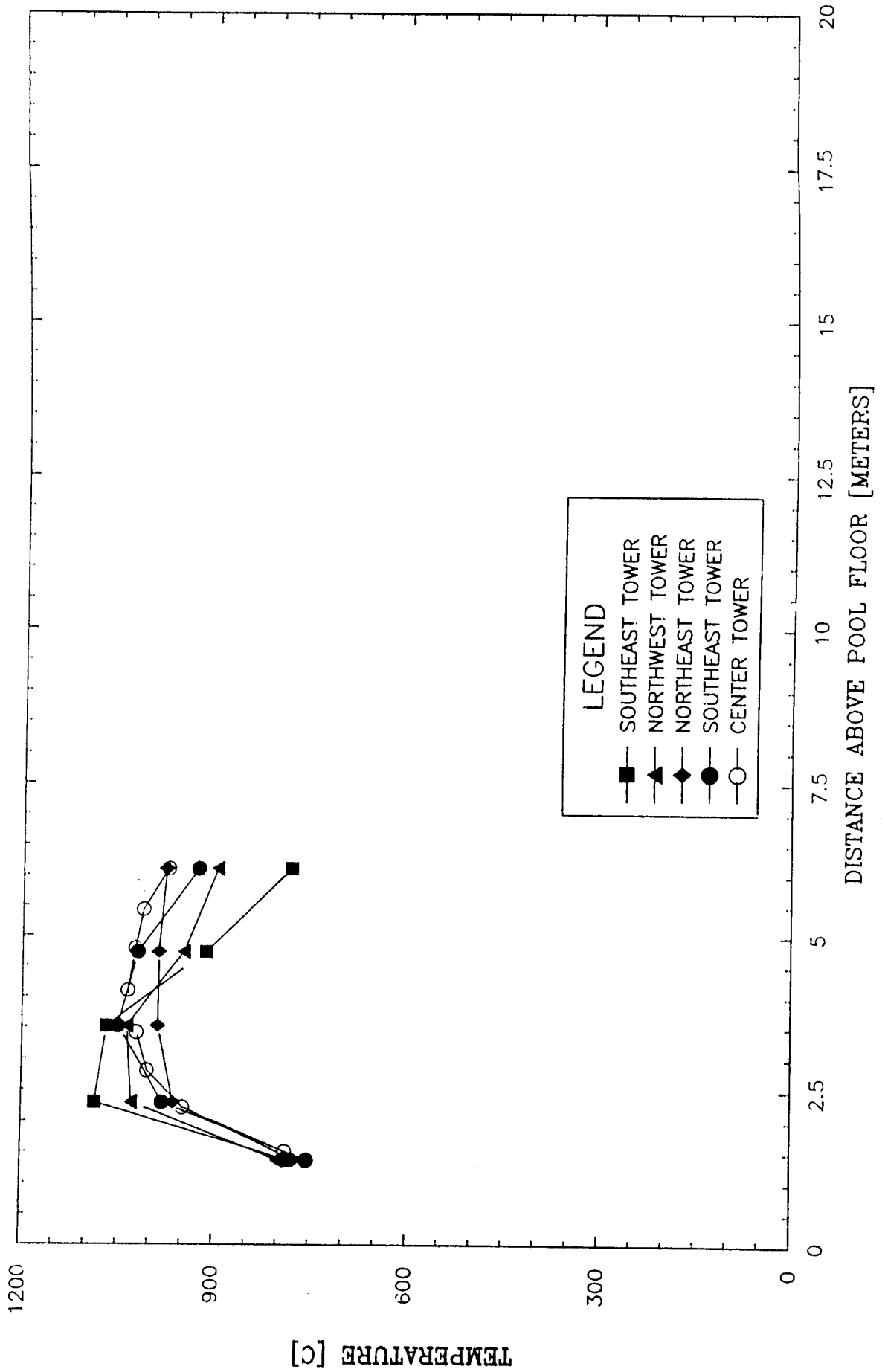


Figure 3.15 Flame Present Temperatures (Trupact-I-Test 1)

TRUPACT 0 FIRE TEST
 FLAME PRESENT TEMPERATURES

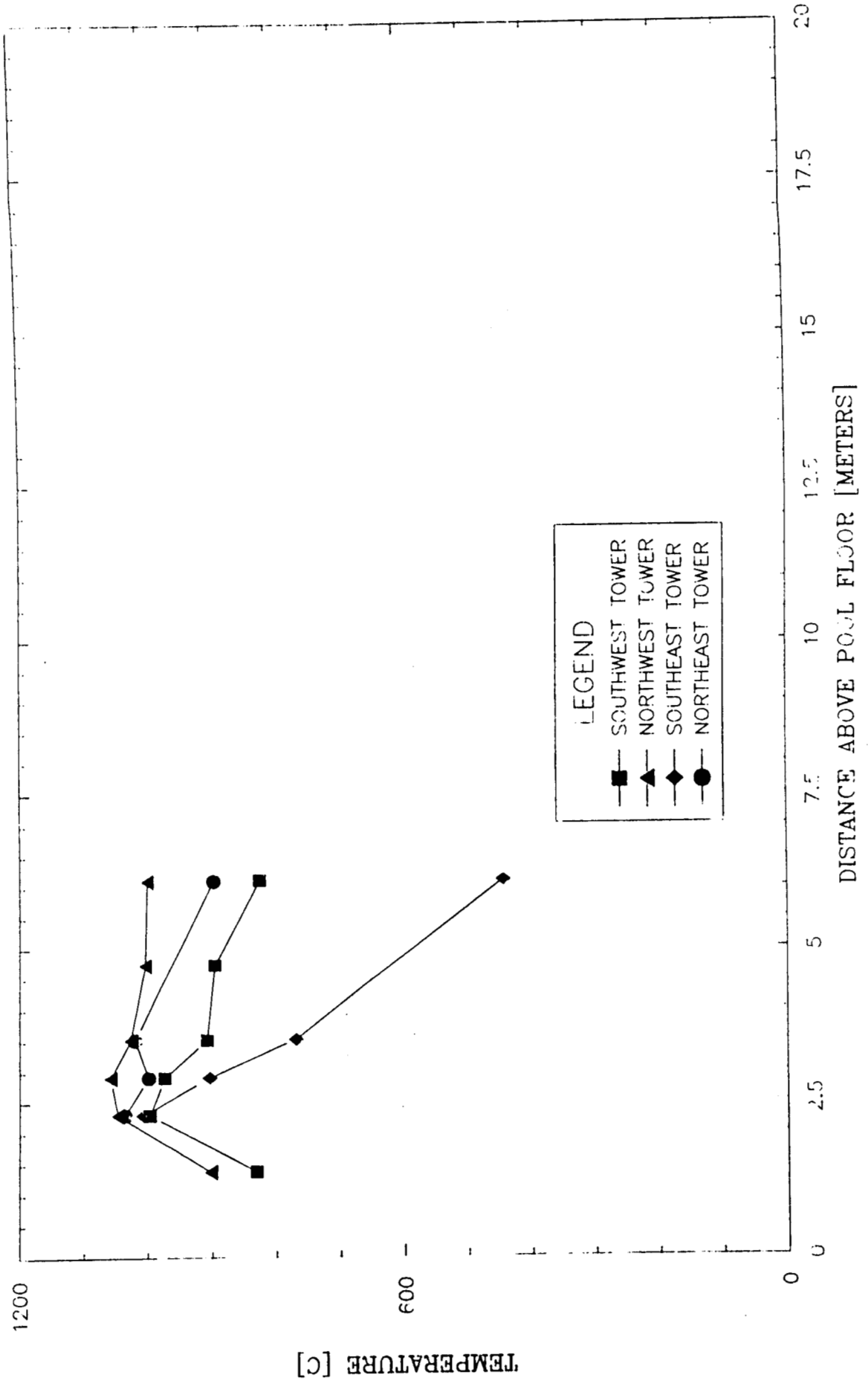


Figure 3.16 Flame Present Temperatures (Trupact-I-Test 0)

IV. GAS VELOCITIES ON THE POOL CENTERLINE

The velocity measurements were made with a low-velocity pitot type probe designed for use at low Reynolds numbers. The design and application of these "bidirectional" probes is described in detail in [6,8]. The velocity probes were mounted at seven vertical stations on the center tower (Figure 2.1); 2.2, 3.4, 4.8, 6.1, 9.1, 12.2, and 15.2 meters above the pool floor as shown in Figure 2.3. A 1.6 mm O.D., inconel sheathed, ungrounded junction, type K thermocouple was used at each probe location to measure the temperature of the gas. These temperatures were used to calculate the density (ρ) of the gas (assumed to be air) which is used in the velocity equation.

$$V = \left(\frac{\Delta P}{\frac{1}{2} \rho C^2} \right)^{1/2}$$

For the lower four stations, the differential pressures (ΔP) were measured with 0 - 0.62 millibar Setra pressure gages (Model 261-1); the differential pressure measurements for the upper three probes used ± 1.2 millibar bidirectional Setra pressure gages. Use of the bidirectional gages for the upper three stations was due to the higher pressures expected and not because of anticipated flow reversals.

The velocity histories are shown in Figures 4.1 and 4.2. Some clipping of signals occur near zero volts in Figure 4.1. The probable cause is from a small amount of noise on the signal lines driving the millivolt signal below zero volts. The reverse velocities at the high stations are likely to be due to the effects of the strong winds late in the test; the probes may be just outside the fire plume. The large fluctuations in the velocities are primarily due to wind effects. The velocity data was conditionally sampled with the flame present signal described in the previous section. The conditionally sampled data represents only 1.5 minutes out of the total test time of 34 minutes (approximately 4 percent). The averages and standard deviations in the measured velocities were calculated and are presented in Table 3.1. The "test" average values and the "conditionally sampled" average values are plotted in Figure 4.3 along with the corresponding values from Trupact-I-Test 1 open pool fire test. The results indicate slightly lower velocities than measured in the previous test.

Figure 4.4 compares the average measured velocities during the "flame present" state with the mean centerline velocity data of McCaffrey [9], which were made in fires which were much smaller. The vertical distance, z , and the velocity, V , have been scaled in a way that normalizes the values with the thermal power of the fire. McCaffrey defines three zones in the fire: continuous flame, intermittent flame, and plume. The point $z/Q^{2/5} = 0.08$ is the end of the continuous flame region, $z/Q^{2/5} = 0.20$ is the end of the intermittent flame region. In the continuous flame region the vertical velocity should vary as

$$\frac{V}{Q^{1/5}} = 6.83 \left(\frac{z}{Q^{2/5}} \right)^{1/2}$$

The value of Q used by McCaffrey was the estimated total heat release. In McCaffrey's work, the flames studied were methane flames. In this case the theoretical maximum heat release (from gross fuel consumption), the estimated total heat release (considering combustion efficiency), and the convective heat release, were very near the same values for a given flame.

In the case of a sooty pool fire that is highly luminous, these values will differ considerably from each other. It is likely that only the convective heat release contributes to the buoyancy, and thus the vertical velocities. The data shown in Figure 4.4 were normalized for the convective heat release.

In an effort to provide for a more direct comparison with Trupact-I-Test 1 velocity data, another conditioning signal was generated. Data from the 2.2, 3.4, 4.8, and 6.1 meter stations was sampled with a conditioning signal generated from the thermocouple temperature history at the 6.1 meter station in the same manner as for the Trupact-I-Test 1 [4,5]. There was a problem with some of the data; at some times the temperature history was high, but the velocity at one or more of the stations was either zero or negative. To correct this inconsistency, the conditioning signal was modified to remove all of the data at any time at which any of the velocities were either zero or negative. By using this conditioning signal, the sample data increased from 1.5 (approximately 4%) to 9.5 minutes (approximately 28%) of the total test time. A comparison of the velocity data generated by using the two conditioning signals generated is shown in table 4.1. Table 4.1 also shows the scaled data as defined by McCaffrey [9] ($[z/Q^{2/5}]$, $[V/Q^{1/5}]$) for the three heat release rates.

TABLE 4.1

Effects Of Conditional Sampling Of The Velocities

Height Above Initial Fuel Surface [meters]	* Velocity ± Std Dev		** Velocity ± Std Dev		Percent Change
	[m/sec]		[m/sec]		
1.42	4.54	1.93	5.79	1.64	28
2.62	8.42	0.99	8.73	1.96	4
3.99	10.70	1.68	10.37	2.13	-3
5.31	12.06	1.82	11.67	2.42	-3
8.36	12.07	2.04	-	-	-
11.41	17.40	3.29	-	-	-
14.46	16.47	2.76	-	-	-

Normalized Data From Video Conditioning Signal

Q Based on

Height Above Initial Fuel Surface [meters]	*** 585 MW Theoretical Maximum Heat Release		535 MW Estimated Total Heat Release		358 MW Estimated Convective Heat Release	
	[z]	$[z/q^{2/5}]$ $[v/q^{1/5}]$	$[z/q^{2/5}]$ $[v/q^{1/5}]$	$[z/q^{2/5}]$ $[v/q^{1/5}]$	$[z/q^{2/5}]$ $[v/q^{1/5}]$	$[z/q^{2/5}]$ $[v/q^{1/5}]$
1.42	0.0070	0.3189	0.0072	0.3246	0.0085	0.3515
2.62	0.0129	0.5914	0.0134	0.0620	0.0157	0.6522
3.99	0.0197	0.7516	0.0204	0.7651	0.0239	0.8288
5.31	0.0262	0.8471	0.0271	0.8624	0.0319	0.9341
8.36	0.0412	0.8478	0.0427	0.8634	0.0501	0.9349
11.41	0.0563	1.2222	0.0583	1.2441	0.0684	1.3477
14.46	0.0713	1.1568	0.0739	1.1760	0.0867	1.2757

* Conditionally sampled data using the video conditioning signal @ 15.2 meters

** Conditionally sampled data using conditioning signal @ 6.1 meters

*** Based on fuel recession rate

NUCLEAR WINTER FIRE TEST CENTER TOWER - VELOCITIES

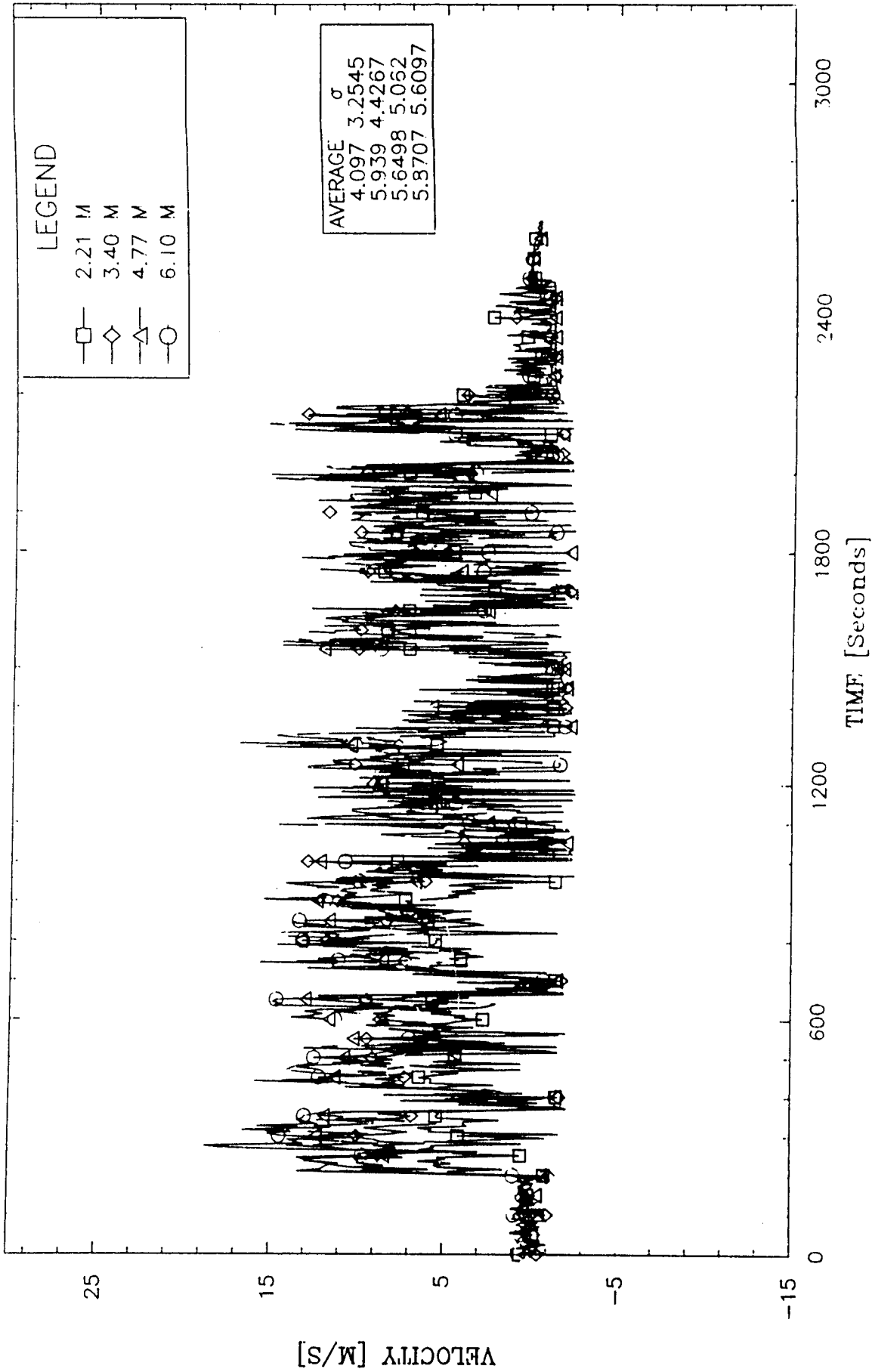


Figure 4.1 Center Tower Velocity Histories

NUCLEAR WINTER FIRE TEST CENTER TOWER - VELOCITIES

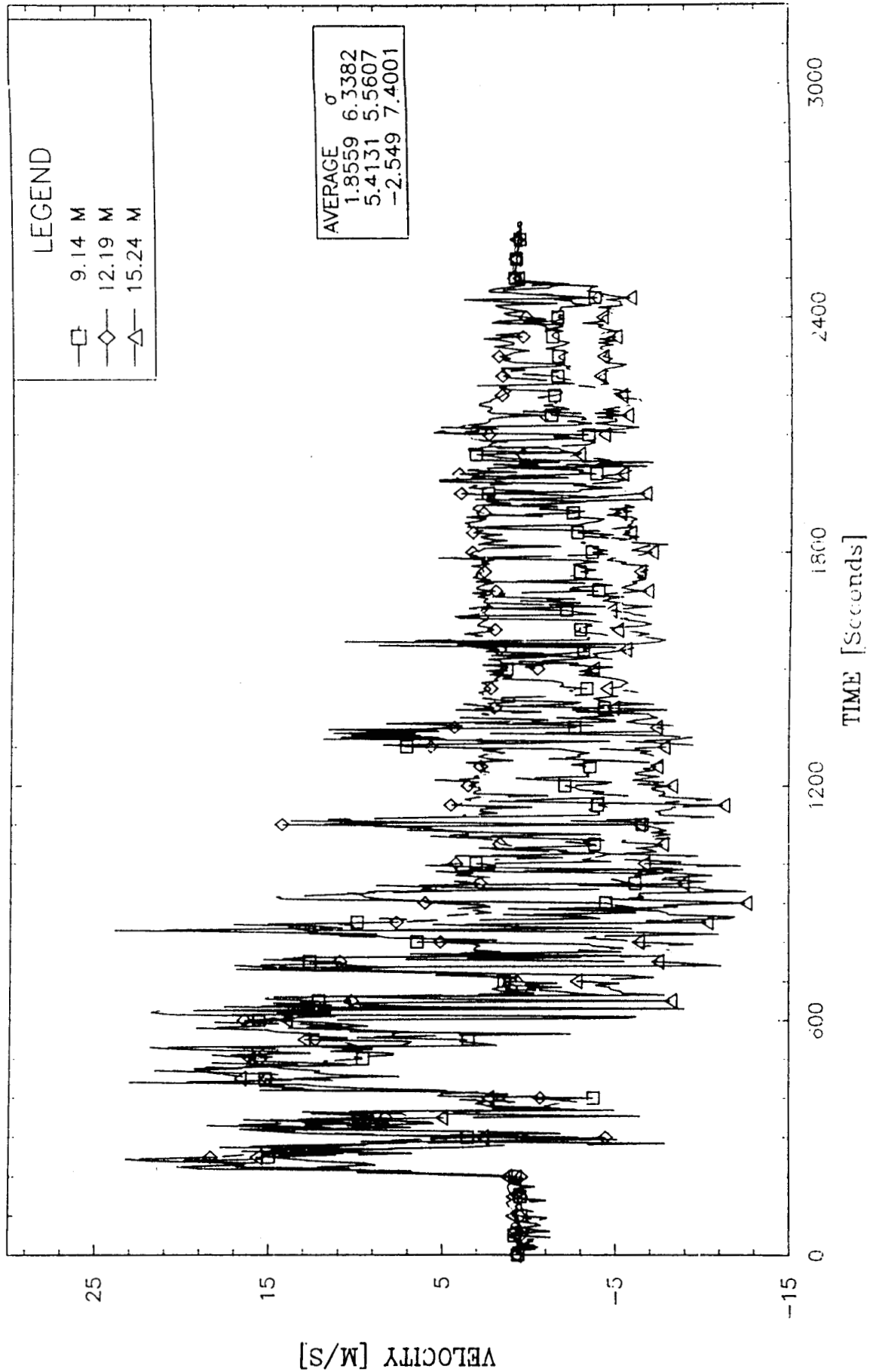


Figure 4.2 Center Tower Velocity Histories

AVERAGE VELOCITIES TWO DIFFERENT FIRE TESTS

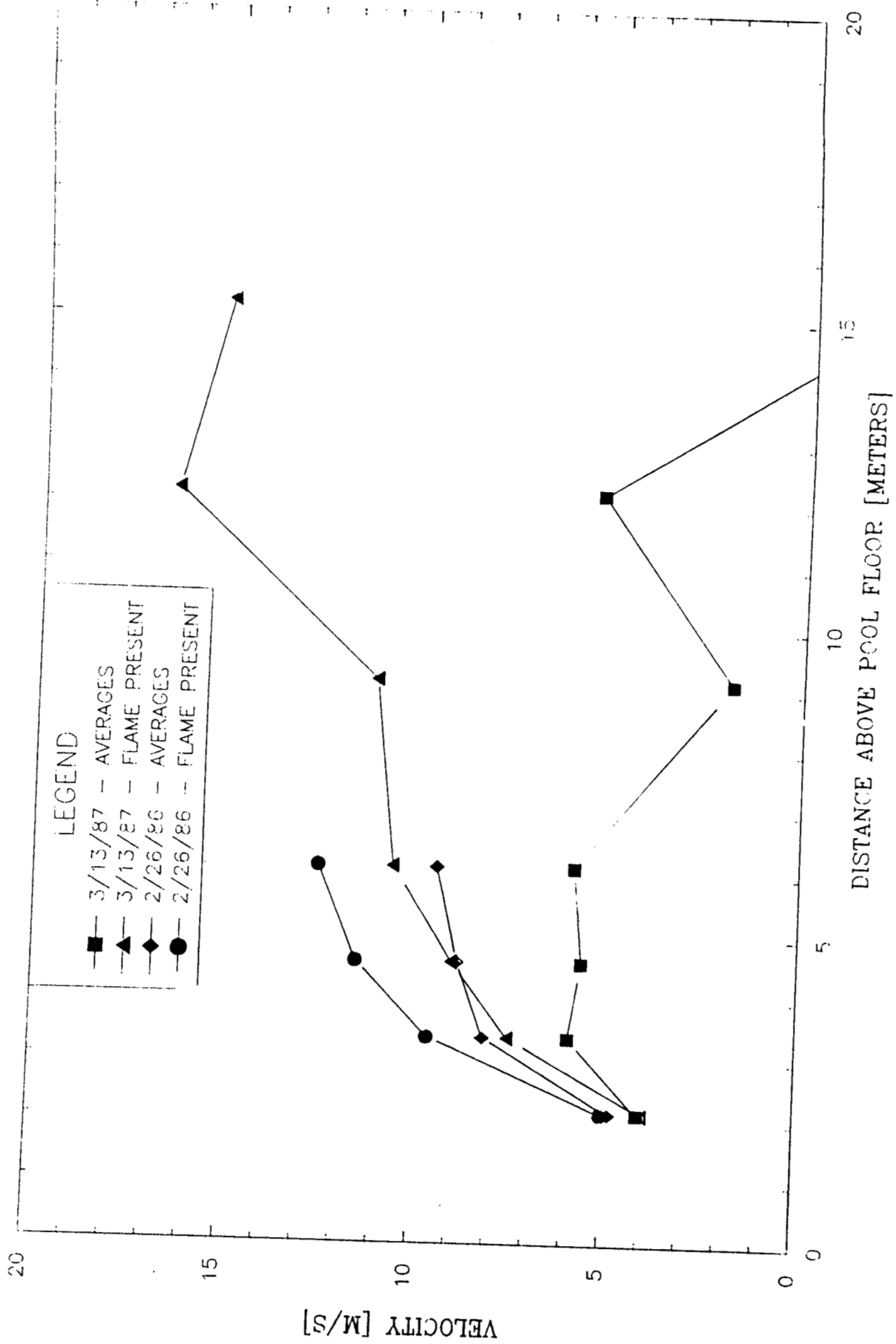


Figure 4.3 Average Velocity vs Elevation

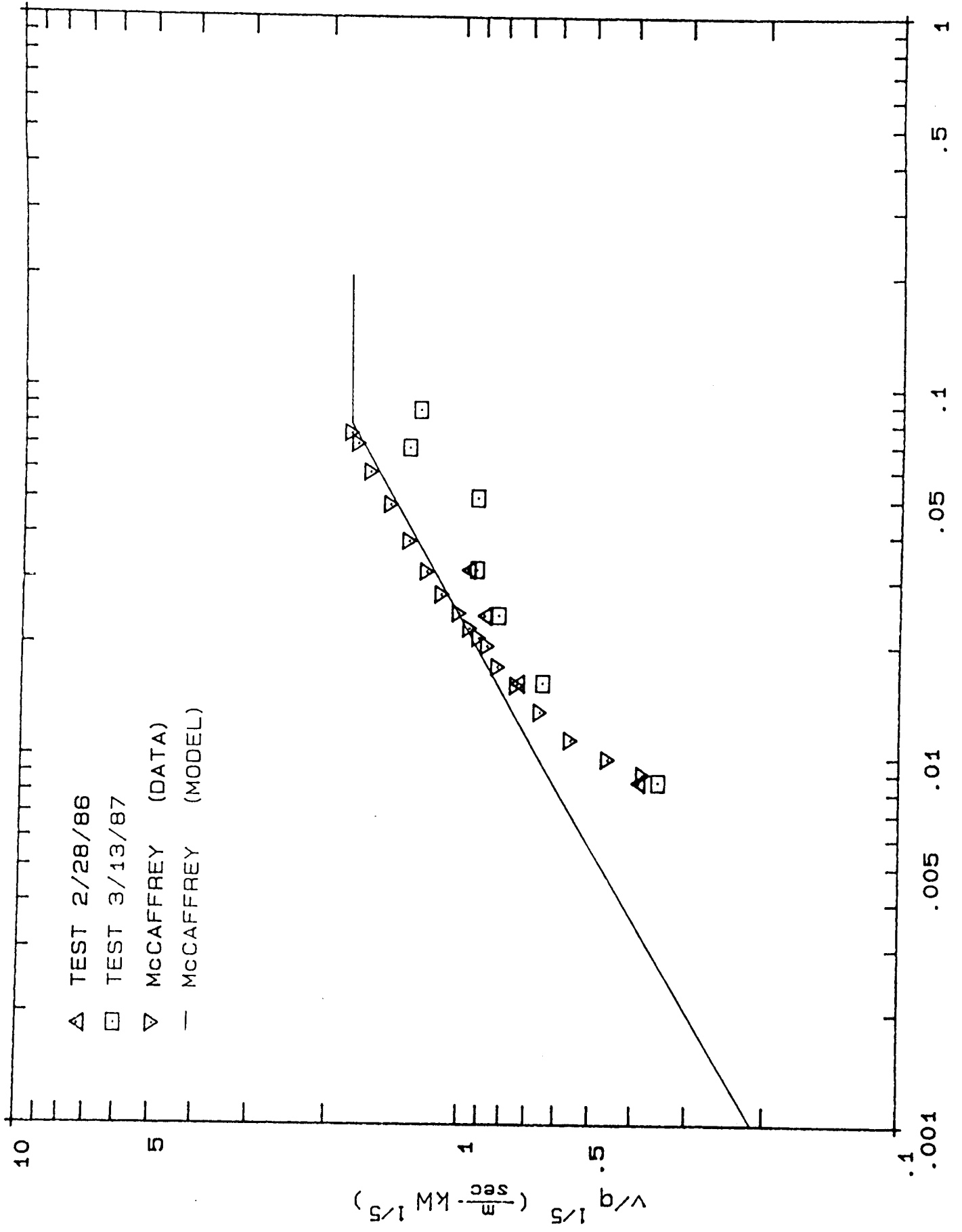


Figure 4.4 Comparison to the Literature $z/q^{2/5} \left(\frac{\text{m}}{\text{KW}} \right)^{2/5}$

V. HEAT FLUX TO THE PLATE CALORIMETER

A plate calorimeter was used to investigate the heat flux to vertical surfaces in fires. The plate calorimeter was positioned about 4.6 m in from the east edge of the pool as detailed in Figure 2.1. The calorimeter was 61 cm in width and 3.05 m in height. Figure 2.4 shows a cutaway view of the calorimeter. The east facing side was constructed of a 1.02 mm thick, mild steel plate which simulates radiation shields which are present on some transportation containers. This thin plate is referred to as a shroud. Spaced 0.95 cm behind the 1.02 mm mild steel plate was a 6.35 mm thick mild steel plate. External, 1.6 mm dia. sheathed thermocouples were placed in the flame about 10 cm off the front surface of the 1.02 mm steel plate. Intrinsic thermocouples were placed on the backface of the 1.02 mm plate, and on the backface of the 6.35 mm plate. The inside of the calorimeter was filled with insulation, and all non-insulated surfaces were painted with Pyromark™ paint. This was done to insure known emissivity values in the gap between the thin and thick plates.

The west side of the plate calorimeter was split in half vertically. The north half was a 19 mm thick plate, the south half, a 6.35 mm plate. The plates were mounted so that the surfaces facing the flames were in the same plane. There were four instrumentation stations located at 4.11, 3.30, 2.49, and 1.68 m from the pool floor. At each station, thermocouples were mounted on the backface of each plate and one protruded about 10 cm into the flames. The calorimeter was mounted so that its bottom surface was 1.37 m from the pool floor.

The backface temperature histories for the walls of two different thicknesses are shown in Figures 5.1 and 5.2. The corresponding west side flame temperature history is included as Figure 5.3. The averages of the flame temperatures over the time of the test indicate that the highest temperatures are found at the lowest station. The average temperature decreases monotonically with elevation. The quasi-equilibrium temperatures of the plates indicate the same trend. The same trend was evident in past tests (eg. TRUPACT-I-Test 1). The 19 mm plate responds much more slowly than the 6.35 mm plate as can be seen by the slower initial heat-up, and the smaller fluctuations overall. Figure 5.4 indicates the relationship between the flame temperatures and the plates' response, for the top station. The top portion of the figure indicates the temperature histories of the flame, the 6.35 mm plate, and the 19 mm plate. It can be noted that for both plates, if the flame temperature is above the plate temperature, the plate temperature will continue rising. If the flame temperature falls below the plate temperature, the plate temperature decreases. Because a large difference exists between the temperatures of the two plates, it is possible for the temperature of one plate to be increasing, while the other plate is cooling off. The net heat flux into each of the two plates was calculated using the SODDIT computer code [10,11]. The results are plotted on the lower part of Figure 5.4. The results clearly show the dependence of the flux on the plates' surface temperatures. Because the 19 mm thick plate remains cool longer than the 6.35 mm thick plate, the flux to it remains positive longer than the flux to the thin plate, and at higher values. These net flux histories correspond, as would be expected, quite well with the derivative of the plates' temperatures. If the flux is positive, the plate is increasing in temperature, and if the flux is negative the reverse is occurring.

Any attempt to compare the flux levels to these two plates should take into consideration the different histories of the plate temperatures. One very simple method of making heat flux comparisons between objects which vary in surface temperature is to compare "cold" wall fluxes.

These are computed by attempting to estimate from the actual flux and surface temperature histories what the flux to a fixed cold temperature wall would be. In this case a cold wall temperature of 278°K, and an effective overall emissivity value of 0.85 were chosen to perform these estimations. The "cold" wall heat flux is then calculated by the following equation:

$$Q_{cw} = Q_{net} + \sigma \epsilon (T_{ff}^4 - T_{cw}^4) \quad 5.1$$

Where the Q_{net} is the net heat flux to the plate given by the SODDIT code, Q_{cw} is the estimated cold wall flux, T_{ff} is the frontface temperature of the plate, and T_{cw} is the assumed 278°K cold wall temperature. The results of these calculations for the two plates of different thicknesses is plotted in Figures 5.5 and 5.6. Note that the calculated cold wall fluxes are always positive, and that the average values agree fairly well between the two plates. This calculation has been performed for a number of different items in a number of different fire tests. The average values of cold wall fluxes measured are listed in Table 5.2, and plotted in Figure 5.7.

The relationship between average cold wall flux and average flame temperature is a very difficult one to discuss from a theoretical point of view. The difficulty exists due to the strongly fluctuating nature of the flame temperature. Appendix A address part of this difficulty by investigating the difference in blackbody radiative flux due to different periodic shapes of fluctuating flame temperature. The general results indicate that as the fluctuations in the flame temperature increase, the radiative flux increases above the blackbody flux calculated from the average flame temperature.

A calculation was performed which tends to raise some questions regarding the cold wall flux calculations. Figure 5.8 shows the value of σT_f^4 ; that is the blackbody flux based on the flame temperature. The average values are given on the figure. This average value is the maximum possible radiative heat flux from the flames to any object. The problem is that these average values are slightly below average values of the calculated cold wall fluxes. A number of possibilities may account for the apparent discrepancy.

- The emissivity value of 0.85 may be too high in Equation 5.1
- The flame emittance may be less than 1.
- The convective flux may be contributing the difference.
- The flame temperatures measured may be low due to radiation errors.

Instead of trying to average the temperatures and fluxes, one can examine the transient values of the net heat flux and measured temperatures. An attempt to determine the relationship between surface temperature, flame temperature and net heat flux is detailed in Appendix B.

Another way to look at the results of the plate calorimeter is to plot the net heat flux to the plate as a function of the front face temperature. Figures 5.9 and 5.10 are these plots for the 6.35 and 19 mm thick plates, respectively.

Turning to the other side of the plate calorimeter, Figure 5.11 shows the temperature history of the 6.35 mm thick plate. The shroud temperature histories are shown as Figure 5.12, and the flame temperatures on the east side of the plate calorimeter in Figure 5.13. Again the trend of decreasing temperature with elevation is evident from these figures. The average flame temperatures are about 170°C higher on the east side of the plate. This is most likely due to

the wind predominantly blowing from the west. Table 5.1 gives the average flame temperatures measured near the various calorimeters in this test.

Looking at Figure 5.12 some high frequency noise is clearly present on the shroud temperature history at the lowest station. The origin of this noise is unknown. It did appear on four other channels : the three pool surface slug calorimeter temperatures, and the pool surface radiometer temperature.

A number of heat fluxes can be defined for the shrouded geometry involved here:

- 1.) Q_{net} - Net heat flux into the 6.35 mm plate can be calculated from the inverse code.
- 2.) $Q_{s \rightarrow p}$ - Heat flux from shroud to plate. Can be calculated from a radiation exchange equation.
- 3.) Q_{sto} - Rate of change of internal energy of the shroud.
- 4.) $Q_{f \rightarrow s}$ - Heat flux from the flame to the shroud can be estimated from the temperature difference and an effective emissivity.
- 5.) $Q_{f \rightarrow p}$ - The flux from the flame to the plate is defined as $Q_{f \rightarrow s} - Q_{sto}$.
- 6.) Q_{cw} - The cold wall heat flux to the shroud. This calculation uses $Q_{f \rightarrow s}$ and the shroud temperature.

The flux from the shroud to the 6.35 mm plate is calculated using the following equation:

$$Q_{s \rightarrow p} = \sigma (0.818) (T_s^4 - T_{ff}^4) \quad 5.2$$

This assumes a shape factor of one and that both surfaces have an emissivity of 0.90. It should be noted here that the emissivities of protected interior surfaces painted with Pyromark™ are assumed to be 0.90, and the exterior surfaces 0.85, throughout this report. The flux from the flame to the shroud was initially calculated using the equation:

$$Q_{f \rightarrow s} = \sigma (0.85) (T_f^4 - T_s^4) \quad 5.3$$

The strong fluctuations in the flame temperature generated high frequency components in the flux calculated in this way. In order to decrease the fluctuations in this quantity, the flame temperature was smoothed prior to the calculation of $Q_{f \rightarrow s}$. The smoothing was done by the following simple method (Simpsons rule) :

$$T_{fs}(\tau) = [T_f(\tau-10 \text{ sec}) + 4 T_f(\tau-5) + 6 T_f(\tau) + 4 T_f(\tau+5) + T_f(\tau+10)] / 16$$

In the calculation of energy storage in the shroud, the equation used was:

$$Q_{sto} = \rho c_p dx dT/d\tau \quad 5.4$$

where dx is the thickness of the shroud, ρ is the density of the shroud material, and c_p is the specific heat of the shroud. The value of $dT/d\tau$ was found by first smoothing the shroud temperature as the flame temperature was smoothed, then taking temperature differences divided by time intervals. Figures 5.14 thru 5.17 gives a comparison of several of the fluxes.

A cold wall flux can also be calculated for the shrouded side of the calorimeter. This Q_{cw} is given by :

$$Q_{cw} = \sigma (0.85) (T_s^4 - T_{cw}^4) + Q_{f \rightarrow s} \quad 5.5$$

Figure 5.18 shows the history and average values of this quantity.

TABLE 5.1 Average Temperatures Near Calorimeters

Measurement Location	Height from Floor [m]	Average [°C]	Std Dev [°C]	Flame Present [°C]
West Side of Plate	4.11	679	286	984
	3.30	737	249	997
	2.49	810	219	1003
	1.68	892	131	908
East Side of Plate	4.11	859	216	1090
	3.30	912	193	1072
	2.49	1012	145	1051
	1.68	1043	84	937
East Shroud	4.11	843	110	
	3.30	896	100	
	2.49	993	86	
	1.68	1027	102	
Around Large Cylinder	Top	459	149	718
	East	963	105	810
	Bottom	926	93	992
	West	696	145	872
Shroud Around Cyl	Top	401	126	
	East	835	84	
	Bottom	--	--	
	West	669	105	

TABLE 5.2
Relationships Between Average Cold Wall Flux
and Average Flame Temperatures for a Variety of Tests and Objects

Test Name	Location	σ_t [°C]	T_{fl} [°C]	Q [Kw/m ²]
DOT Test A	Bottom	118	912	110.1
Large Cylinder	South	242	765	78.8
	Top	228	679	61.5
	North	124	871	89.9
	Bottom	88	918	113.6
DOT Test B	South	184	746	66.3
Large Cylinder	Top	227	595	55.1
	North	109	958	101.1
	Bottom	117	937	115.5
DOT Test C	South	178	778	67.7
Large Cylinder	Top	218	680	64.4
	North	137	952	105.6
	Bottom	149	459	31.1
N-WINTER Test Large Cylinder	East	105	963	90.7
	Bottom	93	926	126.7
	West	145	696	61.7
	Top	149	459	31.1
TRUPACT I Test 1 6.35 mm Plate	4.93	303	846	110.8
	4.62	294	855	112.6
	4.32	275	886	116.0
	4.01	262	902	122.7
	3.10	198	964	137.8
	2.49	149	1003	146.9
	4.11	286	679	96.0
N-WINTER 19 mm Plate	3.30	249	737	97.2
	2.49	219	810	117.2
	1.68	131	892	133.9
	4.11	286	679	89.1
N-WINTER 6.35 mm Plate	3.30	249	737	92.6
	2.49	219	810	110.9
	1.68	131	892	132.8
	4.11	286	679	89.1
N-WINTER Shrouded Plate	3.30	193	912	107.2
	2.49	145	1012	138.4
	1.68	84	1043	146.9
	4.11	216	859	93.7

TABLE 5.2 (continued)
Relationships Between Average Cold Wall Flux
and Average Flame Temperatures for a Variety of Tests and Objects

Test Name	Location	σ_i [°C]	T_f [°C]	Q [Kw/m ²]
N-Winter Test 10 cm cal (east)	Top	**	**	123.8
	South	**	**	118.2
	Bottom	**	**	138.0
	North	**	**	144.7
N-winter 10 cm cal (west)	Top	**	**	149.9
	South	**	**	139.5
	Bottom	**	**	144.6
	North	**	**	156.2

** No thermocouple at this location.

NUCLEAR WINTER FIRE TEST BACKFACE OF WEST 6.35 MM PLATE

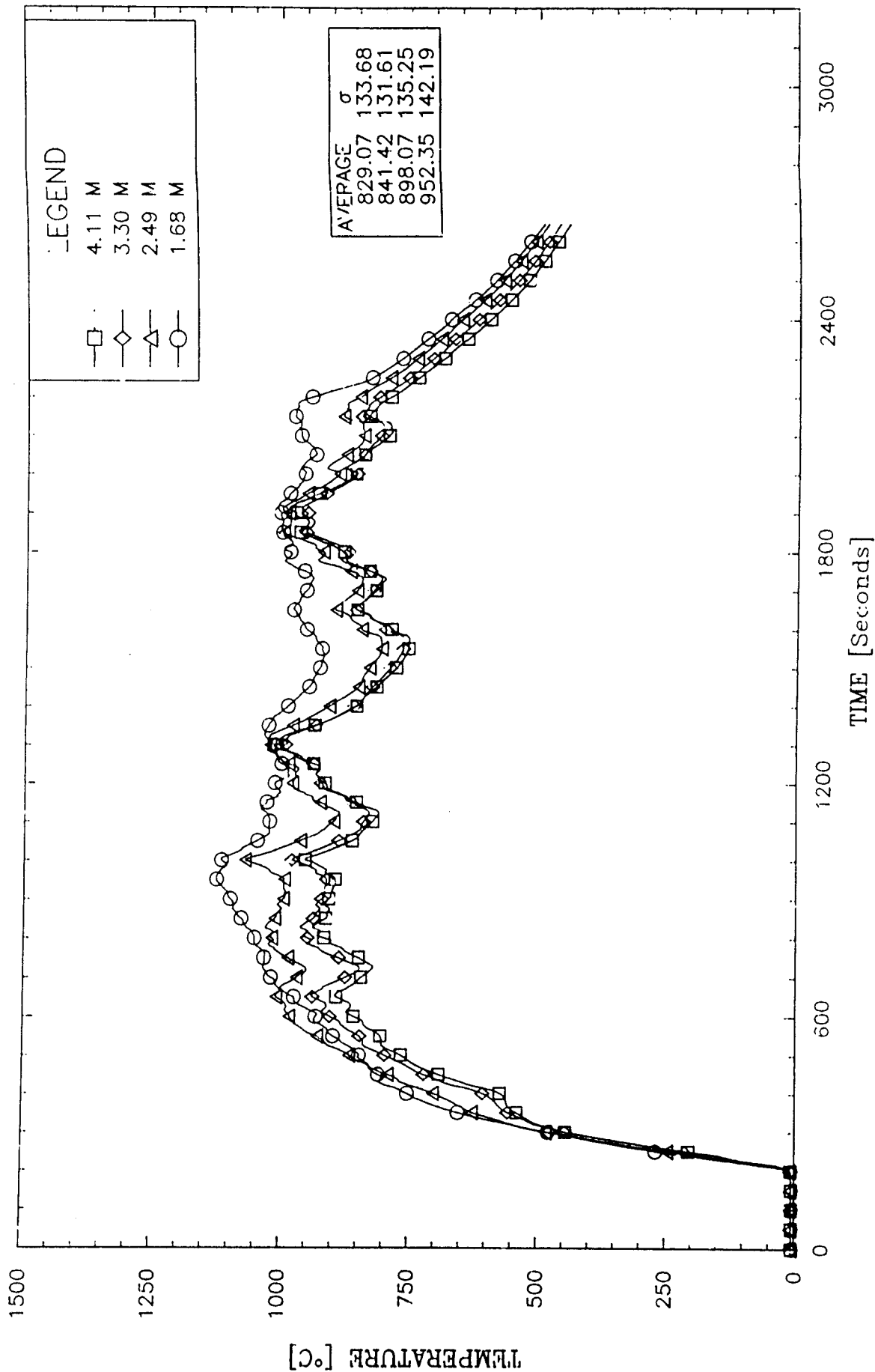


Figure 5.1 Backface Temperature on West 6.35 mm Plate Calorimeter

NUCLEAR WINTER FIRE TEST BACKFACE OF WEST 19 MM PLATE

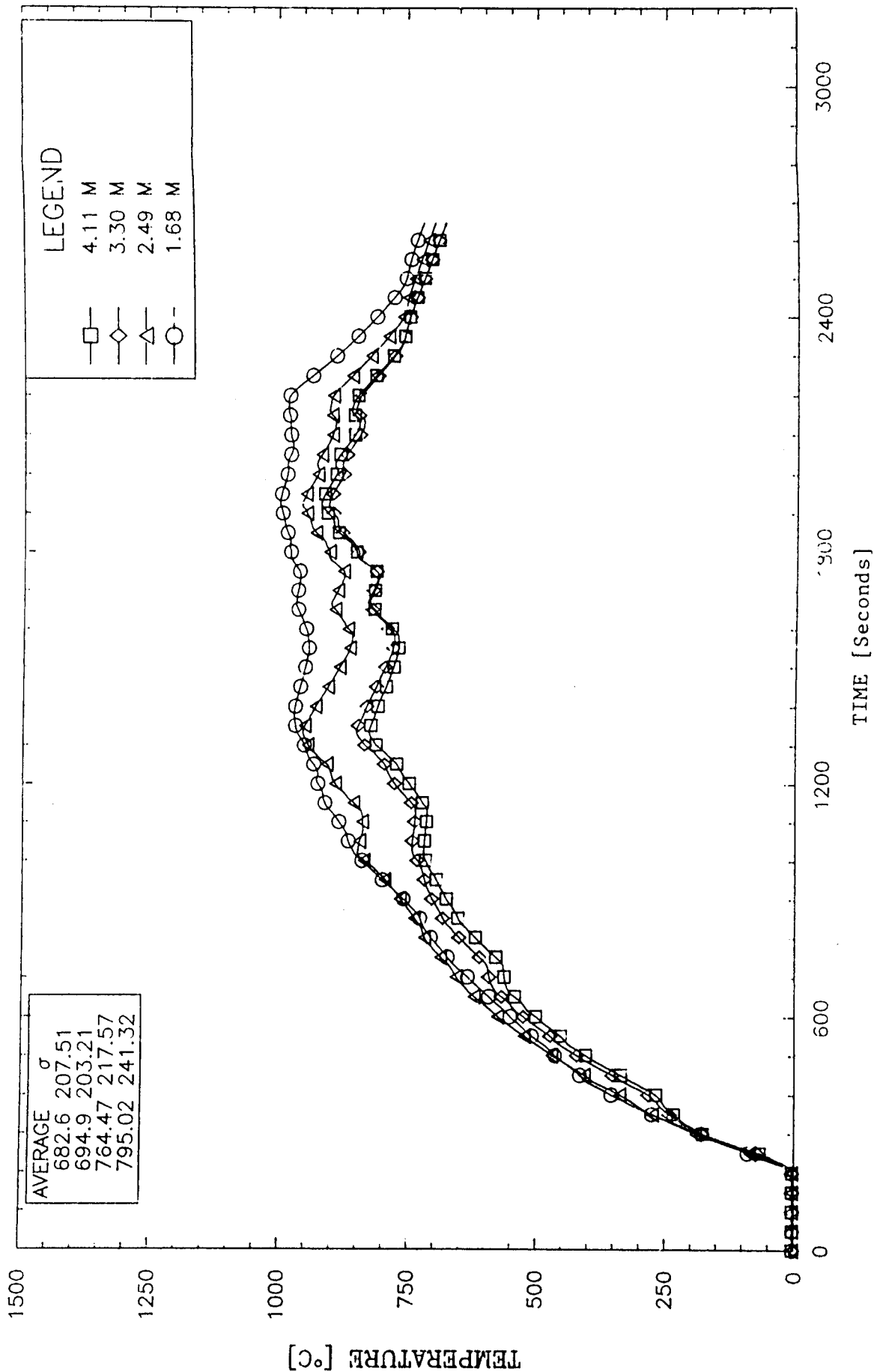


Figure 5.2 Backface Temperature on West 19 mm Plate Calorimeter

NUCLEAR WINTER FIRE TEST FLAME TEMPS - WEST SIDE OF PLATE

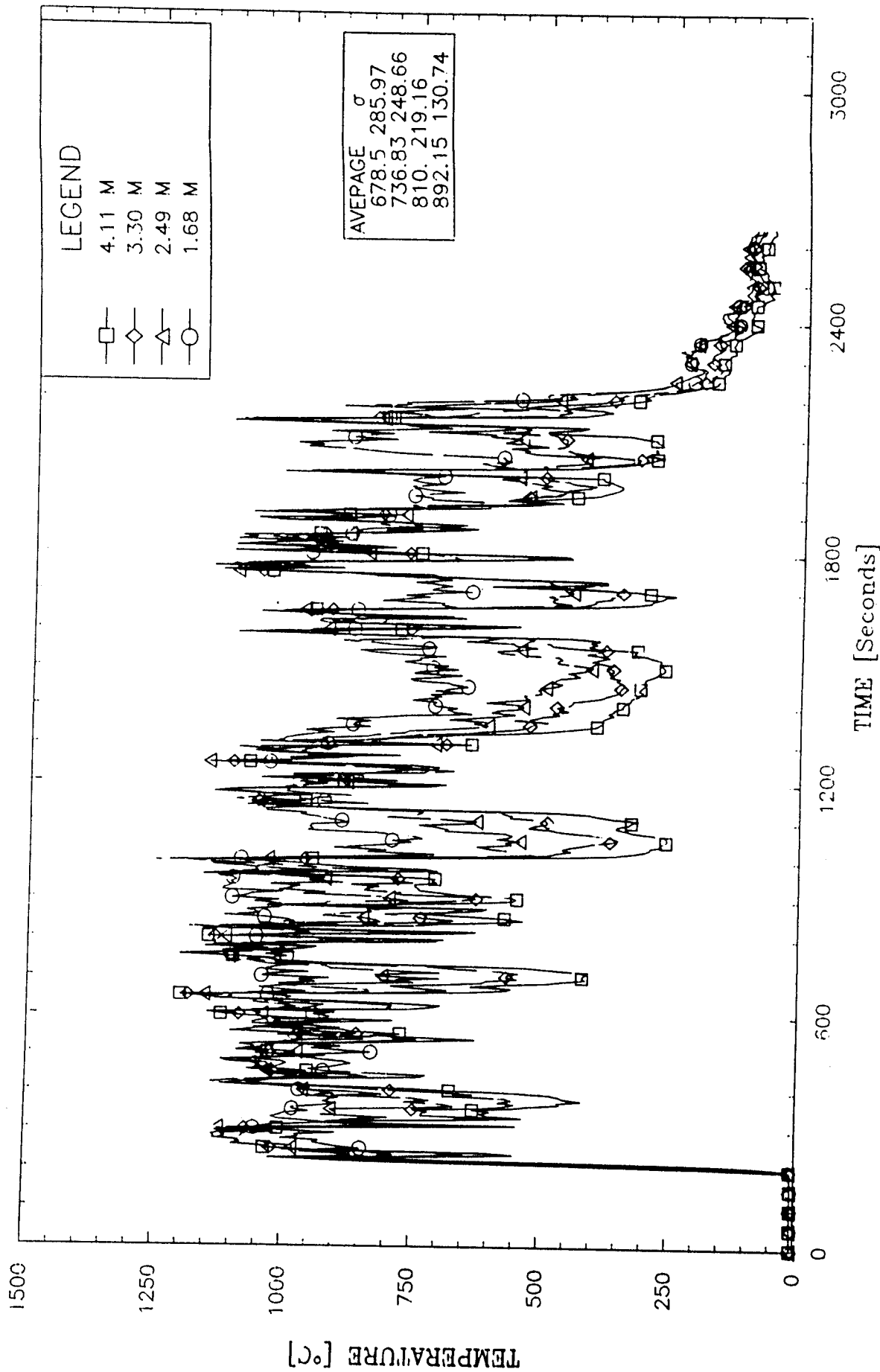
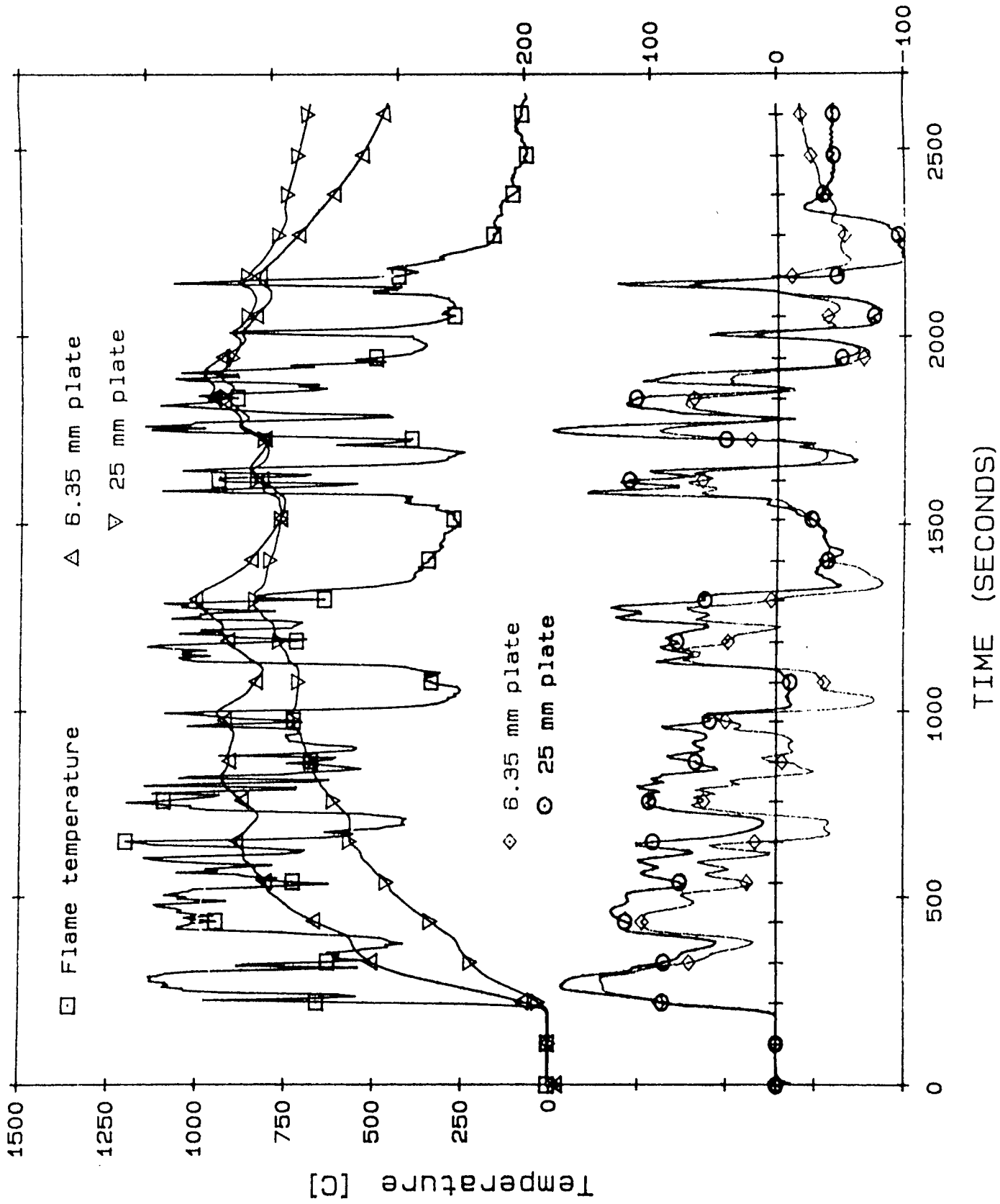


Figure 5.3 Flame Temperatures on West Side of Plate Calorimeter

FIGURE 5.4 - Fluxes and Temperatures: West 4.11 Meter station



NUCLEAR WINTER FIRE TEST
WEST 6.35 MM PLATE - COLD WALL FLUX

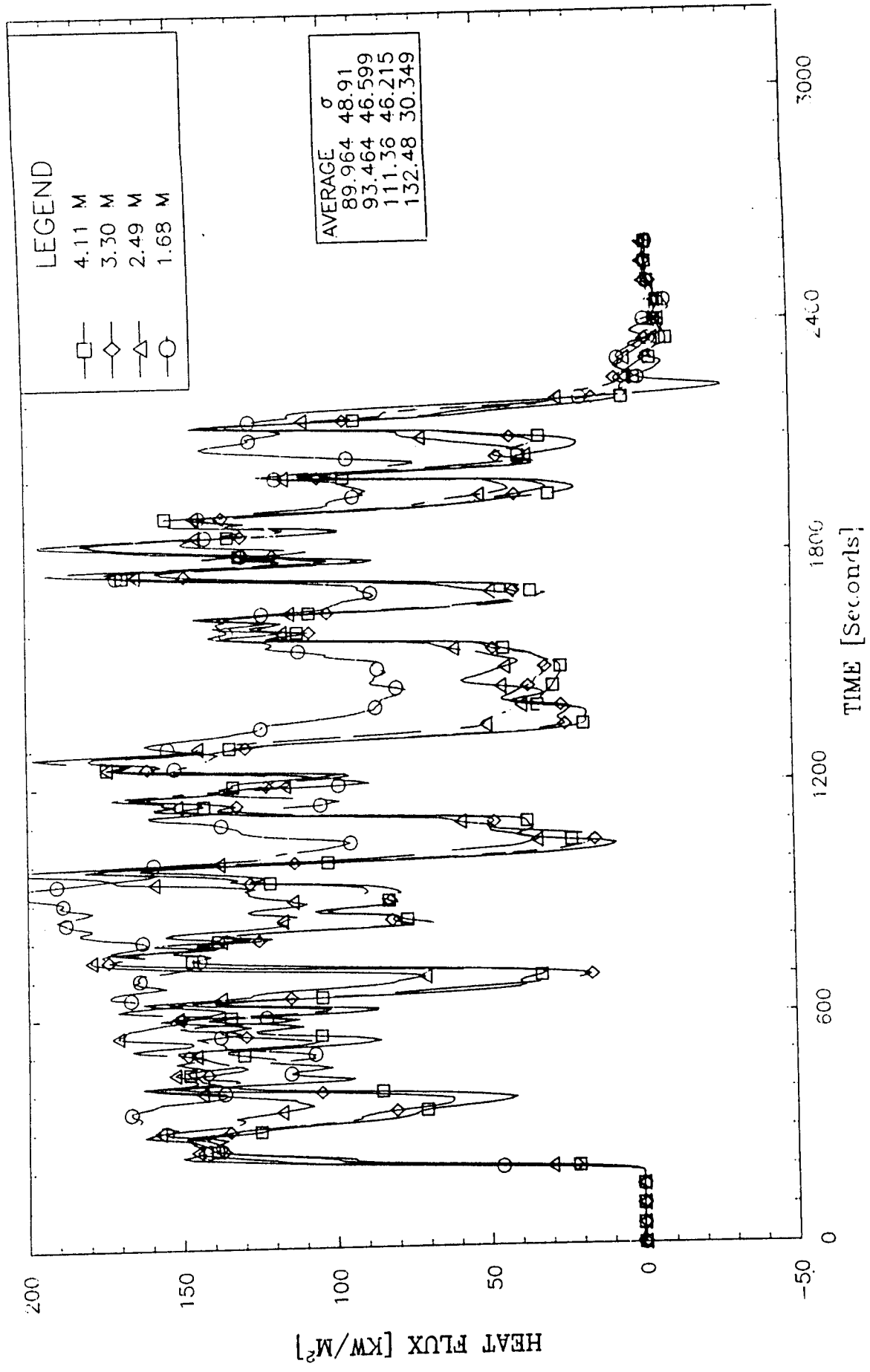


Figure 5.5 Cold Wall Heat Flux to West 6.35 mm Plate Calorimeter

NUCLEAR WINTER FIRE TEST
WEST 19 MM PLATE - COLD WALL FLUX

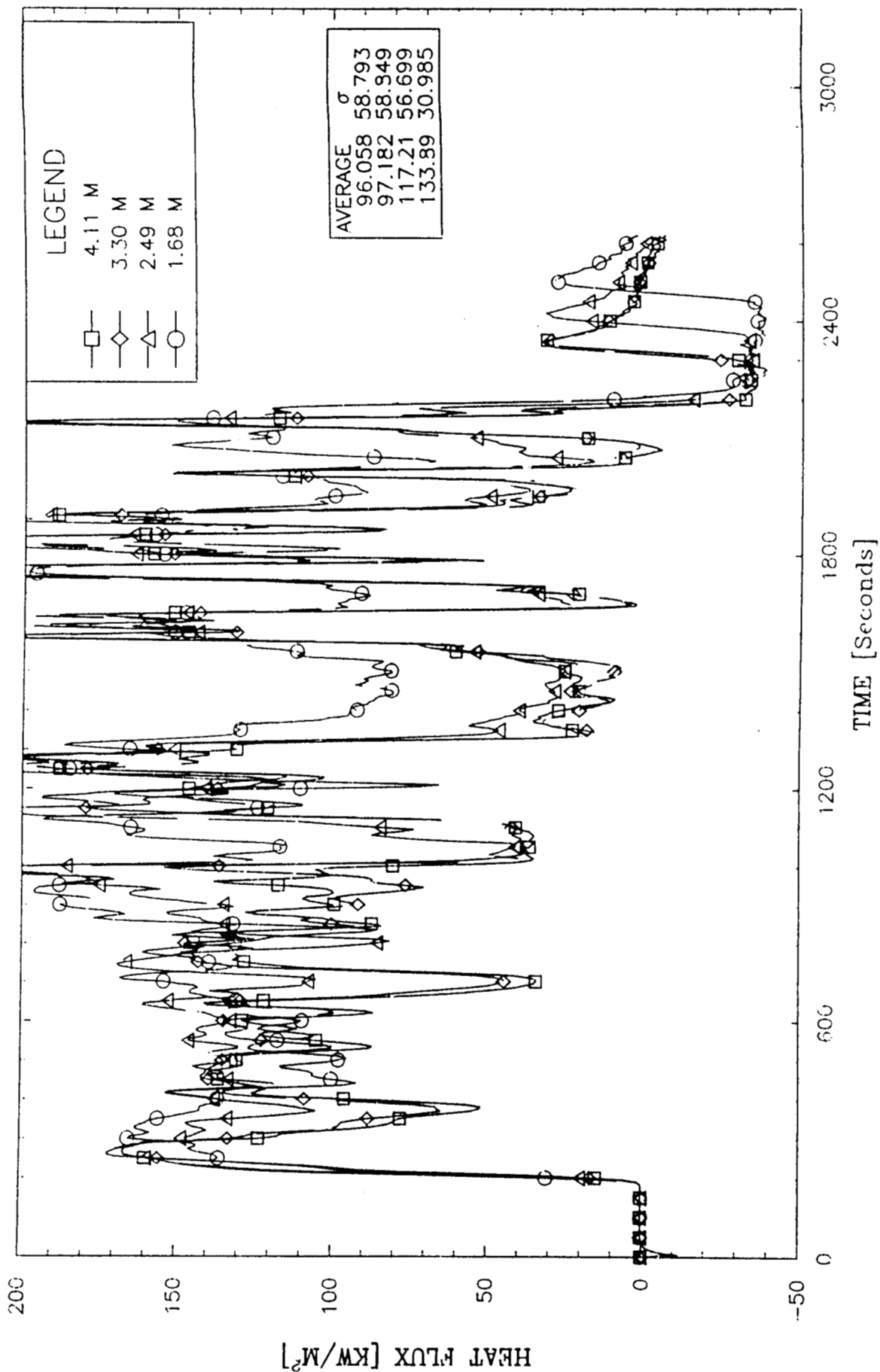


Figure 5.6 Cold Wall Heat Flux to West 19 mm Plate Calorimeter

HEAT FLUX vs FLAME TEMPERATURE

(AVERAGE VALUES)

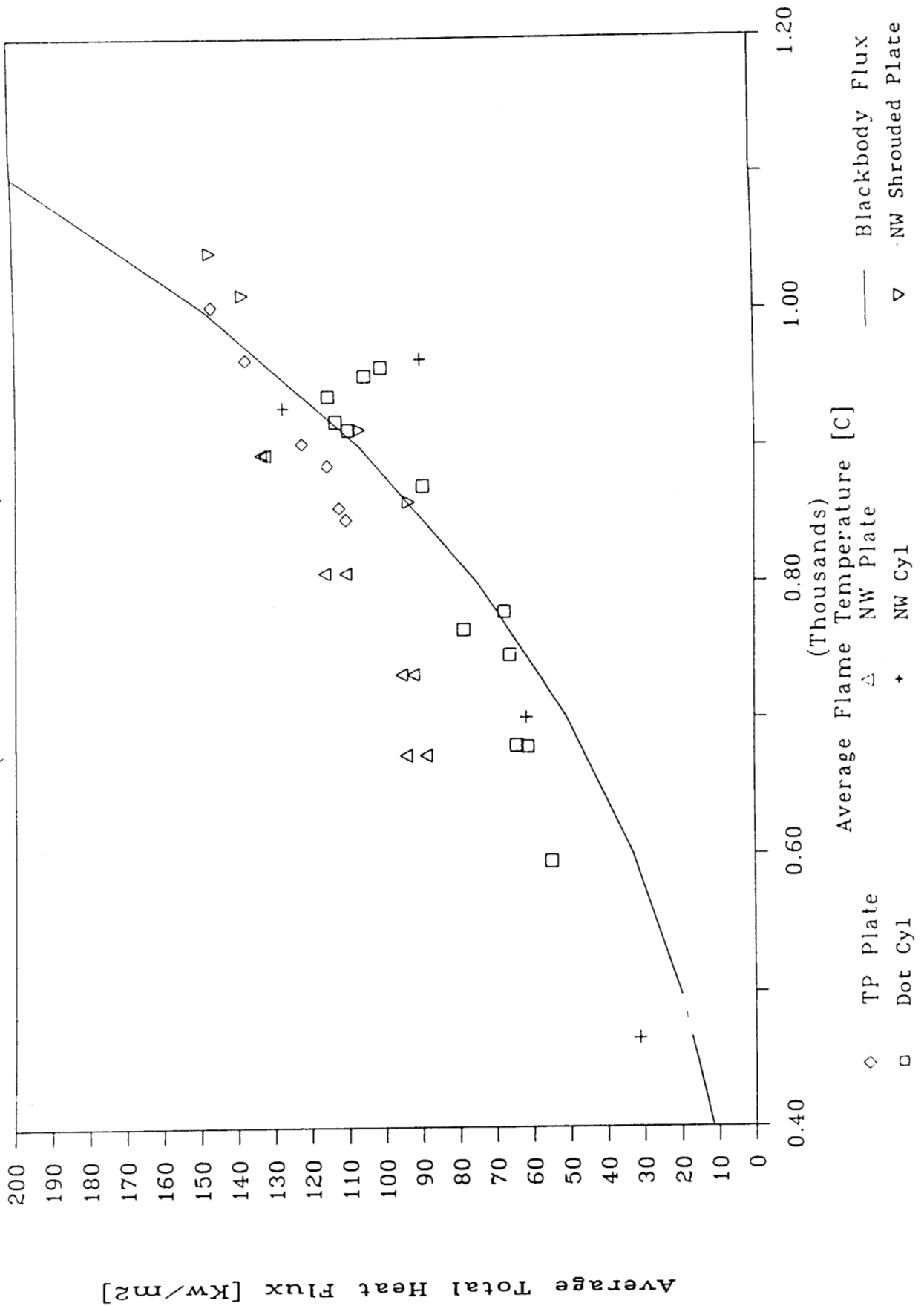


Figure 5.7 Average Cold Wall Flux vs Average Flame Temperature

NUCLEAR WINTER FIRE TEST
WEST FLAME TEMPS - BLACKBODY FLUXES

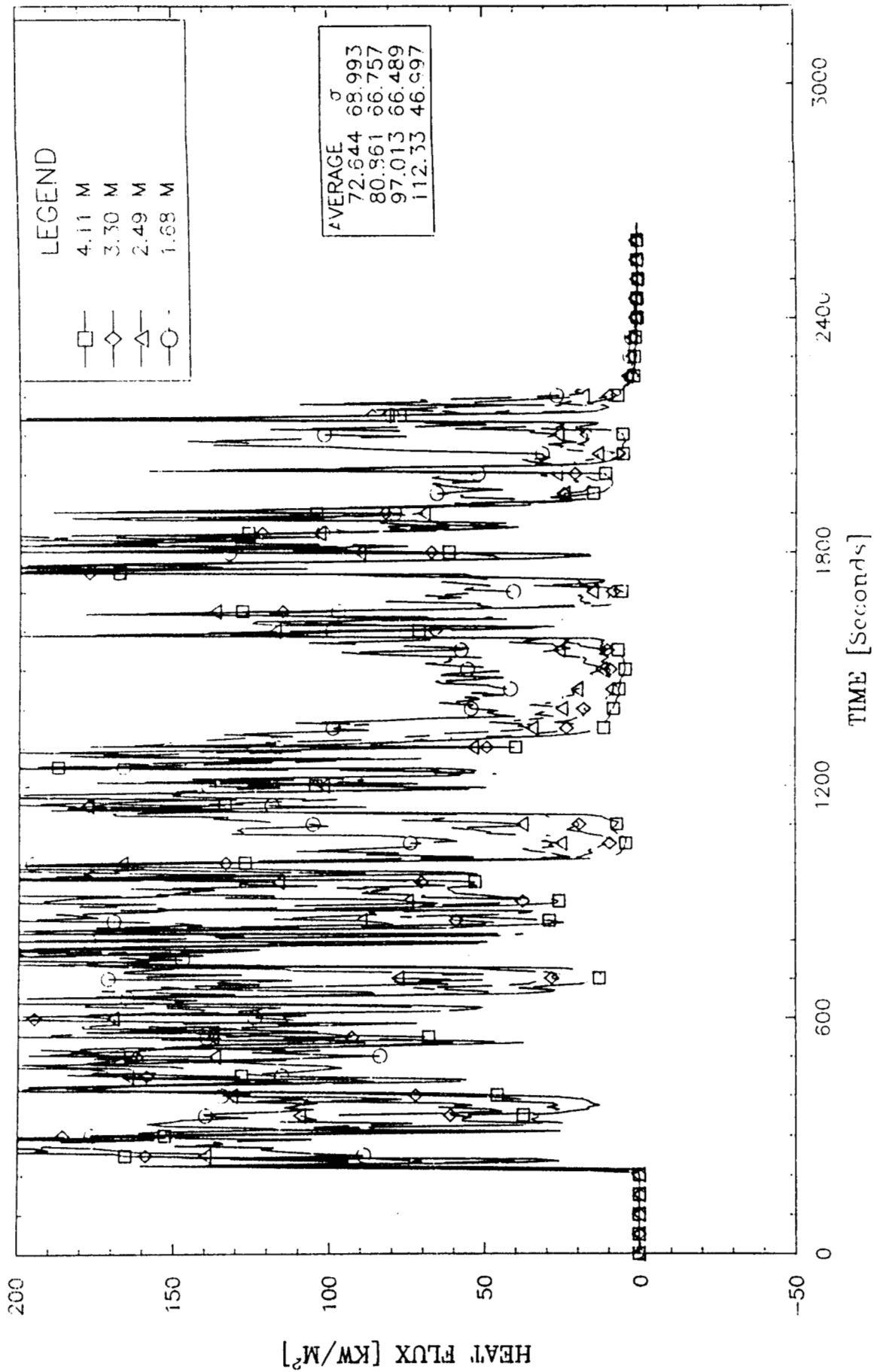


Figure 5.8 Blackbody Fluxes Calculated From Flame Temperatures

NUCLEAR WINTER FIRE TEST
WEST 6.35 MM PLATE - FLUX VS TEMPERATURE

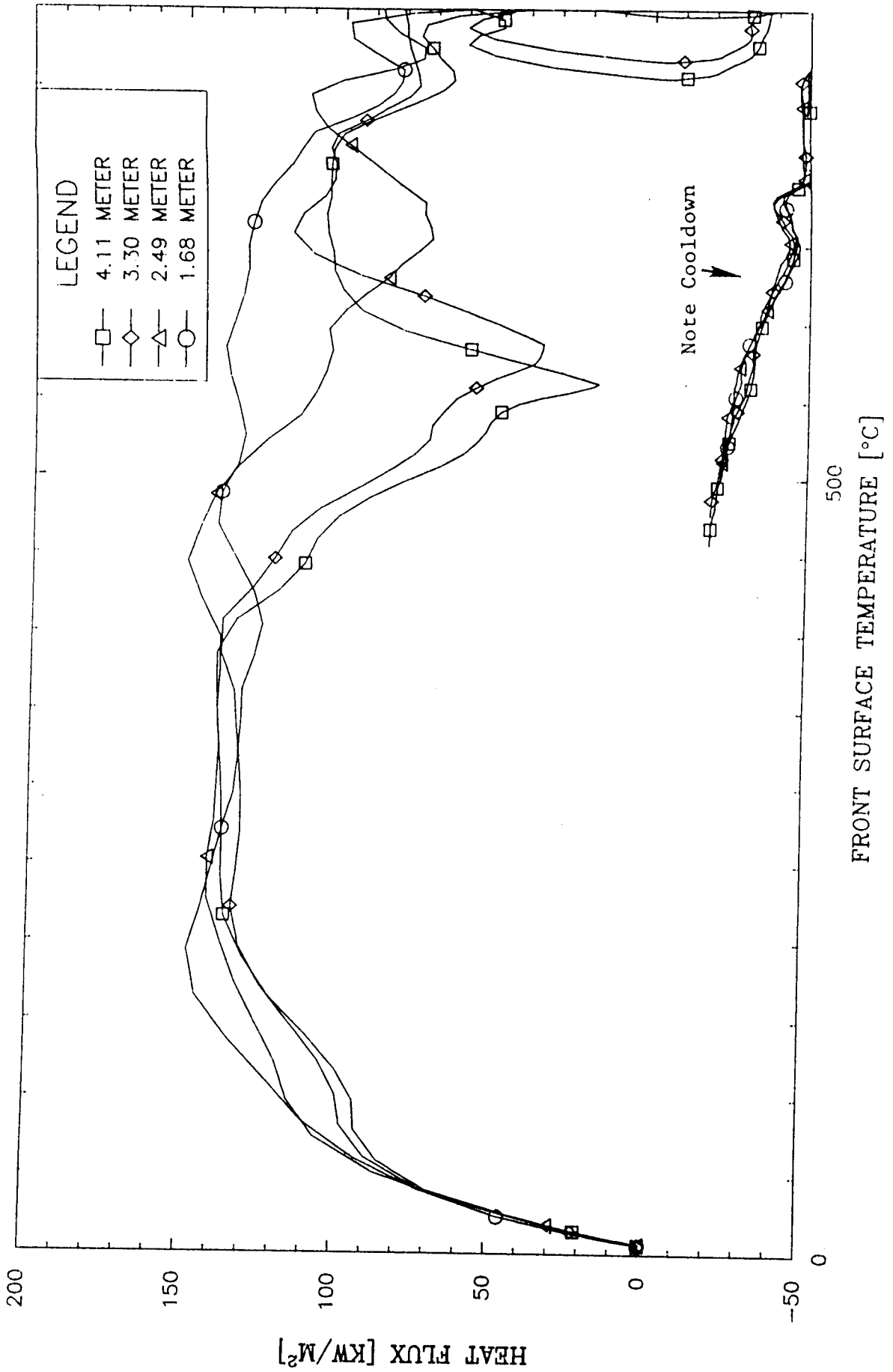
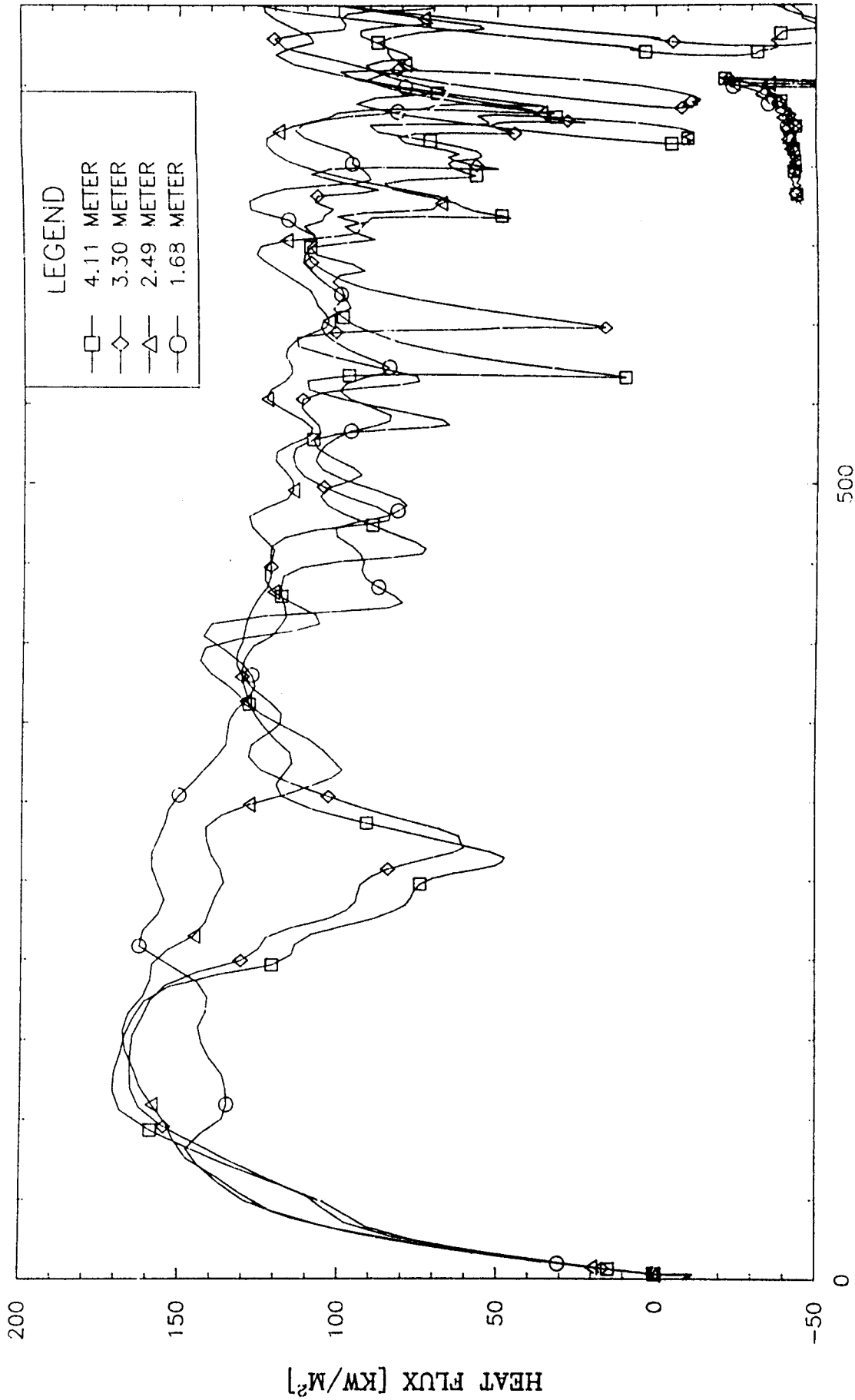


Figure 5.9 Flux vs Surface Temperature West 6.35 mm Plate

NUCLEAR WINTER FIRE TEST
WEST 19 MM PLATE - FLUX VS TEMPERATURE



FRONT SURFACE TEMPERATURE [°C]

500

0

-50

HEAT FLUX [KW/M²]

200

150

100

50

0

-50

Figure 5.10 Flux vs Surface Temperature West 19 mm Plate

NUCLEAR WINTER FIRE TEST BACKFACE OF EAST 6.35 MM PLATE

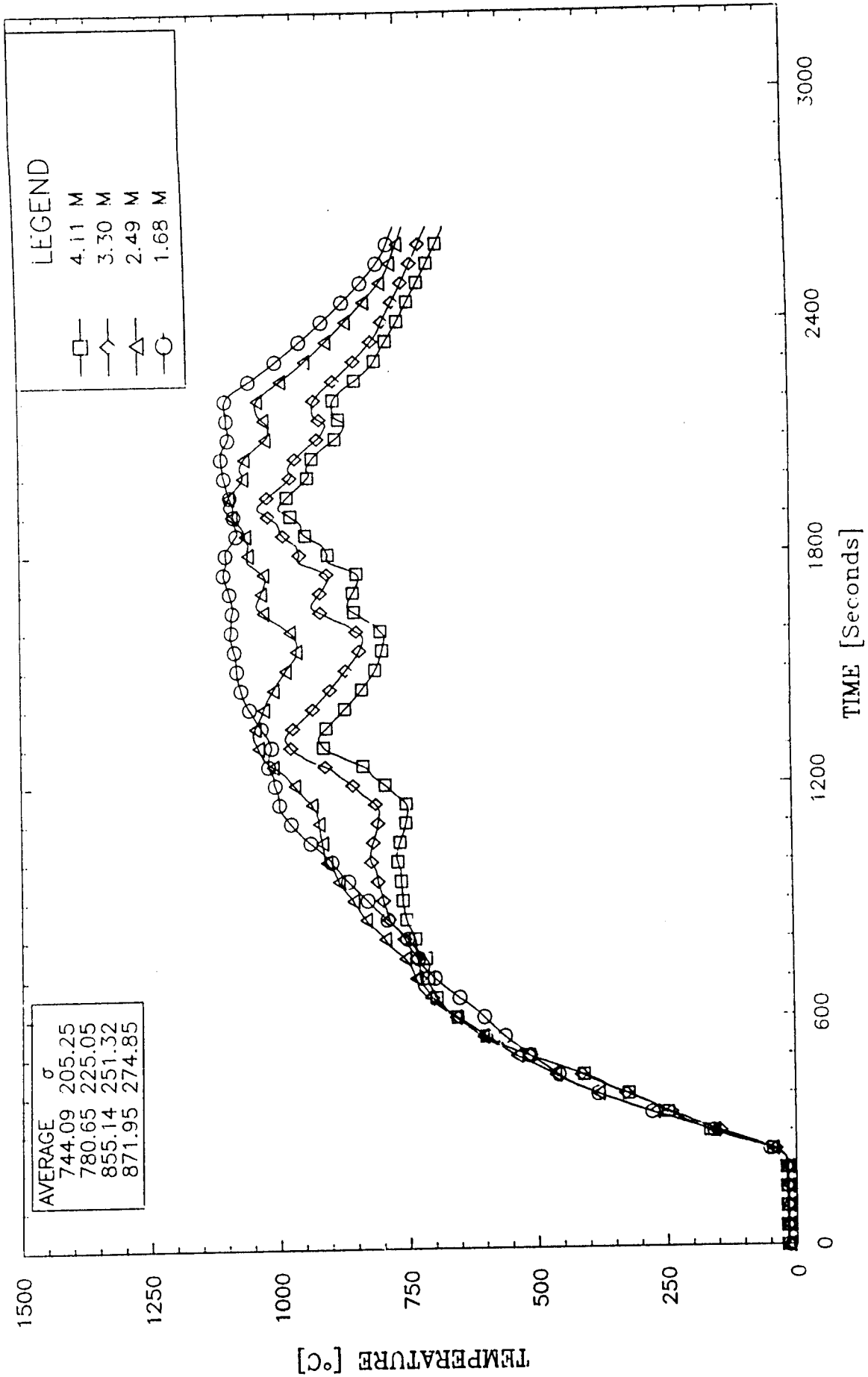


Figure 5.11 Backface Temperature of East 6.35 mm Plate Calorimeter

NUCLEAR WINTER FIRE TEST TEMPERATURE OF EAST SHROUD

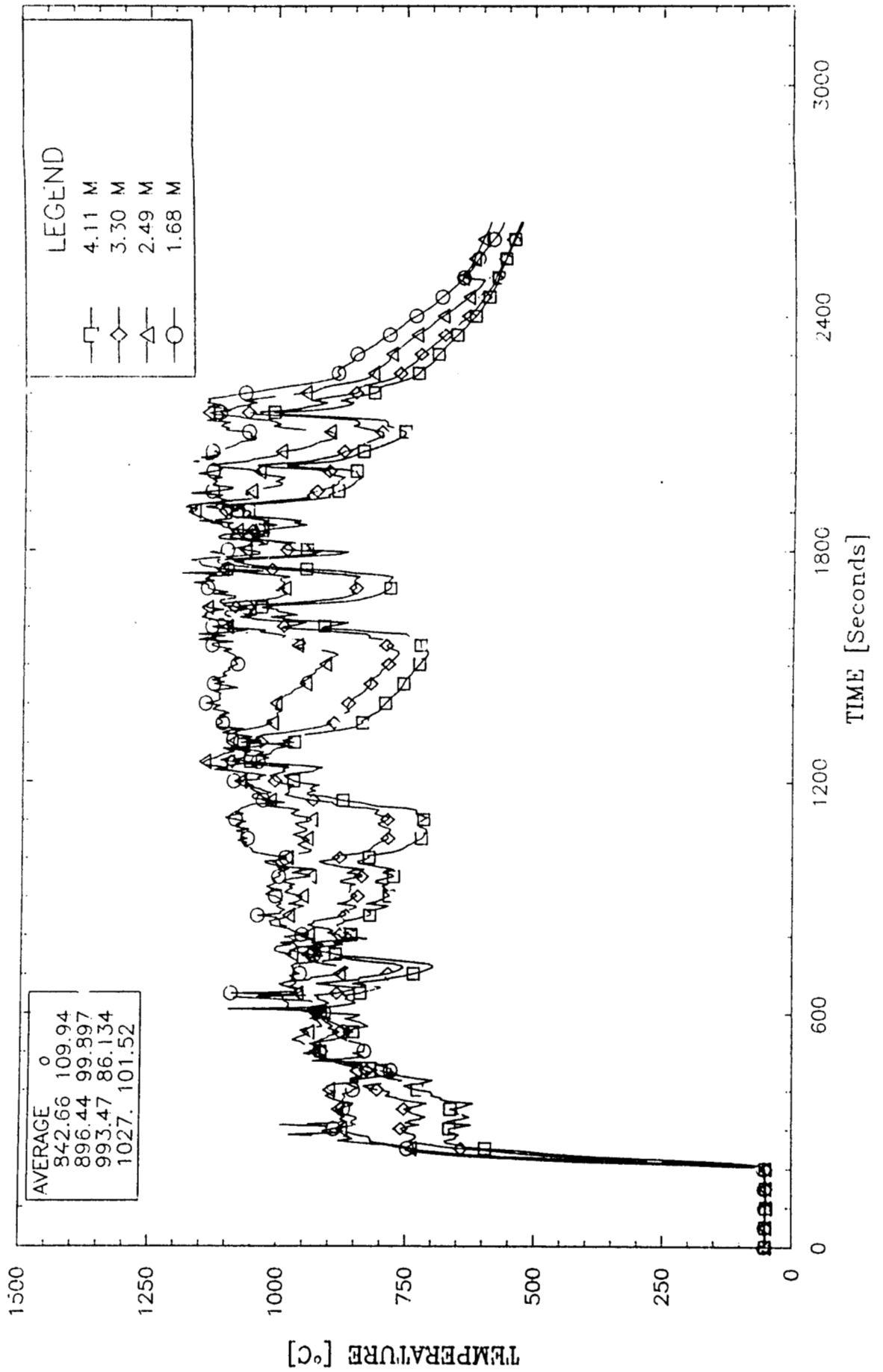


Figure 5.12 Temperature of East Shroud

NUCLEAR WINTER FIRE TEST
 FLAME TEMPS - EAST SIDE OF PLATE

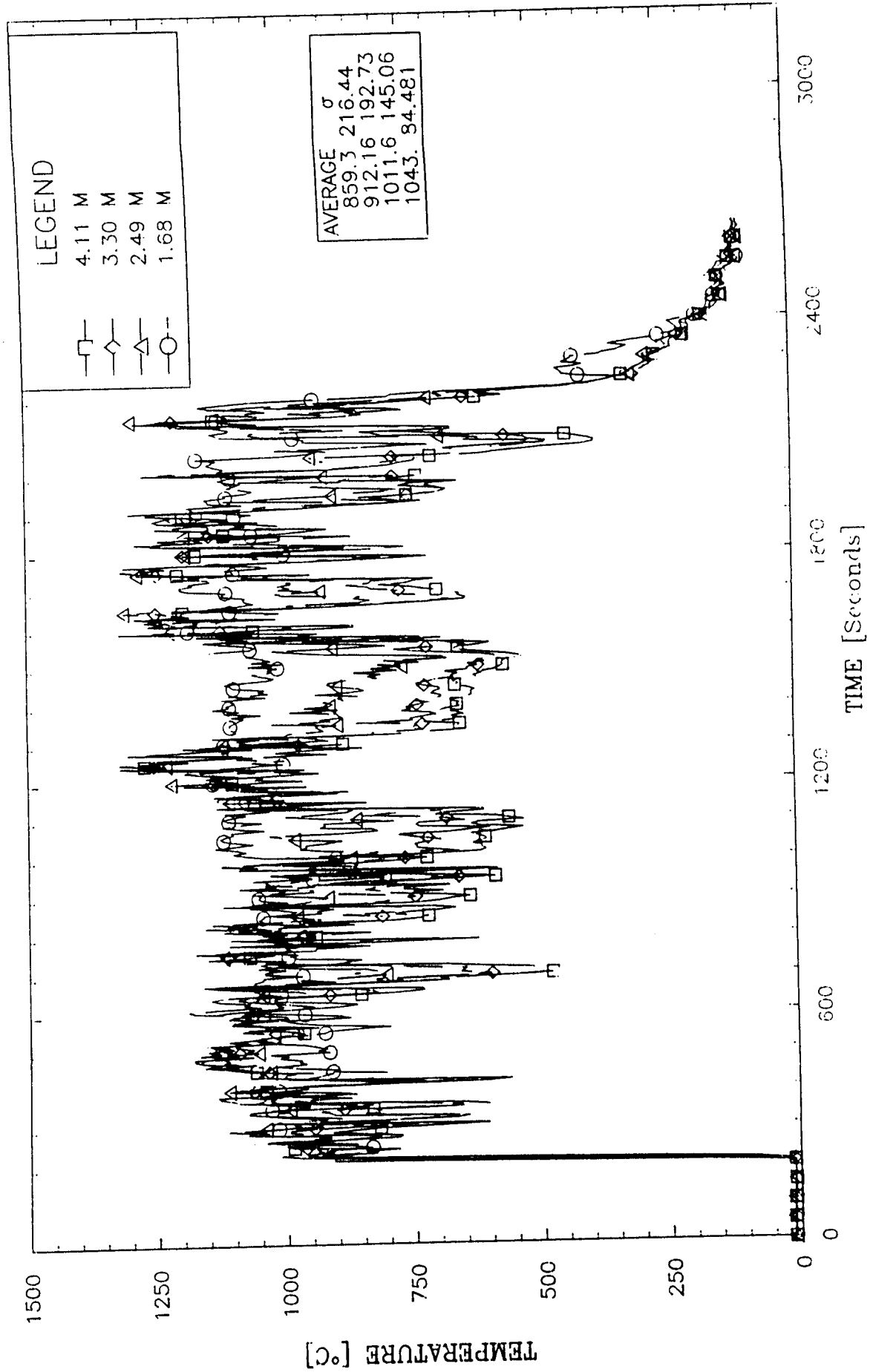


Figure 5.13 Flame Temperature on East Side of Plate Calorimeter

NUCLEAR WINTER FIRE TEST
FLUX COMPARISON - 4.11 METER STATION

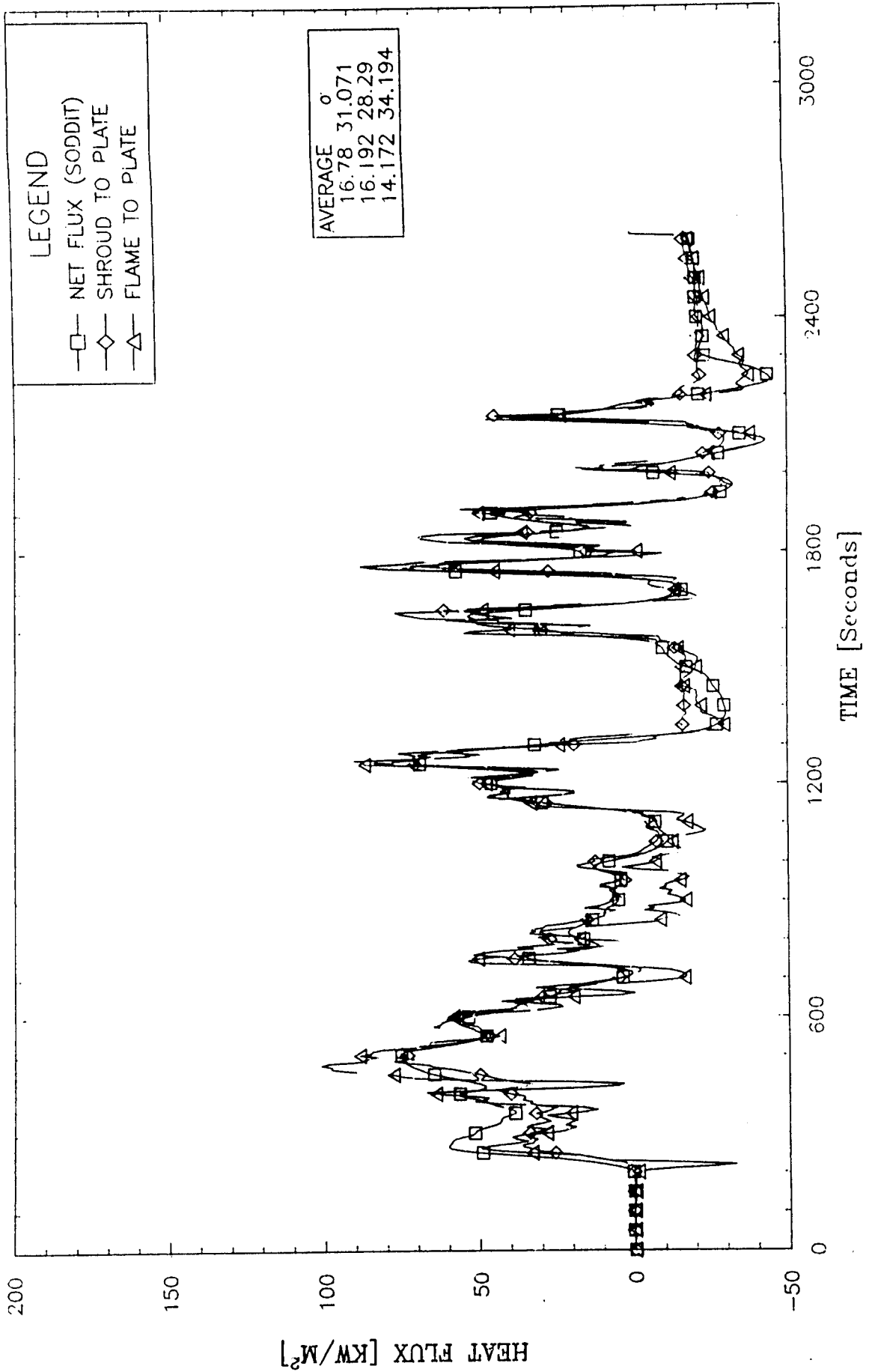


Figure 5.14 Comparison Between Three Heat Flux Calculations - 4.11 m Station

NUCLEAR WINTER FIRE TEST FLUX COMPARISON - 3.30 METER STATION

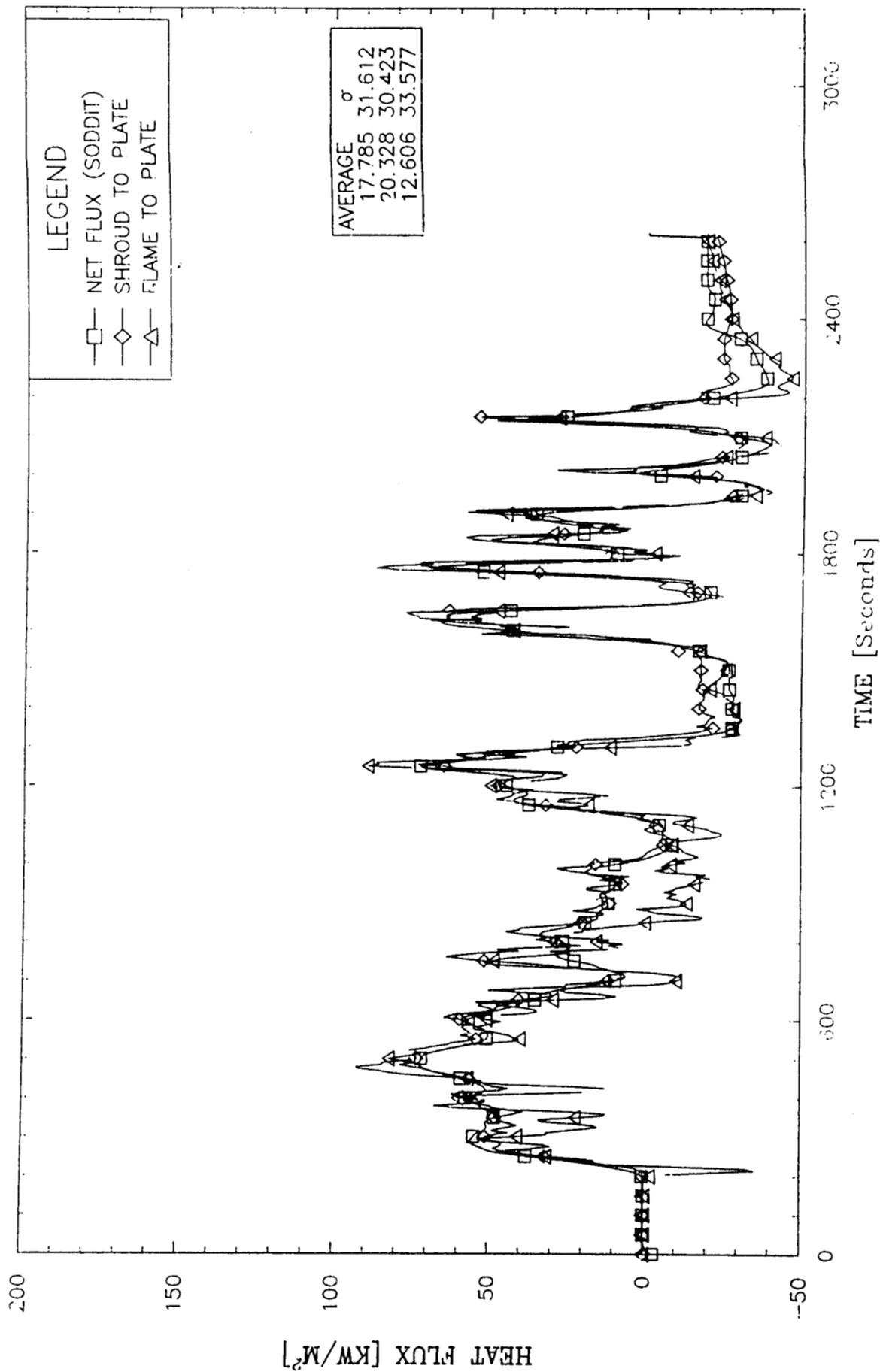


Figure 5.15 Comparison Between Three Heat Flux Calculations - 3.30 m Station

NUCLEAR WINTER FIRE TEST FLUX COMPARISON - 2.49 METER STATION

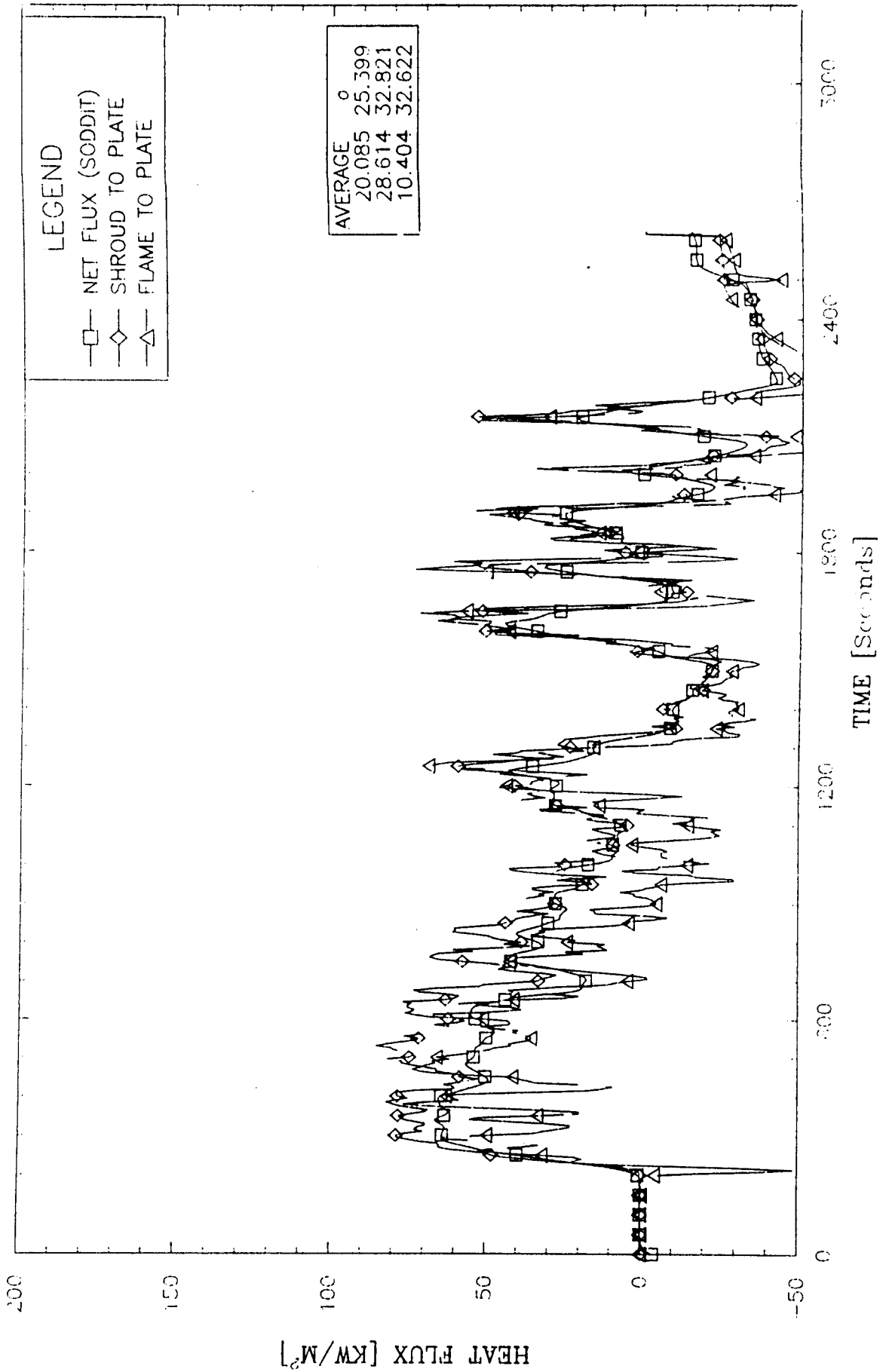


Figure 5.16 Comparison Between Three Heat Flux Calculations - 2.49 m Station

NUCLEAR WINTER FIRE TEST FLUX COMPARISON - 1.68 METER STATION

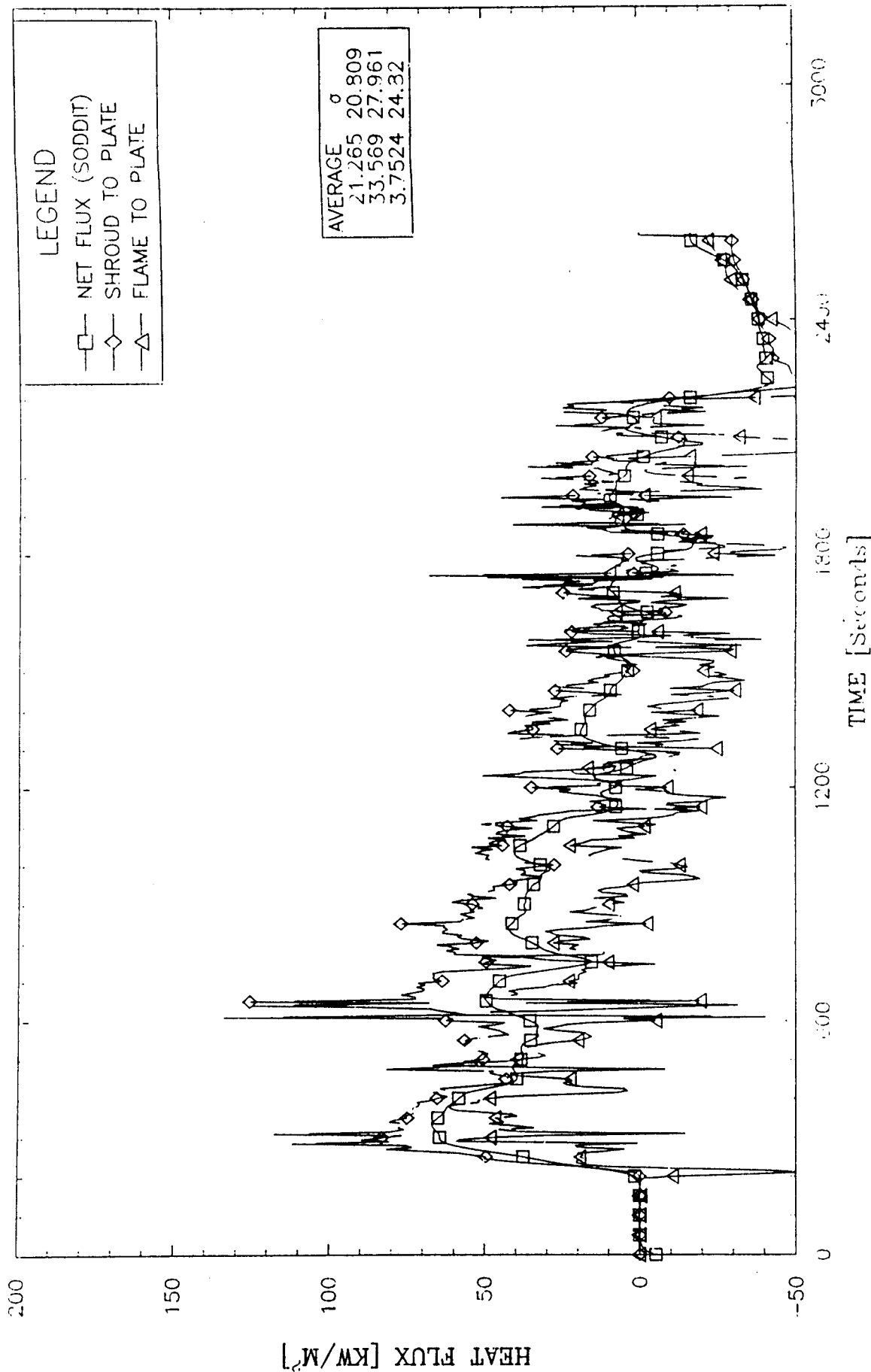


Figure 5.17 Comparison Between Three Heat Flux Calculations - 1.68 m Station

NUCLEAR WINTER FIRE TEST
EAST PLATE - COLD WALL FLUX TO SHROUD

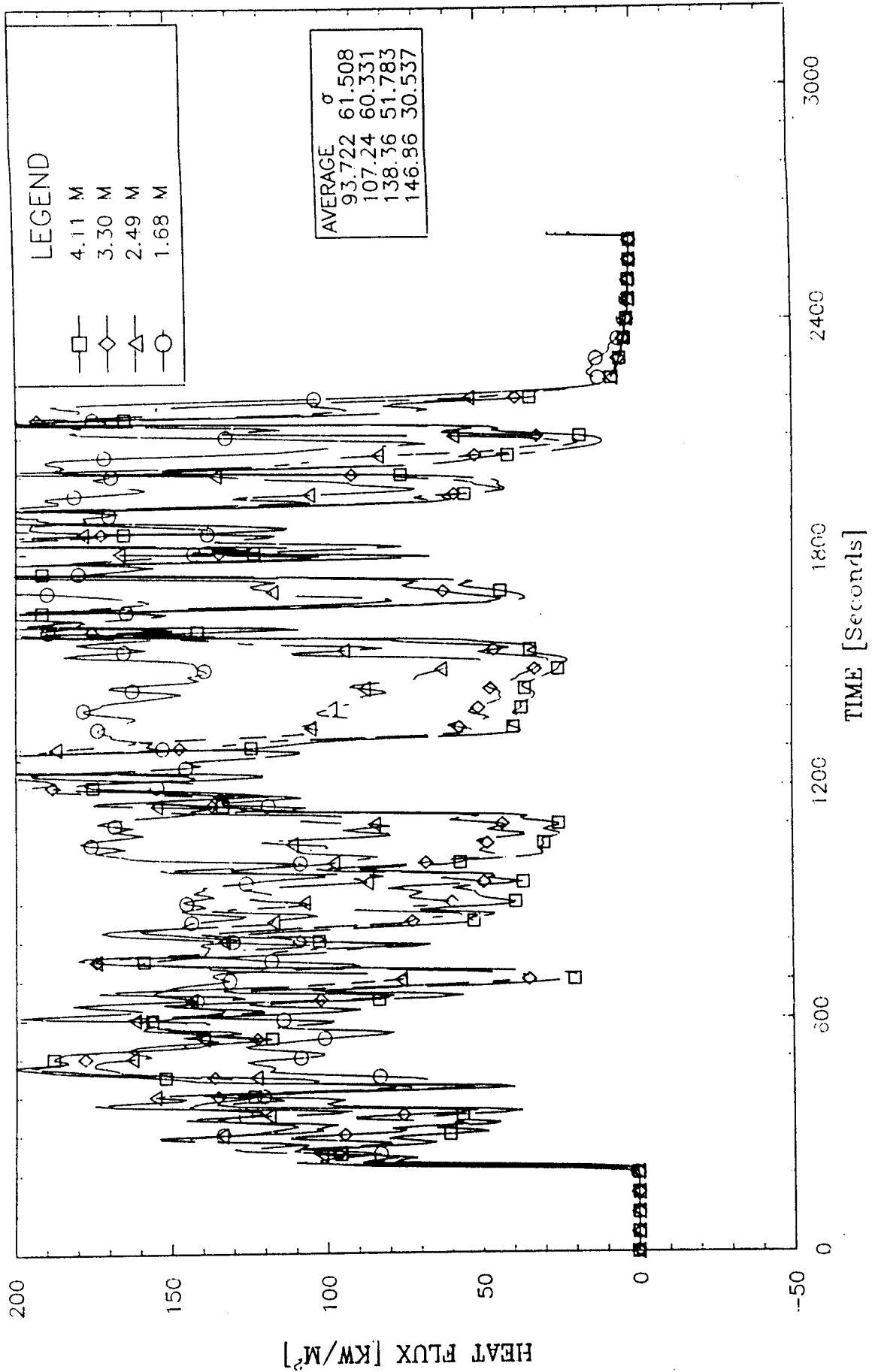


Figure 5.18 Cold Wall Heat Flux to shroud

VI. HEAT FLUX TO LARGE CYLINDRICAL CALORIMETER

A description of the large cylindrical calorimeter was included in Section II. Measurements of temperature were made in the flames near the calorimeter surface, at the exposed surface, at the steel backface/insulation interface, and 2.54 cm into the insulation, on the north end of the calorimeter. Transpiration radiometers were also included on the north end in an effort to measure the radiative component of the heat flux. The south end was covered with a thin steel shroud. The south end had thermocouples on the inner surface of the shroud, and on the steel backface/insulation interface. The data from the unshrouded north end of the calorimeter will be discussed first.

Figure 6.1 shows the steel backface temperature histories measured at the four angular stations. The predominant winds were from the west and south during this test so it is not surprising to find the highest temperatures on the east and bottom of the calorimeter. The wind frequently caused the top and west side of the calorimeter to be exposed. The flame temperatures near the calorimeter, Figure 6.2, show similar trends. The maximum average temperatures being measured on the lower and east sides of the calorimeter. Figure 6.3 shows the measured surface temperatures on the north end of the calorimeter. These surface temperature measurements were made with Nanmac thermocouples. Again the highest temperatures were recorded on the bottom of the calorimeter. The surface measured temperatures are slightly above the measured backface temperatures during the test and drop below the backface temperatures during the post-test cool down period. This makes sense as the heat flux is into the calorimeter during the test and reverses when the fire stops. The temperature was also measured in the insulation 2.54 cm inside the steel backface. These temperatures show the same trends as all other measurements, see Figure 6.4.

The shrouded south end of the calorimeter had thermocouples on the backface of the thick steel wall, and on the inner surface of the thin steel shroud. Figure 6.5 indicates the backface temperature history. Comparing this figure with the corresponding one on the north end (Figure 6.1) reveals similar trends with lower temperatures overall on the south end. The lower temperatures indicate that the heat flux into the thick steel calorimeter is less on the shrouded end than on the exposed end. This is the expected result because the shroud is a radiation shield. The shroud temperature histories are plotted in Figure 6.6. The thermocouple on the bottom surface was damaged prior to the test so results on the lower surface are unfortunately not available. The three temperatures which are plotted indicate the expected trend. The upcoming discussion will indicate that the data on the west side of the shroud are not reasonable after $t=1200$ seconds. It is interesting to compare the average temperature of the shroud to average flame temperatures:

Station	<u>South Shroud</u>		<u>North Flames</u>	
	Average Temperature [°C]	σ_t	Average Temperature[°C]	σ_t
East	835	84	963	105
West	669	105	696	145
Top	401	126	459	150

The average temperatures are fairly close, with the flames slightly above the shroud as expected. The fluctuations in the flame temperatures are much higher than the fluctuations in the shroud temperatures.

The transpiration radiometers all failed in this test so no results have been included from these devices in this report.

From the available data a number of analyses can be performed.

1.) Net heat flux into the thick steel walls can be estimated from the backface temperature histories for both the shrouded and unshrouded ends.

2.) The Nanmac measurements can be compared with surface temperature estimates from inverse codes.

3.) Cold wall fluxes can be estimated by adding a constant times the estimated surface temperature raised to the fourth power.

4.) Heat flux into the shrouded thick wall can also be estimated from the estimated thick wall surface temperature and the known shroud temperature. All surfaces were painted with Pyromarktm paint prior to testing in order to insure known emissivity values.

Examining the unshrouded north end of the calorimeter first, Figure 6.7 shows the net heat flux to the calorimeter as a function of the surface temperature. This method of plotting allows comparisons to be made between objects of differing thermal massiveness. It also allows comparisons to be made with the results of previous tests. The cold wall flux was also calculated by the method described in the previous section (Eqn 5.1). Figure 6.8 shows the time history of this cold wall flux. The average values are included on the Figure, and also in the table 5.2.

Table 6.1 was prepared to allow comparisons to be made directly between the DOT calorimeter tests and the current results. This table gives values of the integrated net heat flux into the calorimeter at 30 minutes after ignition of the fire. The values given for the DOT tests are averages over three axial stations and three tests. The DOT tests used calorimeters of the same material and physical dimensions as the current test. The calorimeters in these tests, however, were positioned with their axes in the east/west direction. Since the wind comes from the west and south a reasonable agreement would be expected between the west station of the current test and the south station of the DOT test. By the same argument the north station of the DOT tests is compared with the east station in the current test. Examining the values it is seen that except for the top stations the agreement is quite good. Secondly, it can be seen that the shroud results in a dramatic decrease in the net flux absorbed by the inner cylinder.

Four Nanmac type thermocouples were mounted in the surface of the calorimeter to allow estimations of the surface temperature. The surface temperature history was also estimated with the inverse code. Figures 6.9 thru 6.12 show differences between the frontface temperatures estimated by SODDIT and those measured with the Nanmacs. In addition, the difference between the front and backface temperatures is also plotted. The Nanmac measurements show a high frequency response to thermal transients. In some cases the Nanmacs give surface temperature measurements which seem consistently higher than the frontface temperature estimates. The discrepancy between the two has not been resolved at this time.

A comparison similar to that performed on the shrouded side of the plate calorimeter (Section V) can be performed on the shrouded cylinder as well. The flux from the shroud to the thick cylinder can be calculated from the shroud temperature, the frontface temperature of the thick cylinder and the known emissivities. In this case, the relationship would be the same as that given in equation 5.2, except that the shape factor is no longer unity. The shape factors in this case are:

$$\begin{array}{lll} F_{s \rightarrow p} = 0.8446 & F_{s \rightarrow s} = 0.0385 & \text{From [12]} \\ F_{s \rightarrow r} = 0.1169 & F_{p \rightarrow r} = 0.0957 & \end{array}$$

Where the subscripts are r=ribs, s=shroud, and p=thick wall. The emissivities were assumed to be 0.9 as before. The assumption is also made that the ribs are insulated surfaces and thus do not participate in the heat transfer. The total heat transfer is given by :

$$a \cdot Q_{s \rightarrow p} = \sigma (17.636) (T_s^4 - T_{ff}^4) \quad 6.1$$

The flux per unit area on the outside of the thick wall is then given by :

$$Q_{s \rightarrow p} = \sigma (0.7949) (T_s^4 - T_{ff}^4) \quad 6.2$$

These flux histories were calculated and compared to the net fluxes into the inner cylinder in Figures 6.13 - 6.16. The results compare fairly well on the east and top sides; however, the comparison on the west side is not good. The curves seem to be in fair agreement until t=1200 seconds at which point the shroud temperature seems to be too high. Looking back at the shroud temperature histories, Figure 6.6, it does seem that the trace of the west temperature takes on a different characteristic at t=1200 sec; this probably indicates there was some type of failure.

TABLE 6.1 - Integrated Heat Flux at 30 Minutes [MJ/m²]

Large Cylindrical Calorimeters

Stations (N-winter)	North End (no shroud)	South End (shrouded)	DOT Stations	DOT Averages
Top	47.4	19.5	180 (Top)	86.4
East	120.3	81.2	270 (N)	127.5
Bottom	152.3	97.8	0 (Bottom)	141.3
West	85.2	30.8	90 (S)	99.8

10 centimeter Calorimeters

	East	West
Top	116.0	134.7
South	111.6	130.9
Bottom	120.2	130.9
North	123.0	134.3

NUCLEAR WINTER FIRE TEST LARGE CYLINDER - NORTH INTRINSICS

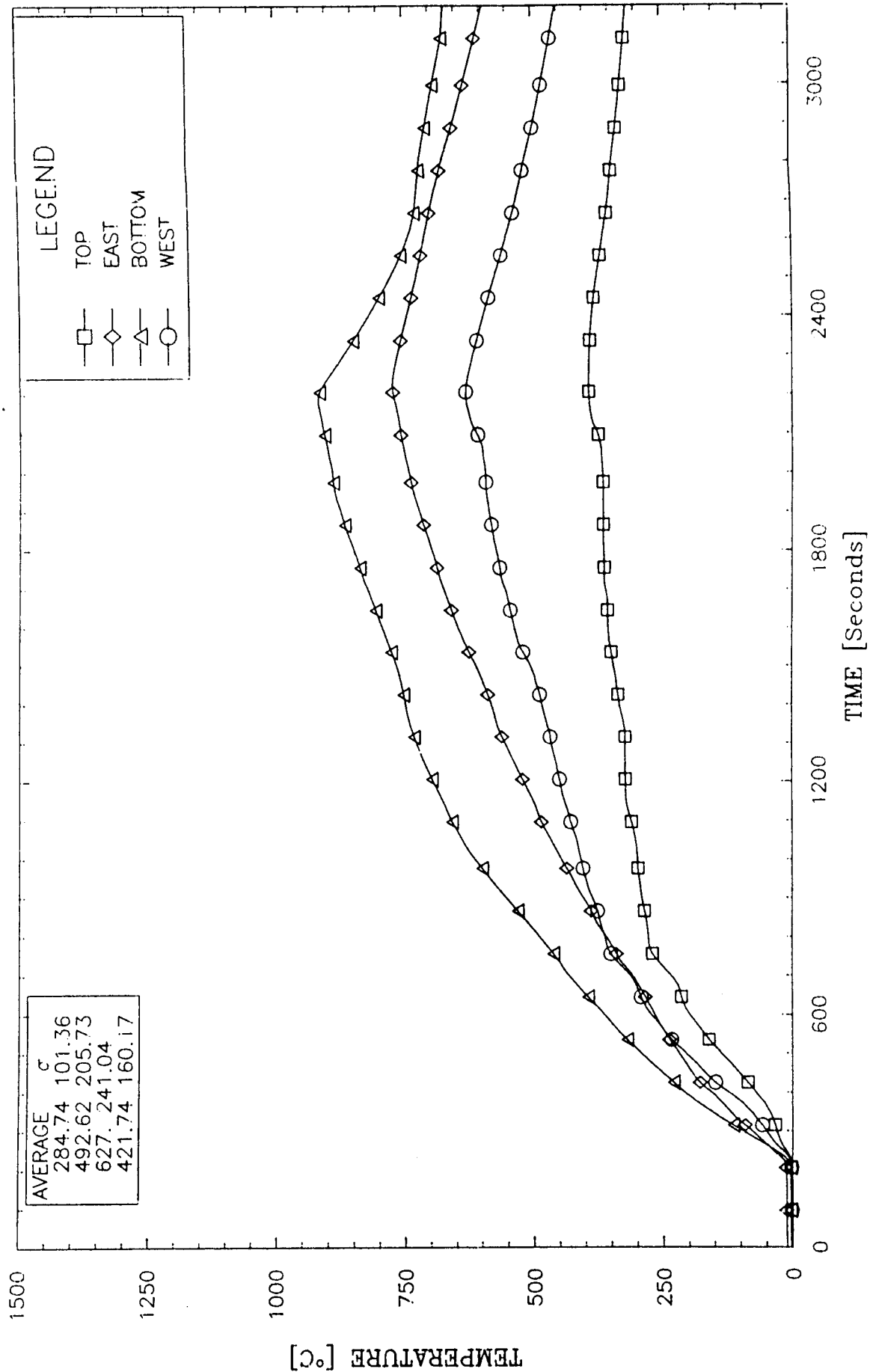


Figure 6.1 Large Cylinder - North Intrinsic

NUCLEAR WINTER FIRE TEST LARGE CYLINDER - NORTH EXTERNALS

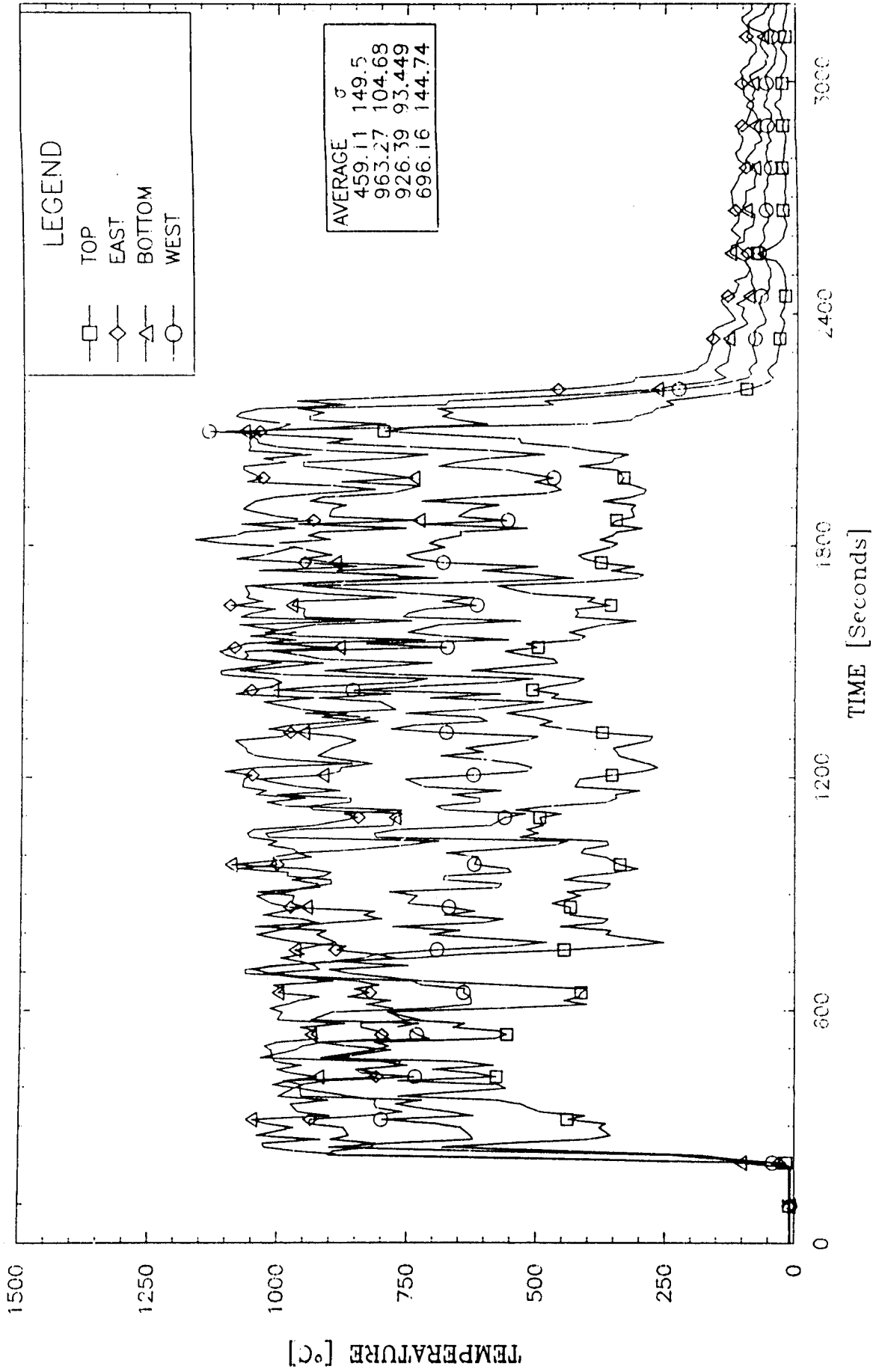


Figure 6.2 Large Cylinder - North Externals

NUCLEAR WINTER FIRE TEST LARGE CYLINDER - NORTH NANMACS

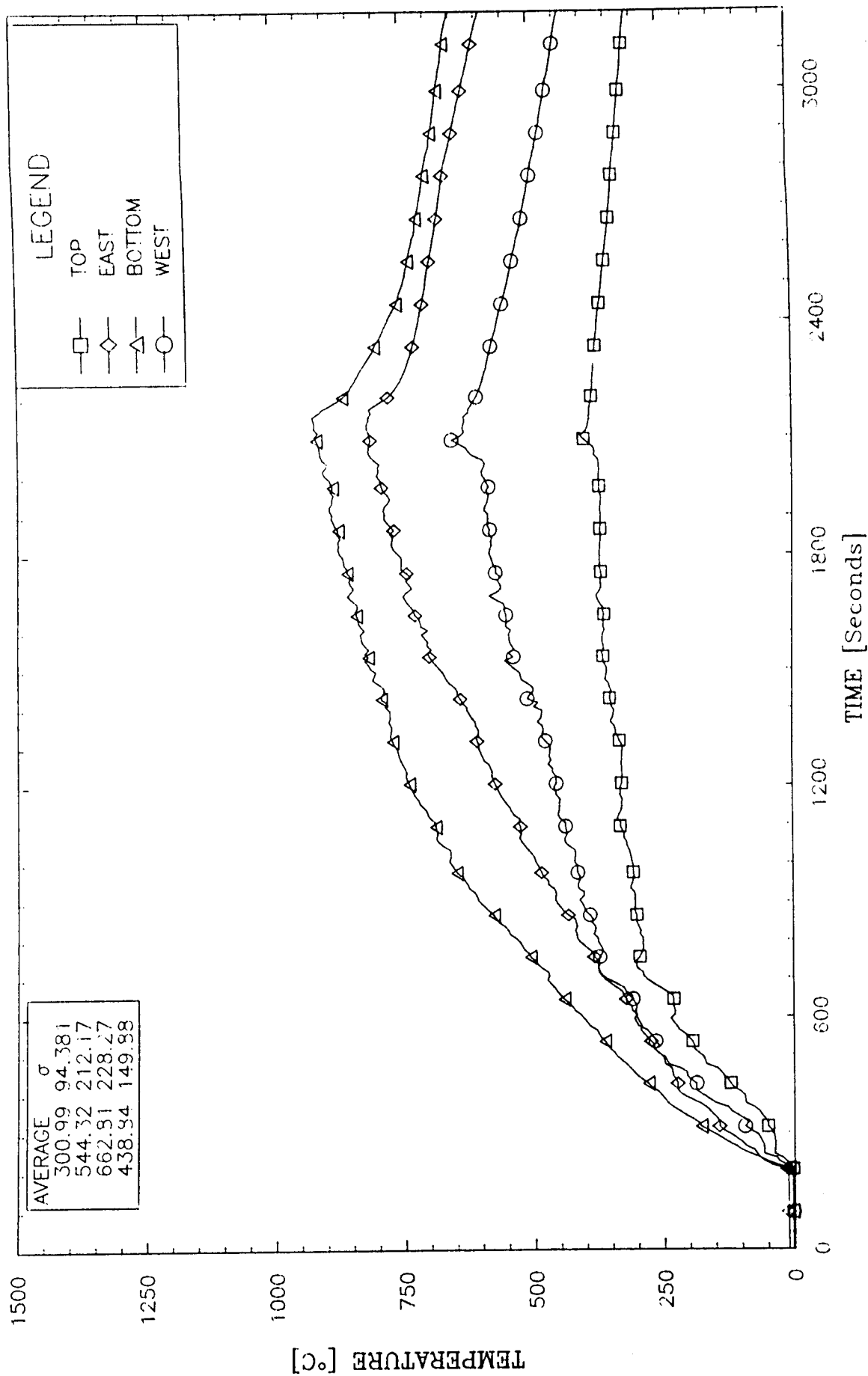


Figure 6.3 Large Cylinder - North Nanmacs

NUCLEAR WINTER FIRE TEST LARGE CYLINDER - INSULATION TEMPERATURES

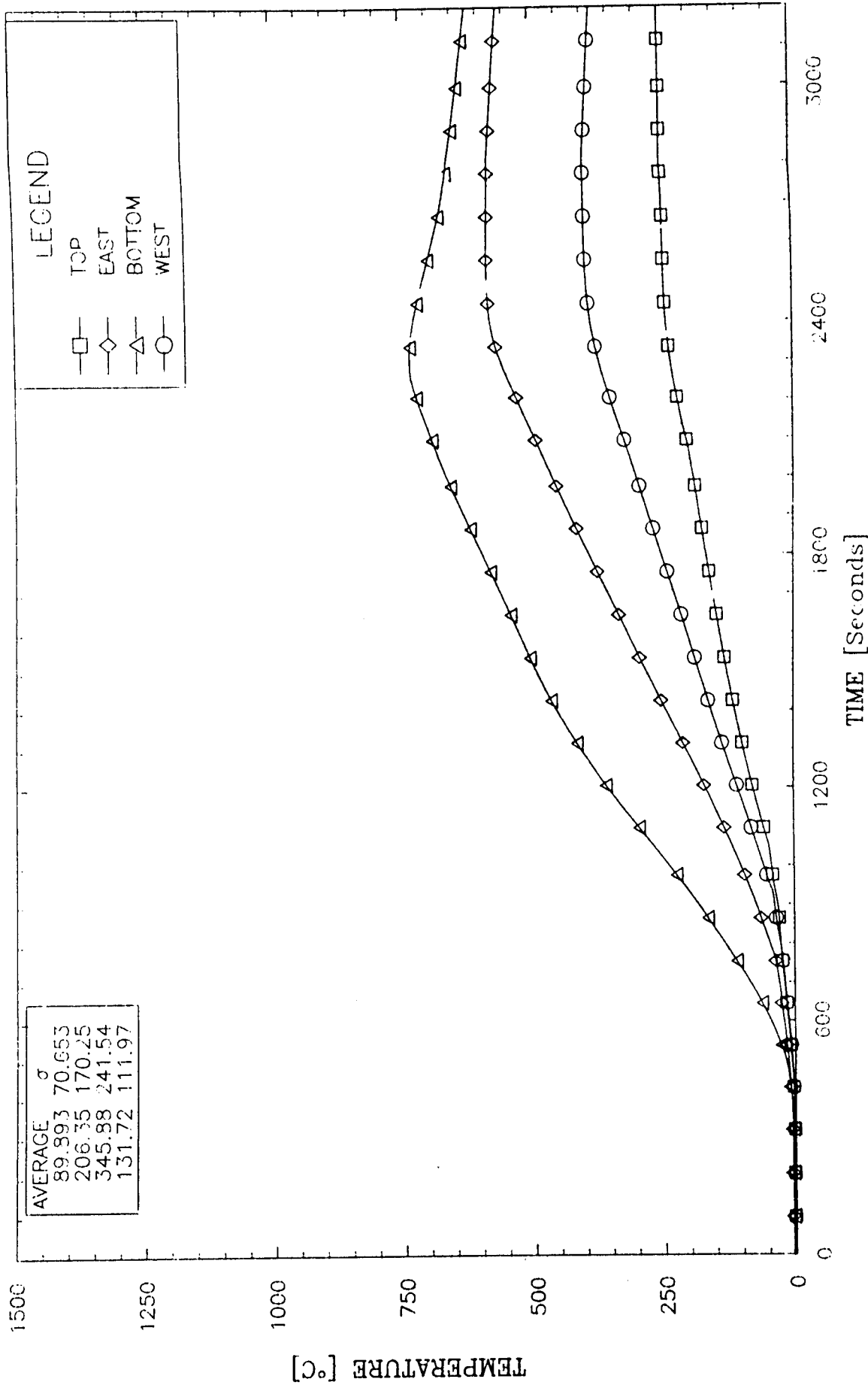


Figure 6.4 Large Cylinder - Insulation Temperatures

NUCLEAR WINTER FIRE TEST LARGE CYLINDER - SOUTH INTRINSICS

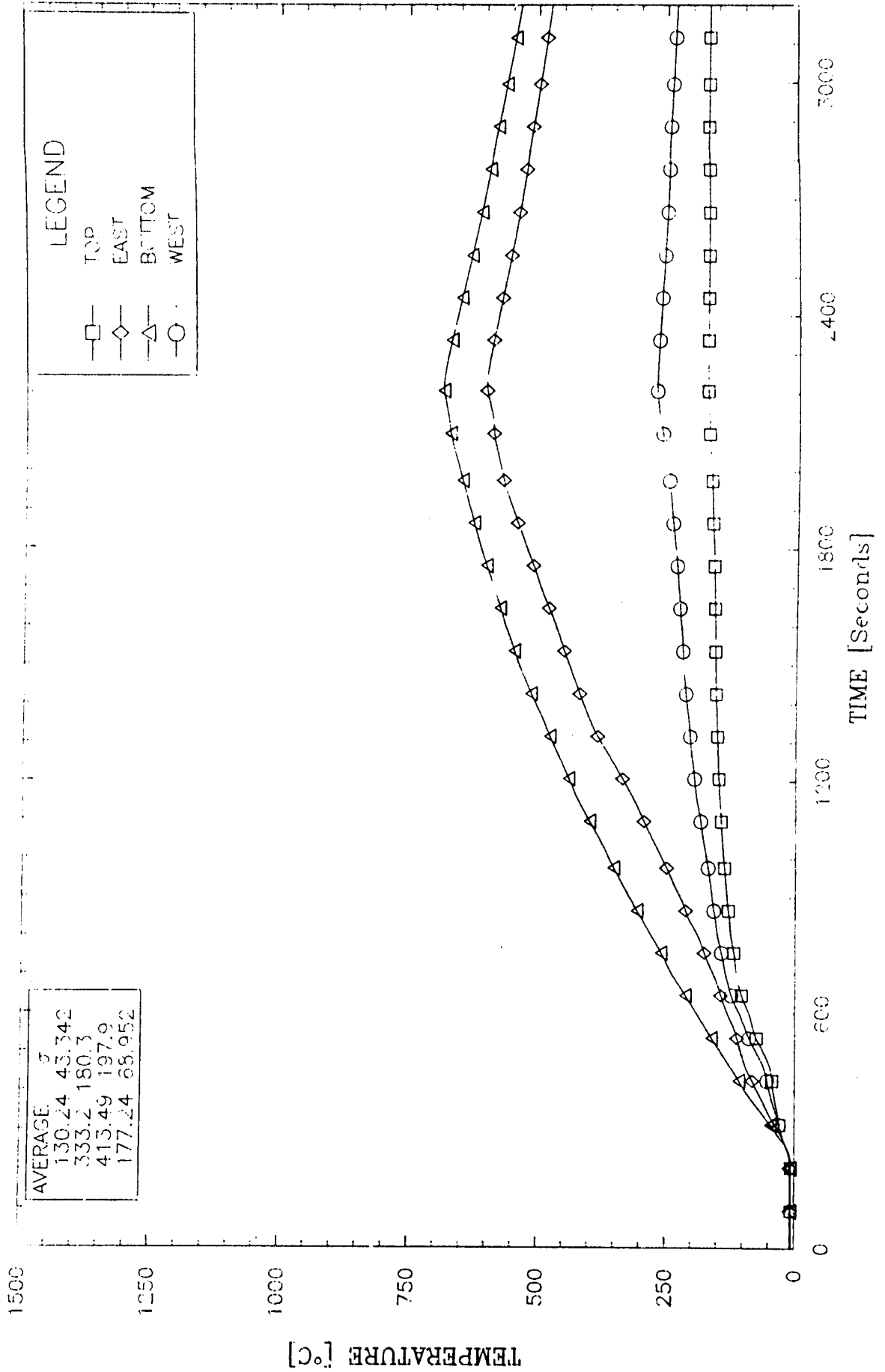


Figure 6.5 Large Cylinder - South Intrinsic

NUCLEAR WINTER FIRE TEST LARGE CYLINDER - SOUTH SHROUD

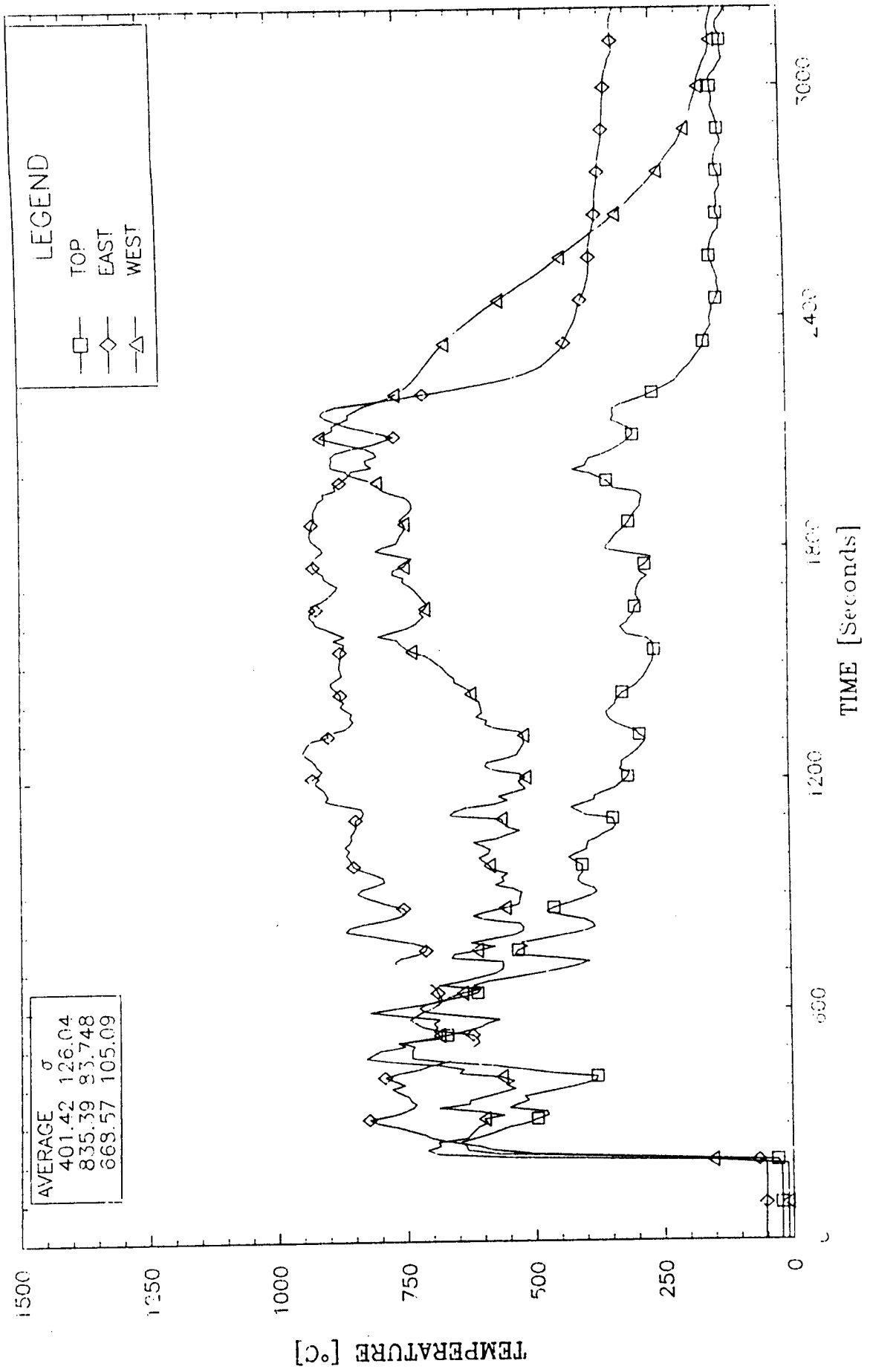


Figure 6.6 Large Cylinder - South Shroud Temperature

NUCLEAR WINTER FIRE TEST
NORTH LARGE CALORIMETER - FLUX VS TEMPERATURE

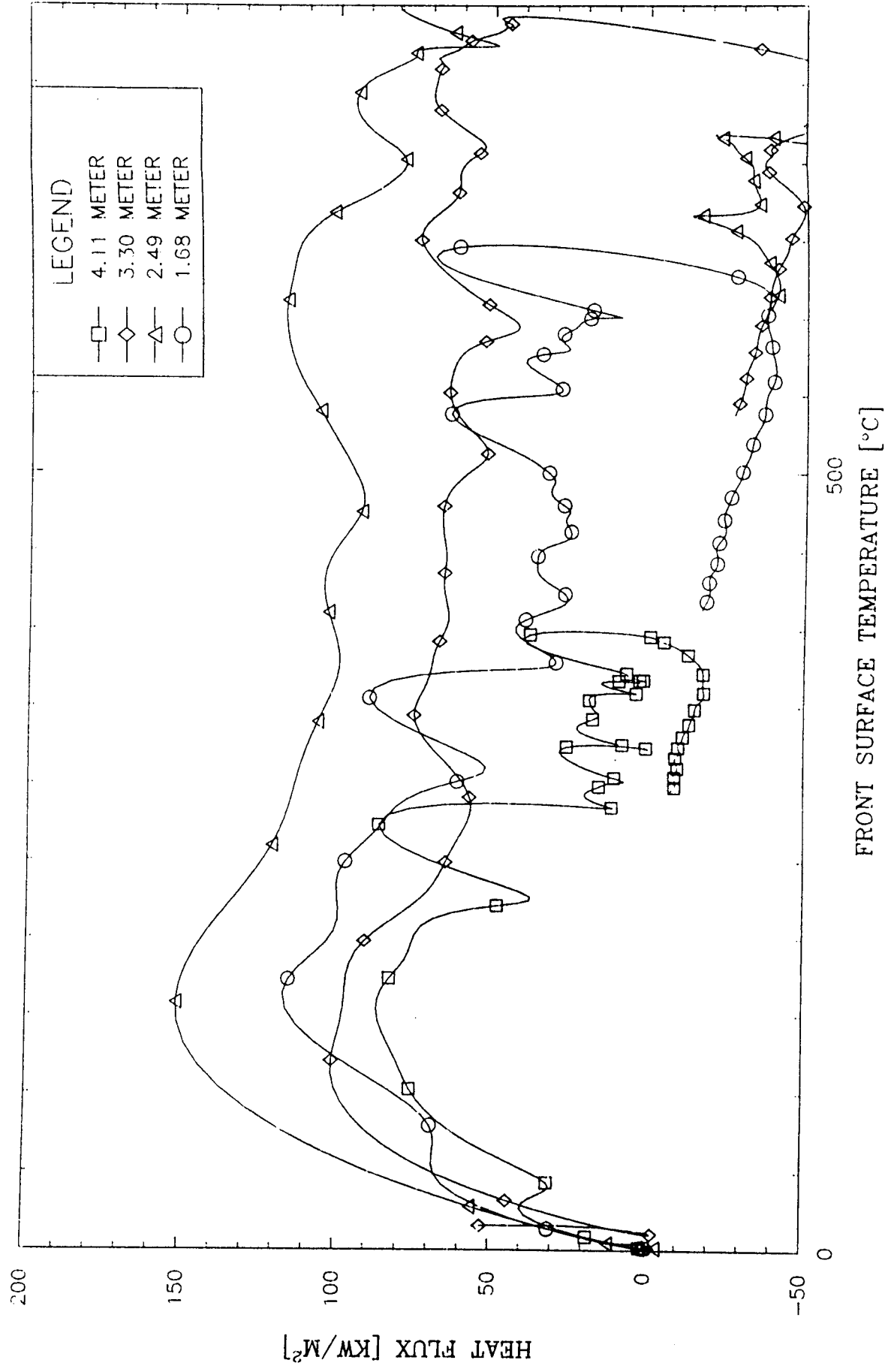


Figure 6.7 Large Cylinder - North Flux vs Surface Temperature

NUCLEAR WINTER FIRE TEST LARGE CYLINDER - NORTH HEAT FLUX

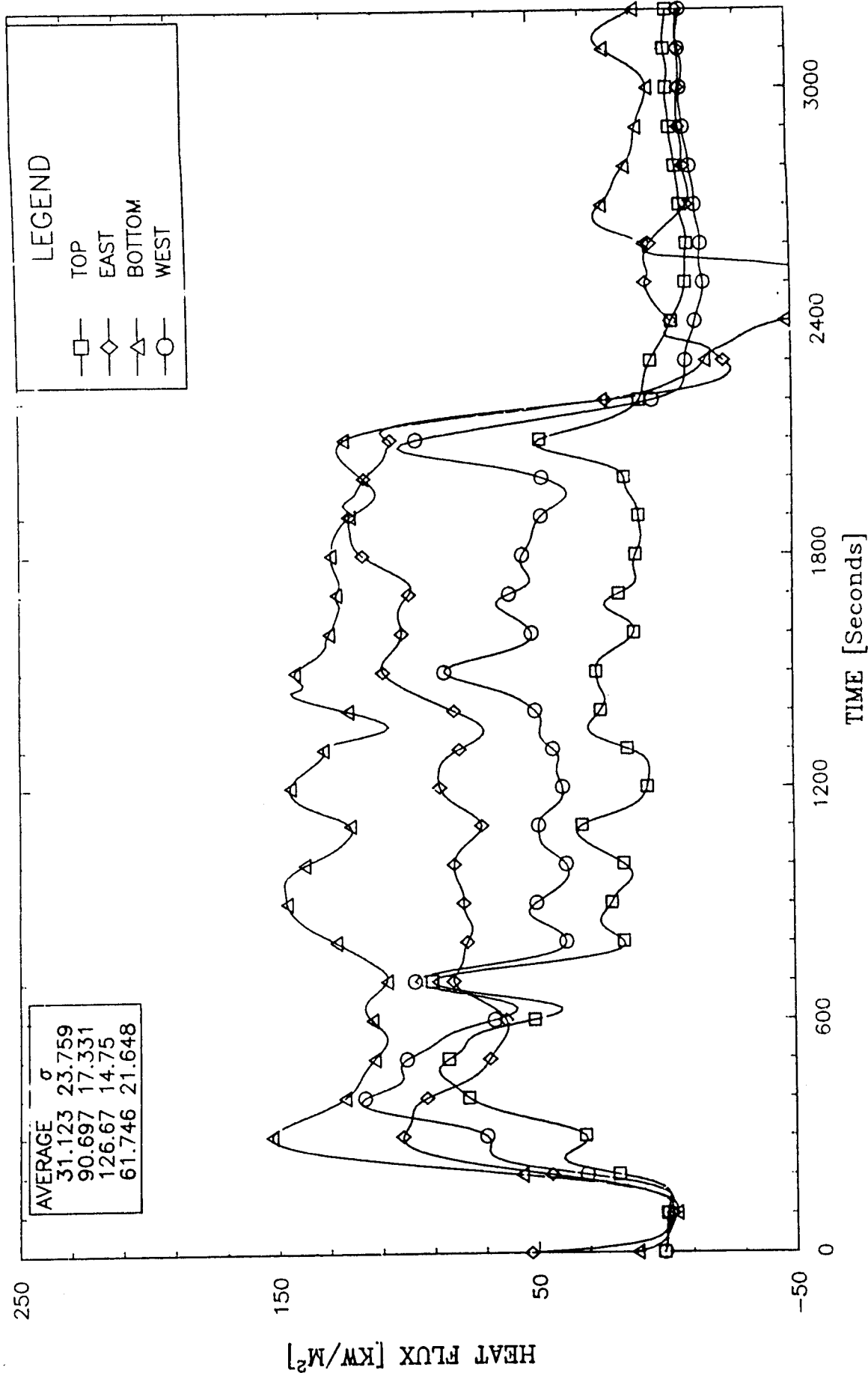


Figure 6.8 Large Cylinder - North Cold Wall Heat Flux

NUCLEAR WINTER FIRE TEST TOP STATION

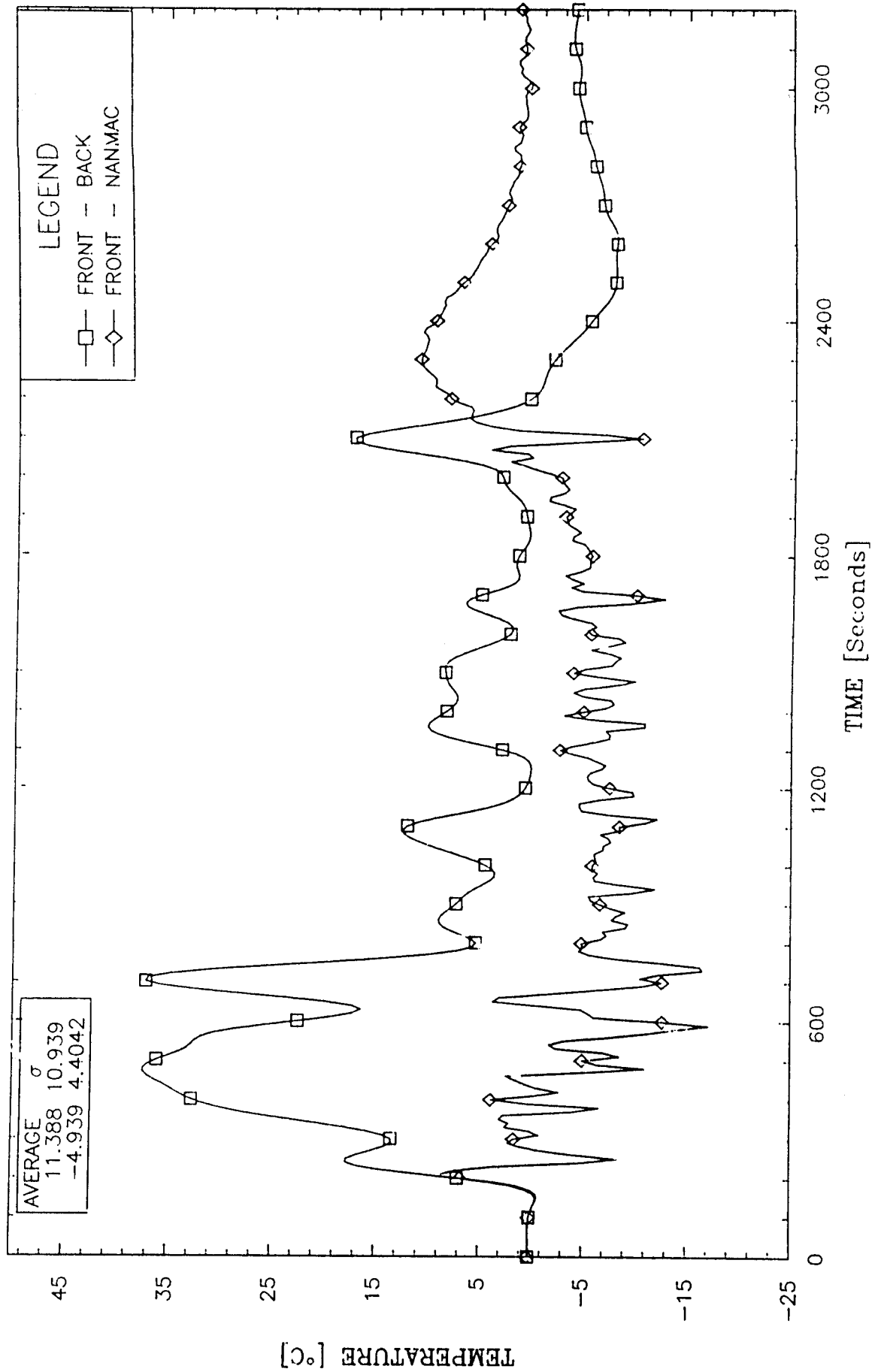


Figure 6.9 Nanmac's SODDIT Surface Temperature Estimates (Top Station)

NUCLEAR WINTER FIRE TEST EAST STATION

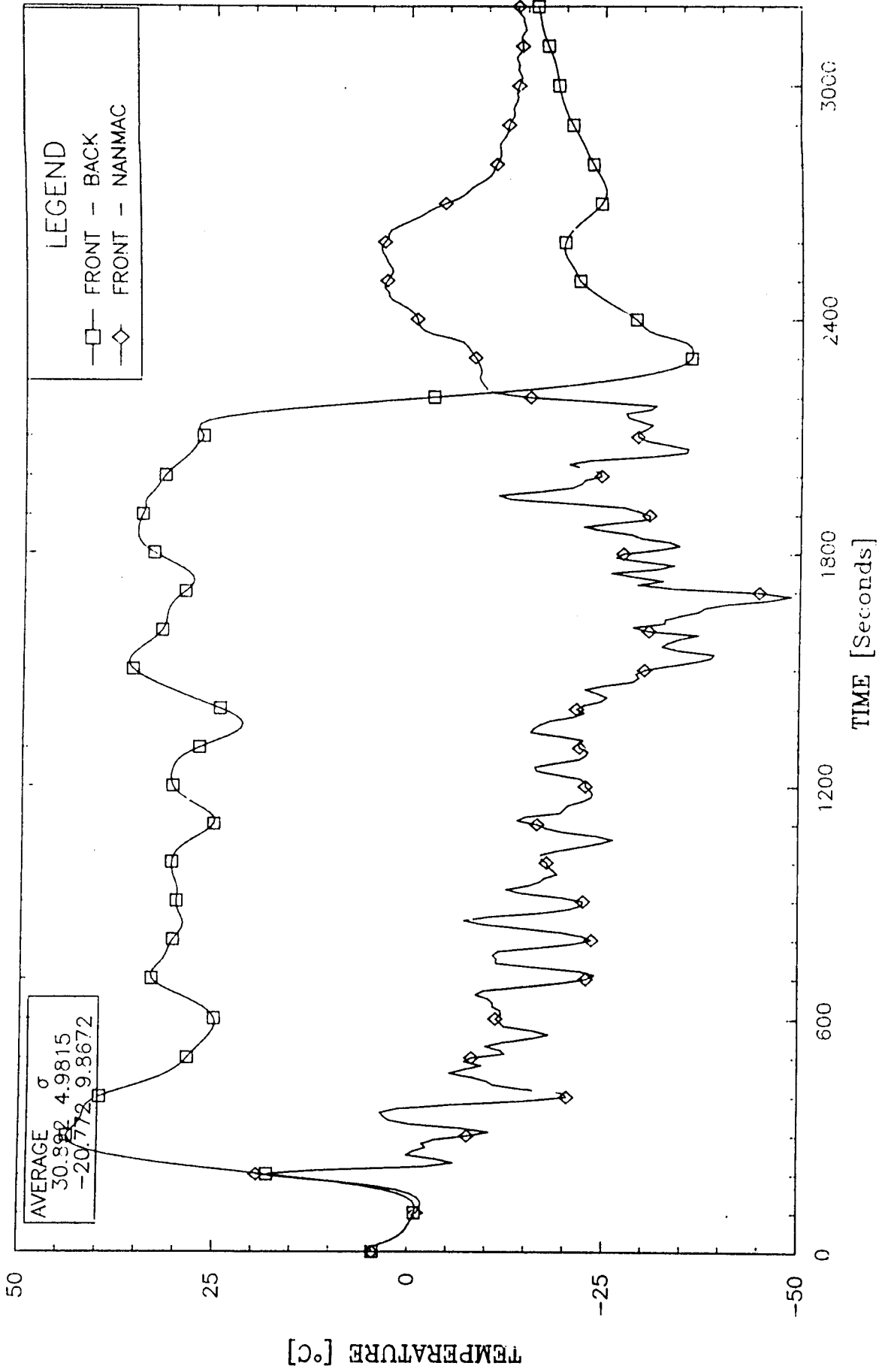
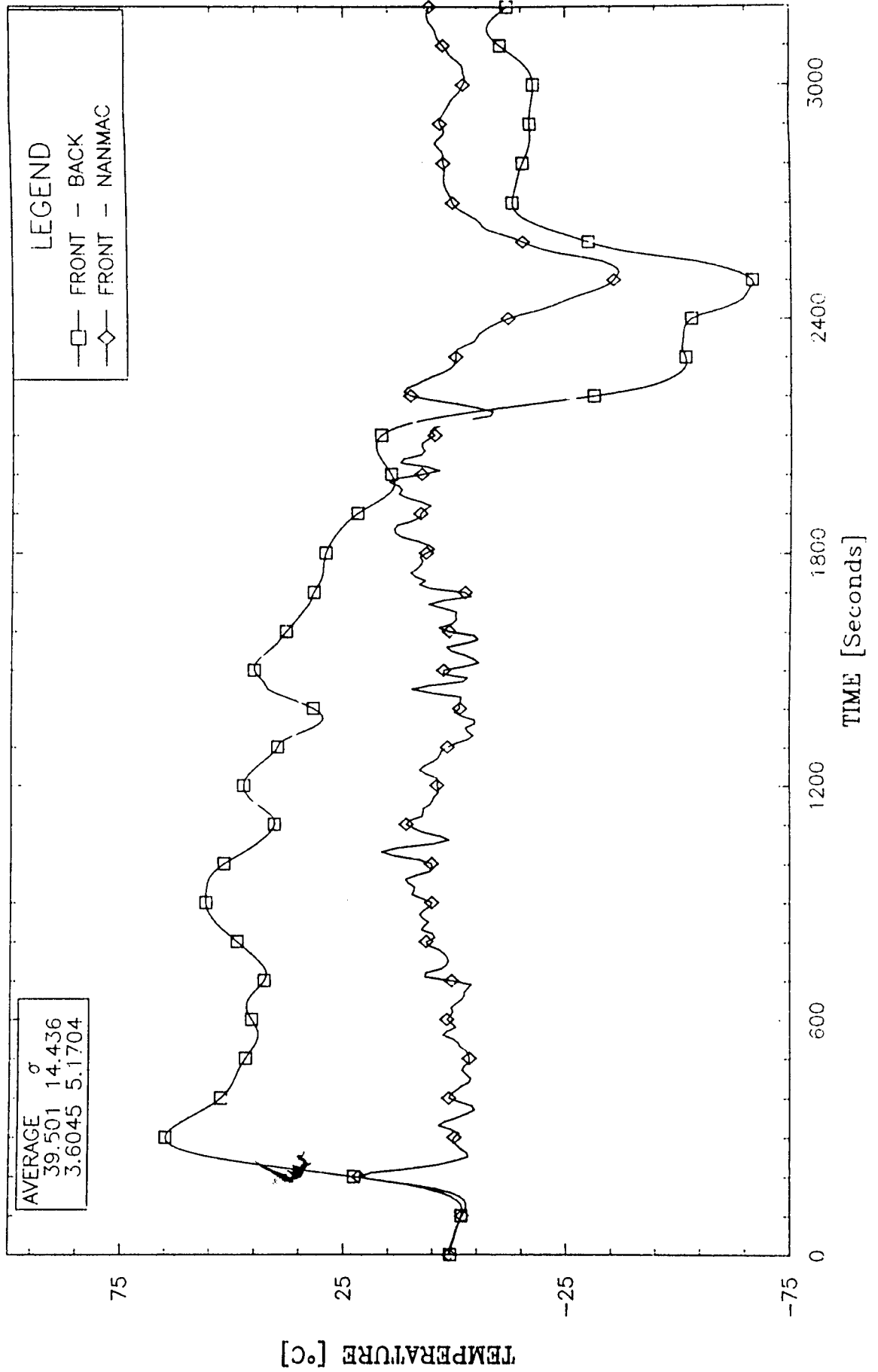


Figure 6.10 Nanmacs vs SODDIT Surface Temperature Estimates (East Station)

NUCLEAR WINTER FIRE TEST BOTTOM STATION



NUCLEAR WINTER FIRE TEST
WEST STATION

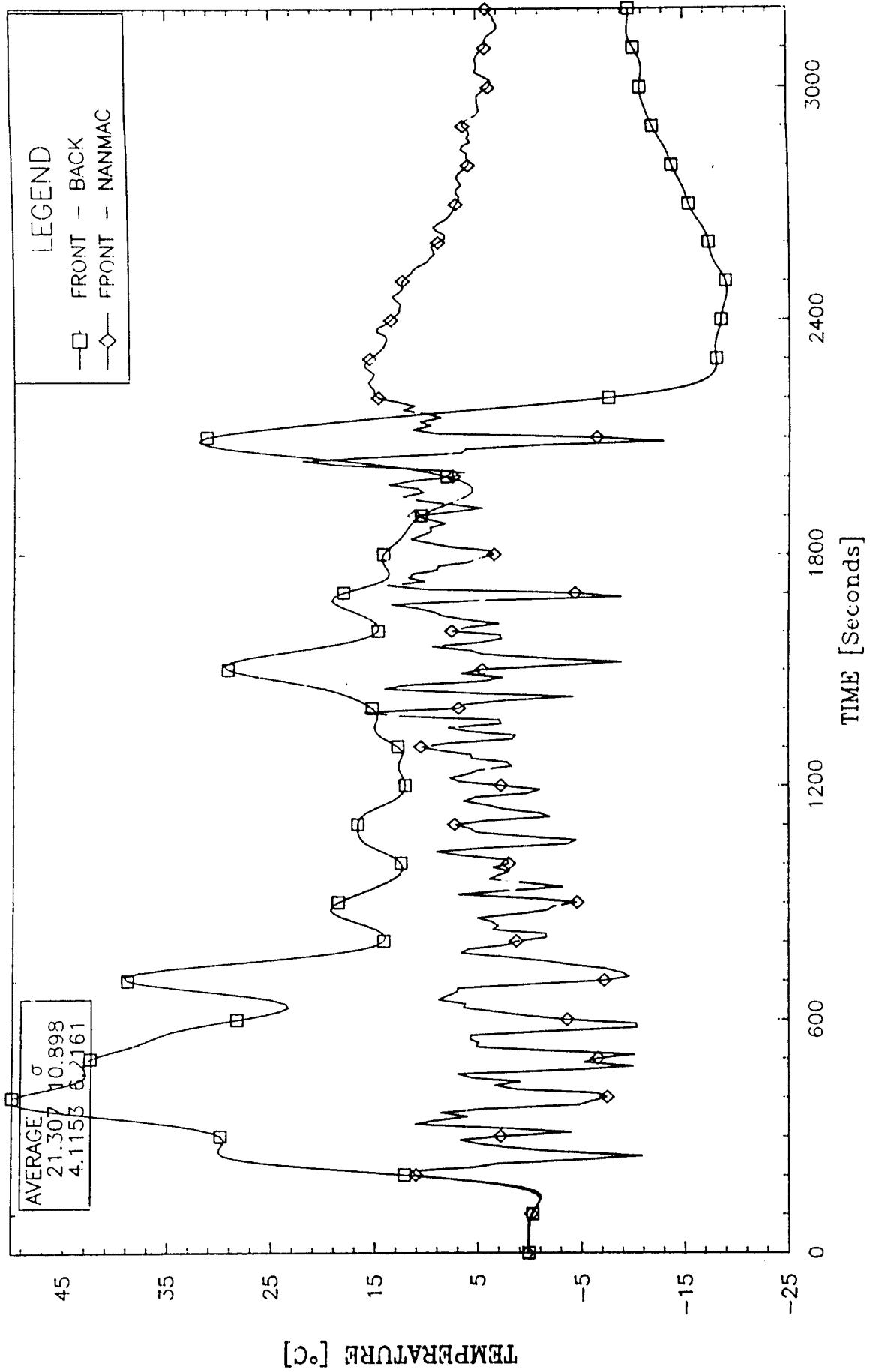


Figure 6.12 Nanmacs vs SODDIT Surface Temperature Estimates (West Station)

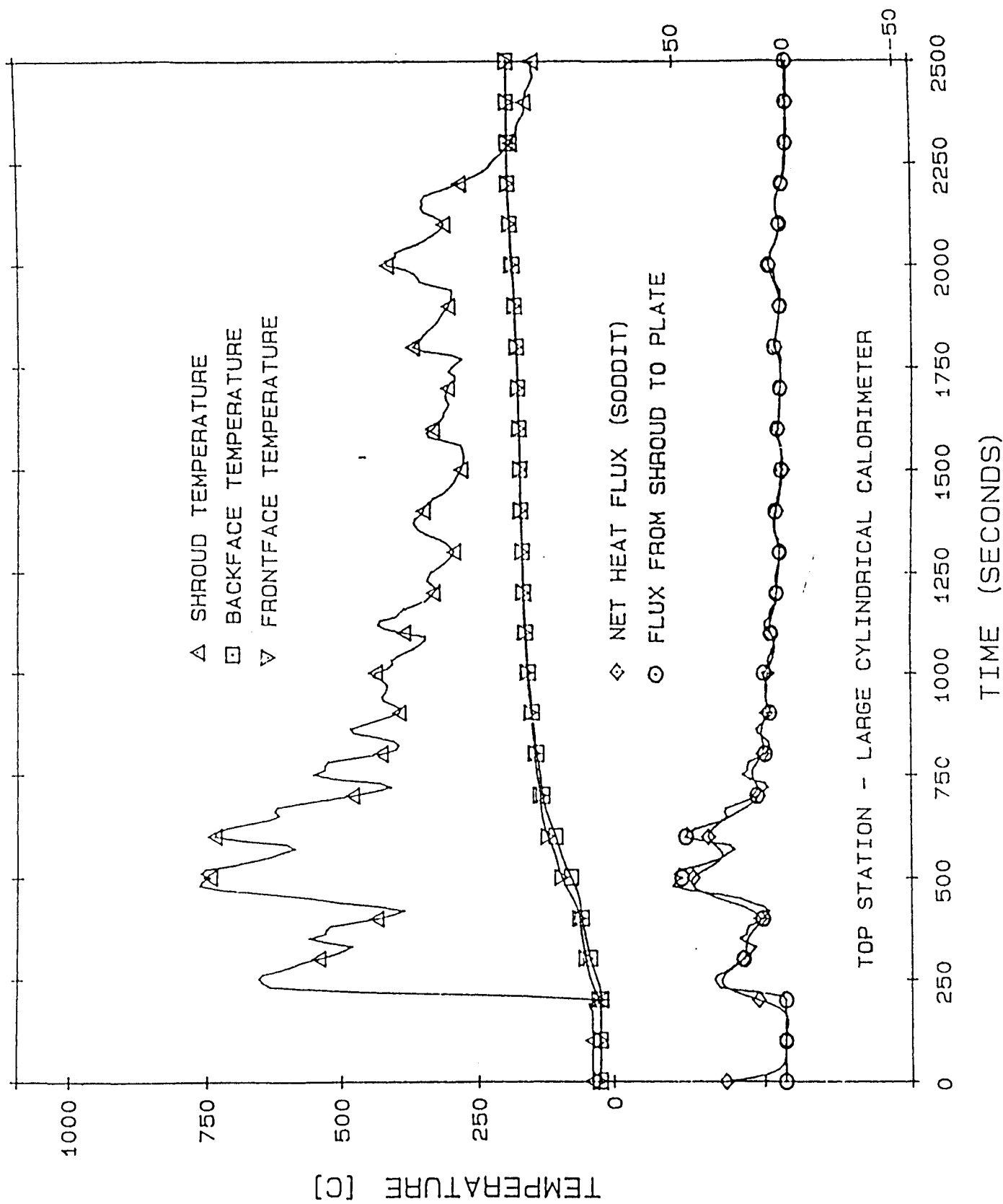


Figure 6.13 Comparison Between Two Heat Flux Calculations (Top Station)

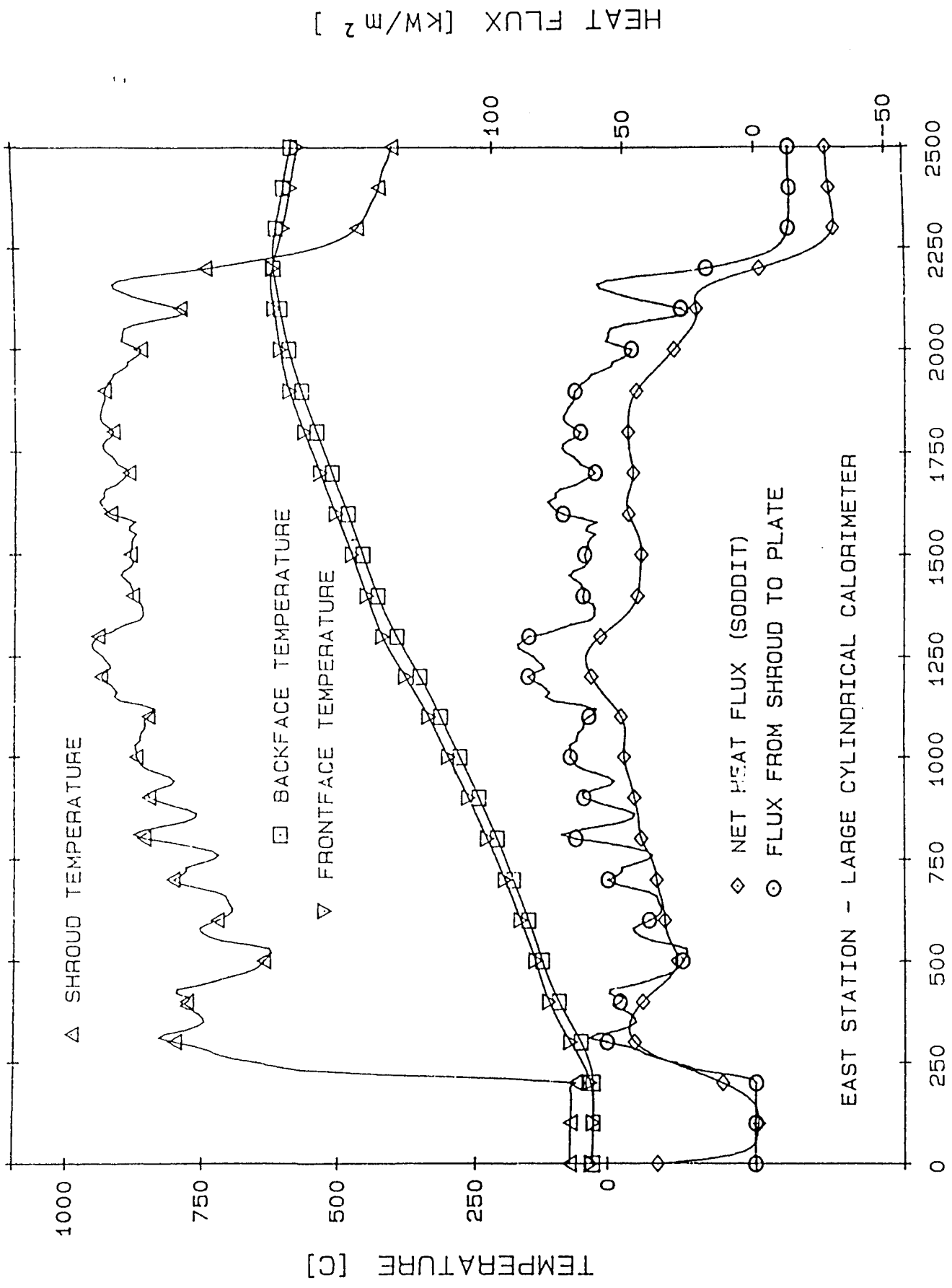


Figure 6.14 Comparison Between Two Heat Flux Calculations (East Station)

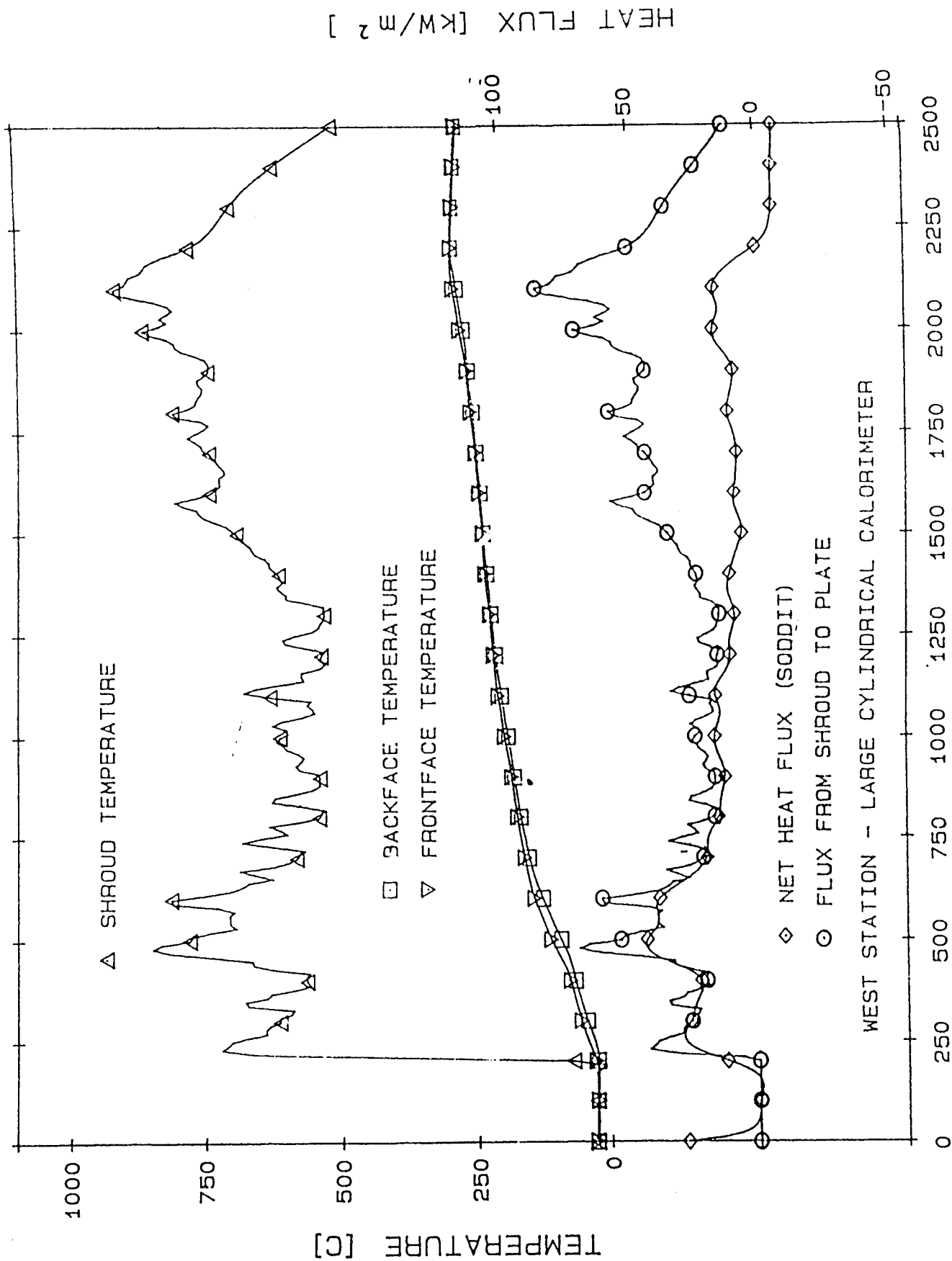


Figure 6.15 Comparison Between Two Heat Flux Calculations (West Station)

VII. HEAT FLUX TO THE 10 CM CYLINDRICAL CALORIMETERS

Heat flux and surface temperature estimates were obtained by using temperature data from thermocouples located at known depths within the calorimeter material. The data was processed by application of an inverse heat conduction code, the Sandia One-Dimensional Direct and Inverse Thermal (SODDIT) code [10,11]. The code utilizes the assumption that the heat transfer is one-dimensional; an assumption that is believed to be reasonable in the case of these calorimeters because of the thermal insulation between the quadrants. The code accounts for the cylindrical geometry of the calorimeters.

The backface steel temperatures for the 10 centimeter calorimeters are plotted in Figures 7.1 and 7.2. Note that the maximum difference in backface temperatures for all stations on a single calorimeter is 95°C for the east calorimeter, and 111°C for the west. The values for the east and west calorimeters track each other closely. The temperature data was conditioned by using a smoothing spline with a 3°C standard deviation. The original temperature data was smoothed and interpolated because the acquisition of resistance values every tenth scan left uneven time intervals, and the inverse code requires even time intervals.

The cold wall heat flux histories for the 10 centimeter calorimeters calculated using Equation 5.1 are plotted in Figures 7.3 and 7.4. The magnitudes of the reported heat flux values are also reasonable, when comparing to heat flux estimates for the 10 centimeter calorimeters in other tests.

Figures 7.5 and 7.6 are plots of the net heat flux to the calorimeters as a function of the front face temperature. These plots are included to allow comparisons to be made with other test results and fire standards.

NUCLEAR WINTER FIRE TEST EAST TEN CM CALORIMETER

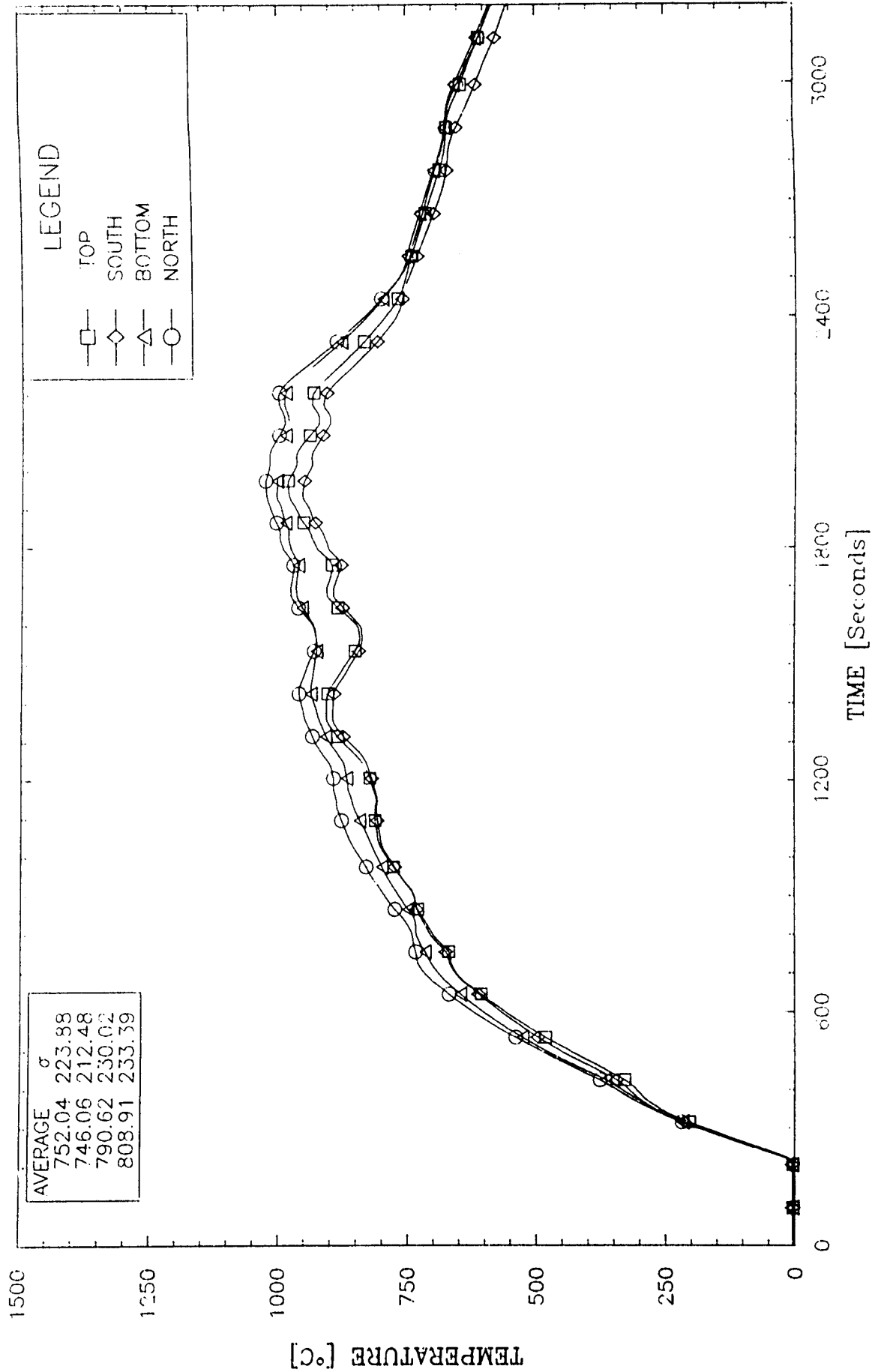


Figure 7.1 East 10 cm Calorimeter Backface Temperatures

NUCLEAR WINTER FIRE TEST
WEST TEN CM CALORIMETER

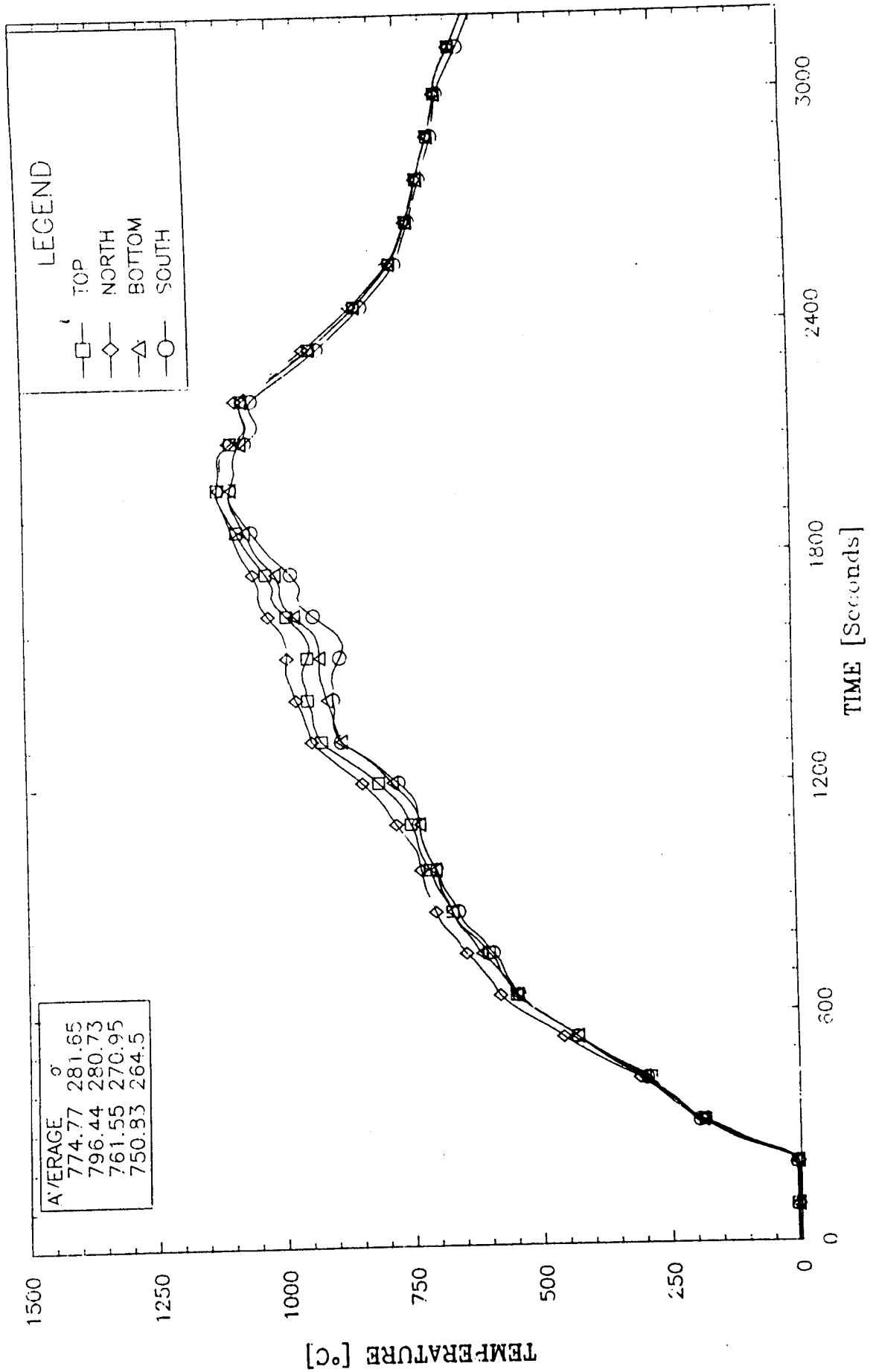


Figure 7.2 West 10 cm Calorimeter Backface Temperatures

NUCLEAR WINTER FIRE TEST
EAST TEN CM CALORIMETER

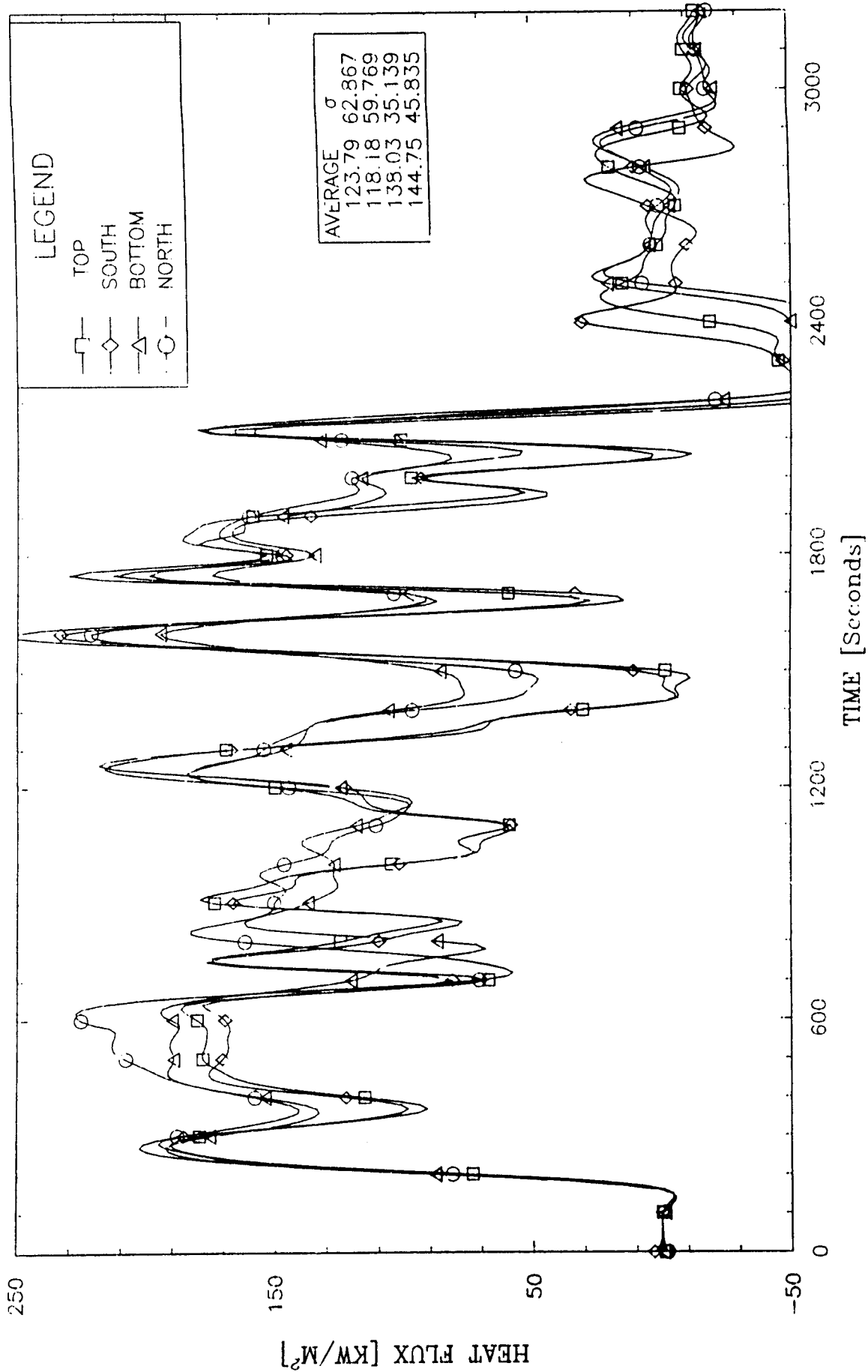


Figure 7.3 East 10 cm Calorimeter Cold Wall Heat Flux

NUCLEAR WINTER FIRE TEST
WEST TEN CM CALORIMETER

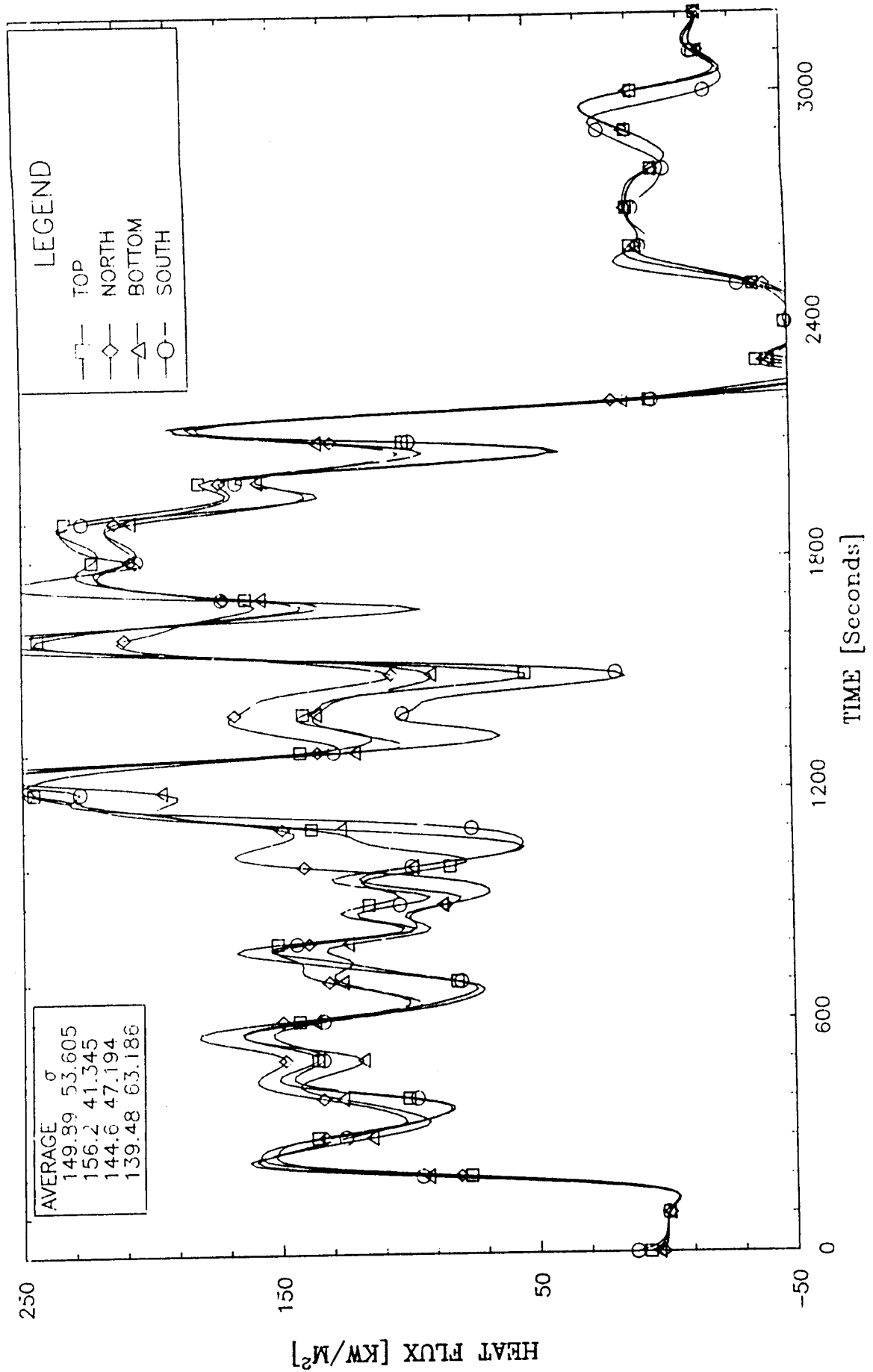


Figure 7.4 West 10 cm Calorimeter Cold Wall Heat Flux

NUCLEAR WINTER FIRE TEST
EAST 10 CM CALORIMETER - FLUX VS TEMPERATURE

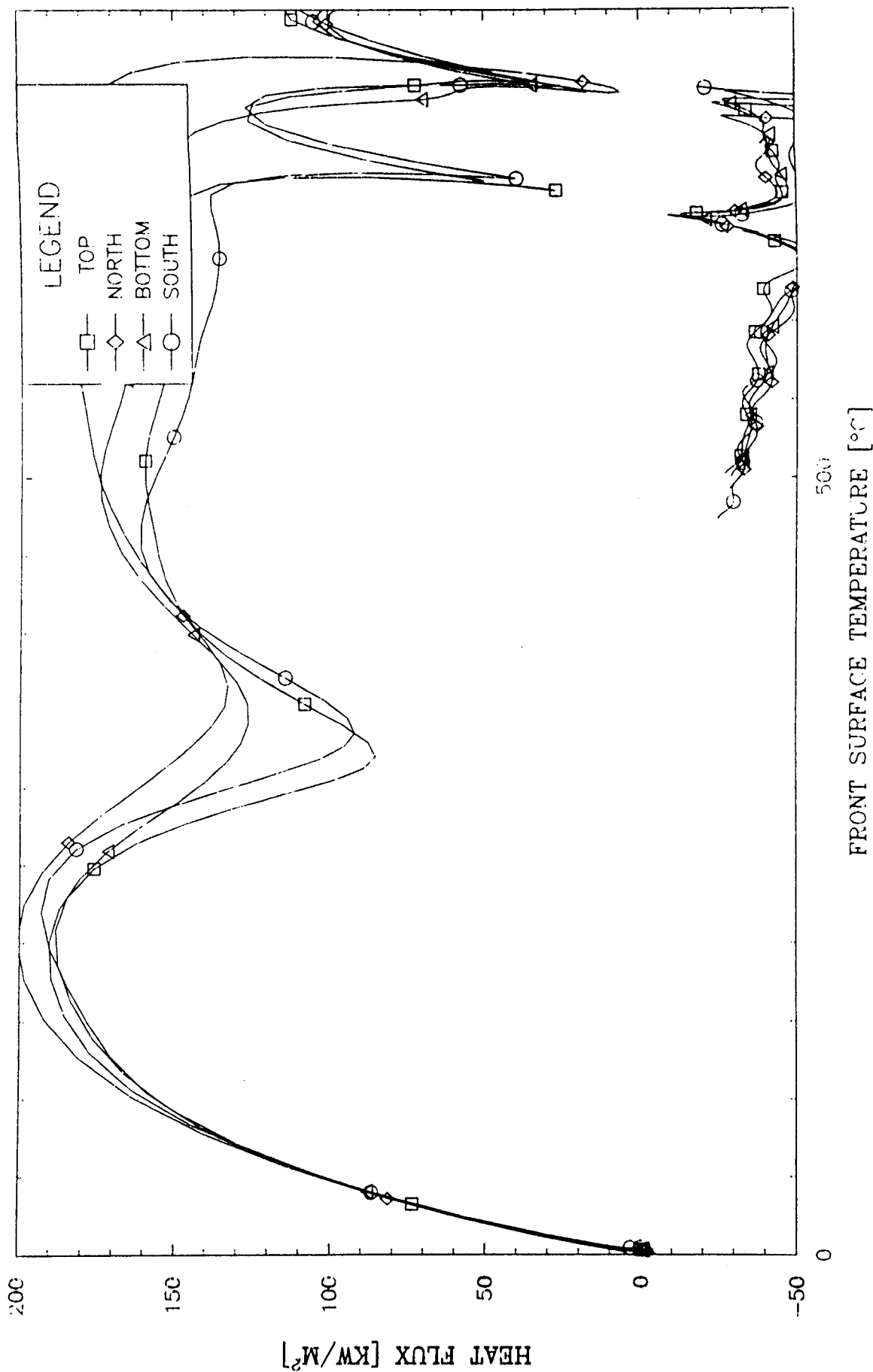


Figure 7.5 East 10 cm Calorimeter Heat Flux vs Surface Temps

NUCLEAR WINTER FIRE TEST
WEST 10 CM CALORIMETER - FLUX VS TEMPERATURE

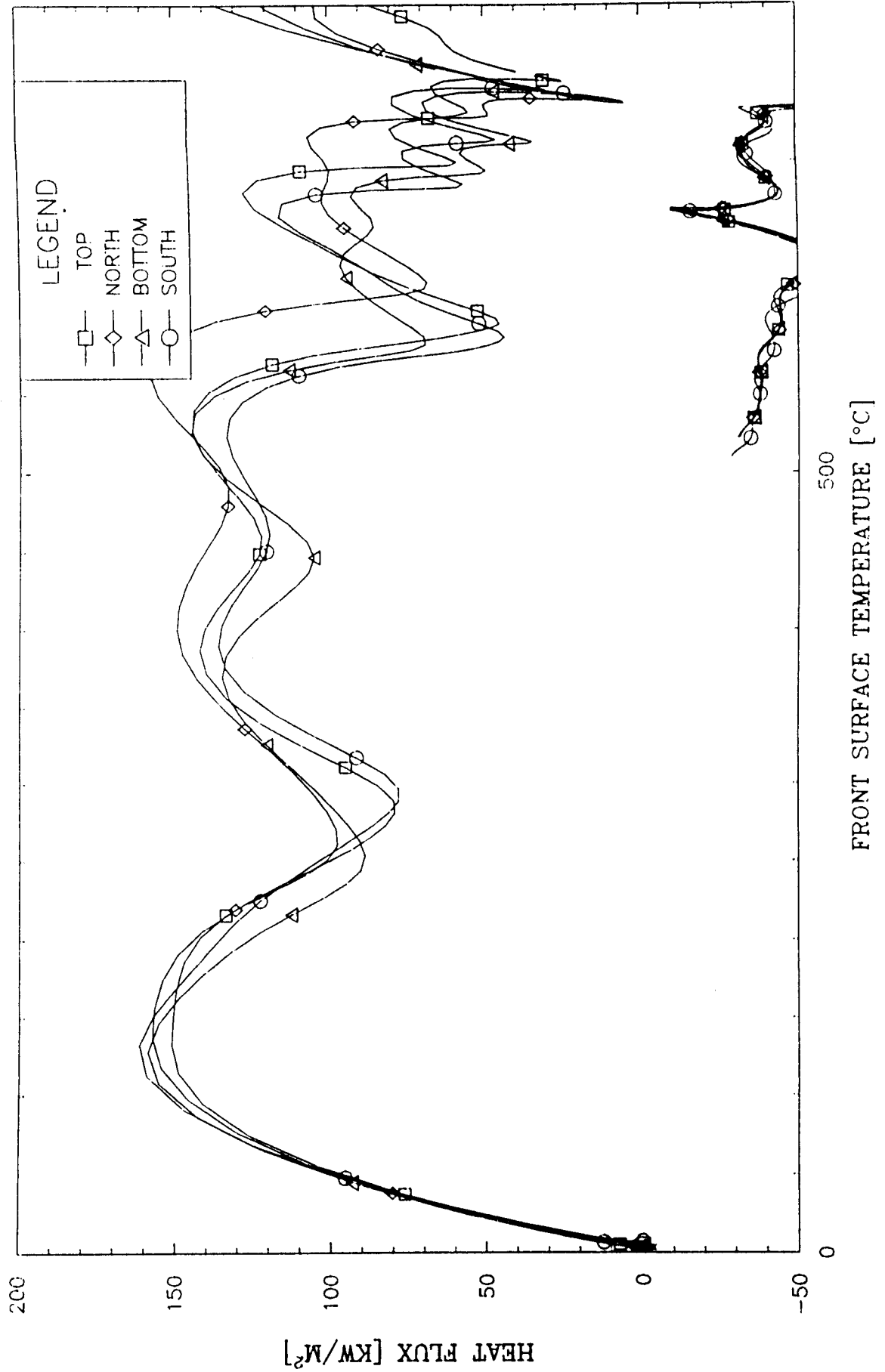


Figure 7.6 West 10 cm Calorimeter Heat Flux vs Surface Temps

VIII. FUEL LEVELS AND BURN RATE

In this test a number of systems were in place to monitor the fuel consumption rate. The amount of fuel supplied to the pool was measured with a meter at the supply tank. The level of liquid in the pool was measured with a sight glass, a pressure transducer, and a float connected to an LVDT. The output from the pressure transducer and LVDT were monitored during the test to quantify any changes in overall burning rate.

Prior to the test the fuel meter read 21743. Initially 65.4 centimeters of water were added to the pool. Next 17.8 centimeters of fuel was added. The fuel meter then read 29594. This indicates an addition of 30185 liters. The meter factor is 3.845 liters per count (1.01566 gallons per count). At about 25 minutes into the test it was determined that more fuel should be added to achieve the desired burn time. At that time an additional 3467 liters were added bringing the total fuel to 33652 liters. The final fuel meter reading was 30496. The fuel temperature was measured to be 5.6 °C.

Figure 8.1 shows a plot of the fuel level in the pool. The plot is derived from the output of the LVDT/float system. The curve was arrived at by converting the change in voltage to centimeters of fuel using the calibration of the device, and the properties of fuel and water, then forcing the post-test value to be zero. The pressure transducer output was much more sensitive to noise which made the zero setting somewhat questionable. It was decided that the LVDT was the more reliable instrument for this type of measurement. The initial value from the plot is 18.24 centimeters which corresponds to 30438 liters of fuel. This is slightly more than the indicated initial fuel load (30185 liters). The slight difference may be due to the evaporation of some water near the end of the test. Since the LVDT data prior to the fuel addition is not used, the loss of water at the end of the test would appear as extra fuel consumed.

The burning rate was estimated in three ways. First the average burning rate can be estimated simply by dividing the total fuel load (33652 liters) by the test duration (2000 seconds). This gives a rate of 0.605 centimeters per minute (1010 liters per minute). A second method is to fit a line to portions of the curve shown in Figure 8.1. The results of this were:

Time period (sec)	liters/min	cm/min
300- 600	806	0.485
600- 900	984	0.589
900-1200	1052	0.630
1200-1500	1030	0.617
1500-1800	1079	0.648

Figure 8.2 indicates the third method, which is to differentiate the curve of Figure 8.1. The average of this derivative over the time 500 to 1600 seconds was 0.612 centimeters per minute (1022 liters per minute).

The fuel burning rate in an open pool fire is governed by the heat flux from the flames above the pool down to the fuel surface. The energy to vaporize the liquid fuel must be obtained from flame radiation. Measurements of heat flux to the pool surface were attempted in this fire

test. Two methods were used here. The first method involves the measurement of total heat flux to a slug calorimeter placed very near the burning fuel surface. A second method involved the direct measurement of the total radiative flux toward the fuel surface with a transpiration radiometer[13].

Figure 2.6 shows a cutaway view of the slug calorimeters used. An axisymmetric, two dimensional, thermal model was used to demonstrate that heat transfer in the calorimeter was one dimensional. As the fuel recedes, more of the calorimeter support is exposed. The model was used to demonstrate that the exposure length did not significantly affect the temperature history of the slug.

The backface temperature profiles from the slug calorimeters are included as Figure 8.3. These temperatures have been smoothed to remove noise which interferes with any heat flux calculation from measured temperatures. The smoothed curves are shown in Figure 8.4. The heat flux to each of the three calorimeters was calculated using the SODDIT code referred to earlier in this report.

At this point the situation becomes quite difficult. We know the flux to a plate of varying (but known) surface temperature and known emissivity. We want to estimate the flux to the boiling fuel surface. A simple estimate of the incident flux can be made. To do this the following flux was calculated:

$$Q_{bf} = \sigma \epsilon (T_{ff}^4 - T_{bp}^4) + Q_{net}$$

where T_{ff} is the frontface temperature of the slug calorimeter, T_{bp} is the fuel boiling point, and Q_{net} is the net flux into the calorimeter. This modified cold wall flux is plotted in figure 8.5.

For comparison, a calculation can be made to estimate the heat flux required to vaporize fuel at the measured rate of recession. This calculation results in an estimated heat flux requirement of:

$$0.00612 \text{ m/min (1/60 min/sec)} \cdot 770 \text{ kg/m}^3 (632.75 \text{ KJ/Kg}) = 49.7 \text{ Kw/m}^2$$

Figures 8.6 and 8.7 show the output voltage and gage temperature of the transpiration gage mounted near the pool center facing vertically. The values measured are way too high to be reasonable due to some problem with the calibration of the gage. The figures have been included to show the general trends.

NUCLEAR WINTER FIRE TEST FUEL LEVEL

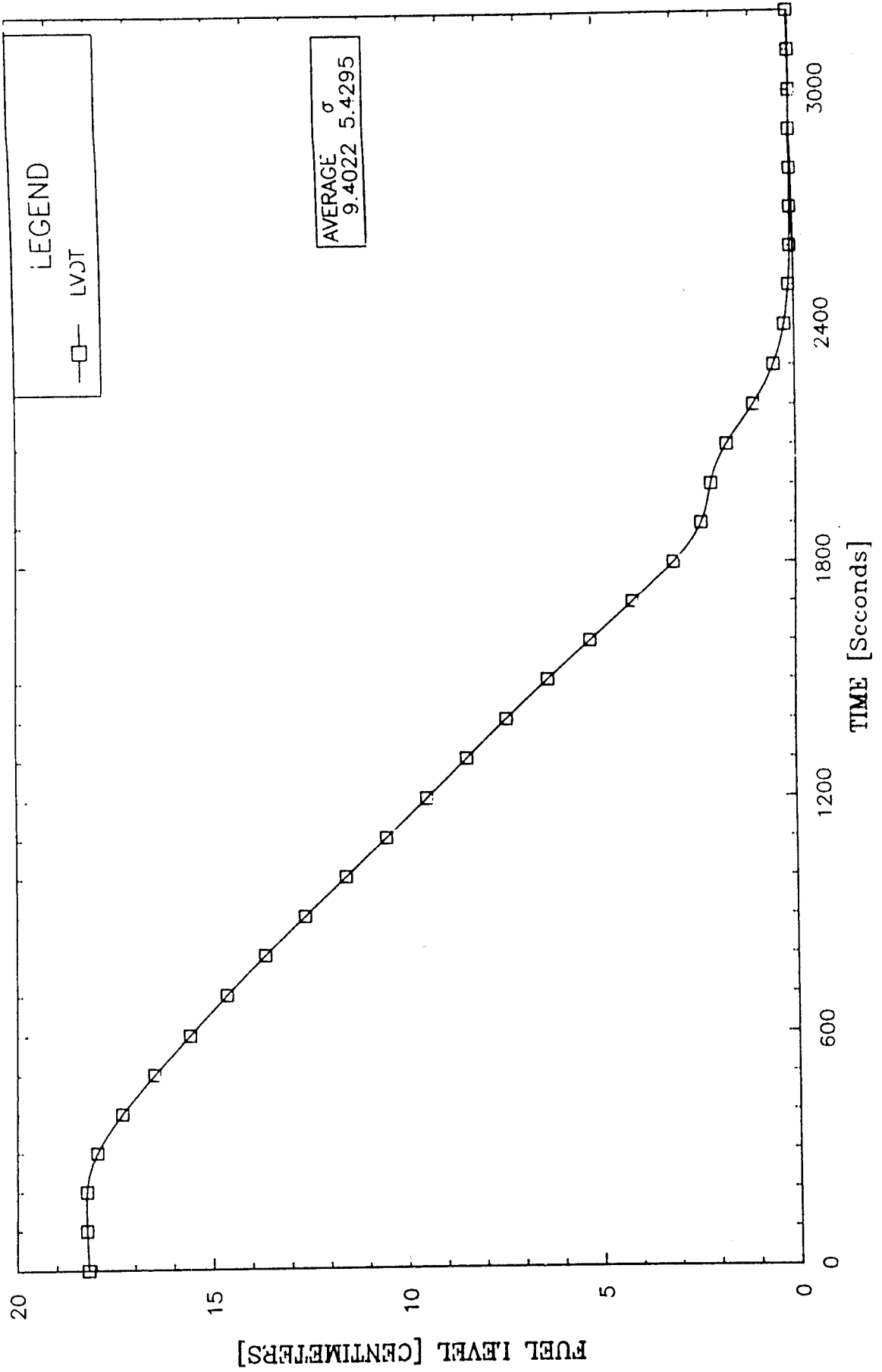


Figure 8.1 Fuel Level

NUCLEAR WINTER FIRE TEST FUEL BURNING RATE

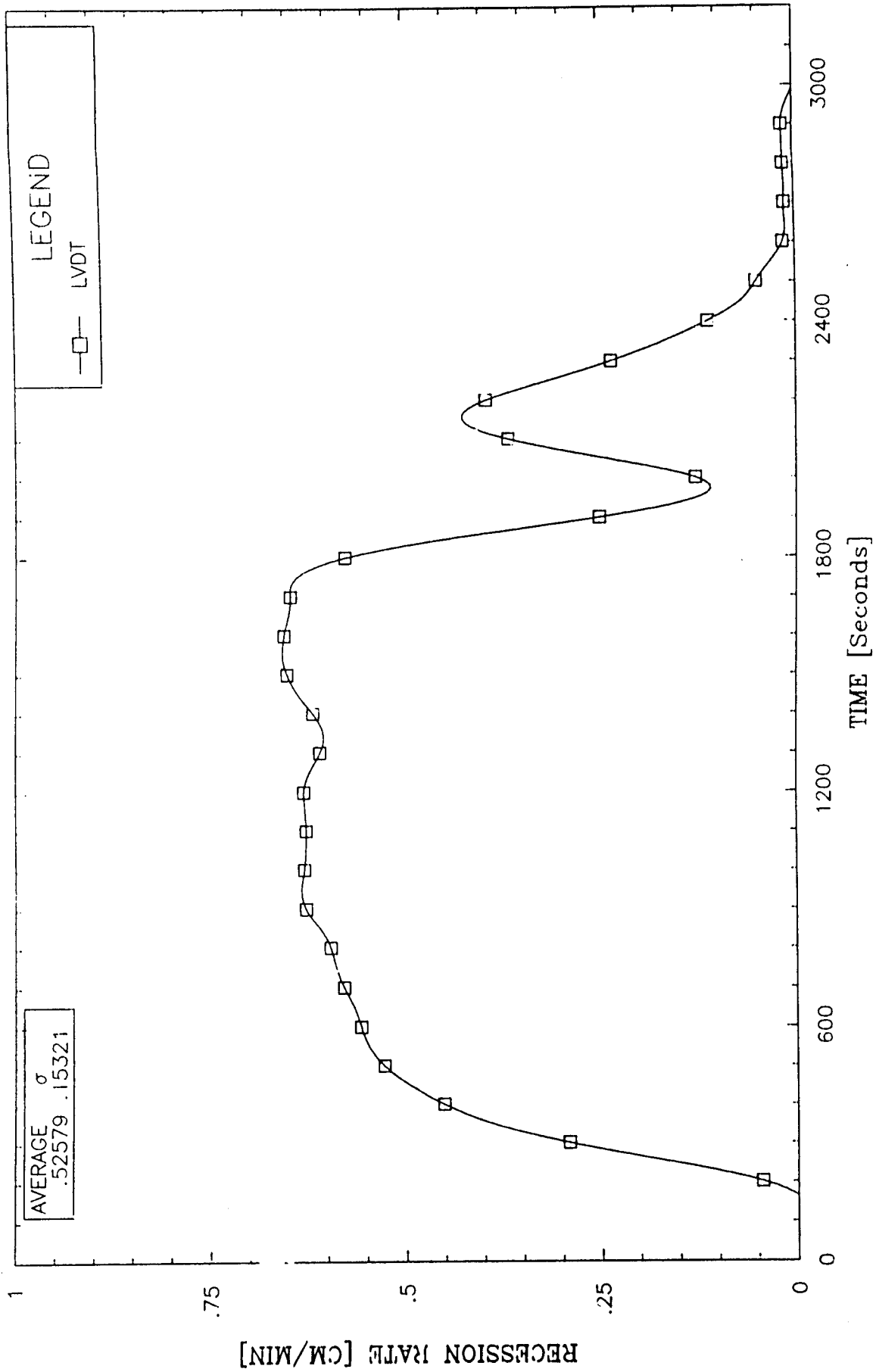


Figure 8.2 Fuel Recession Rate

NUCLEAR WINTER FIRE TEST POOL SURFACE CALORIMETERS

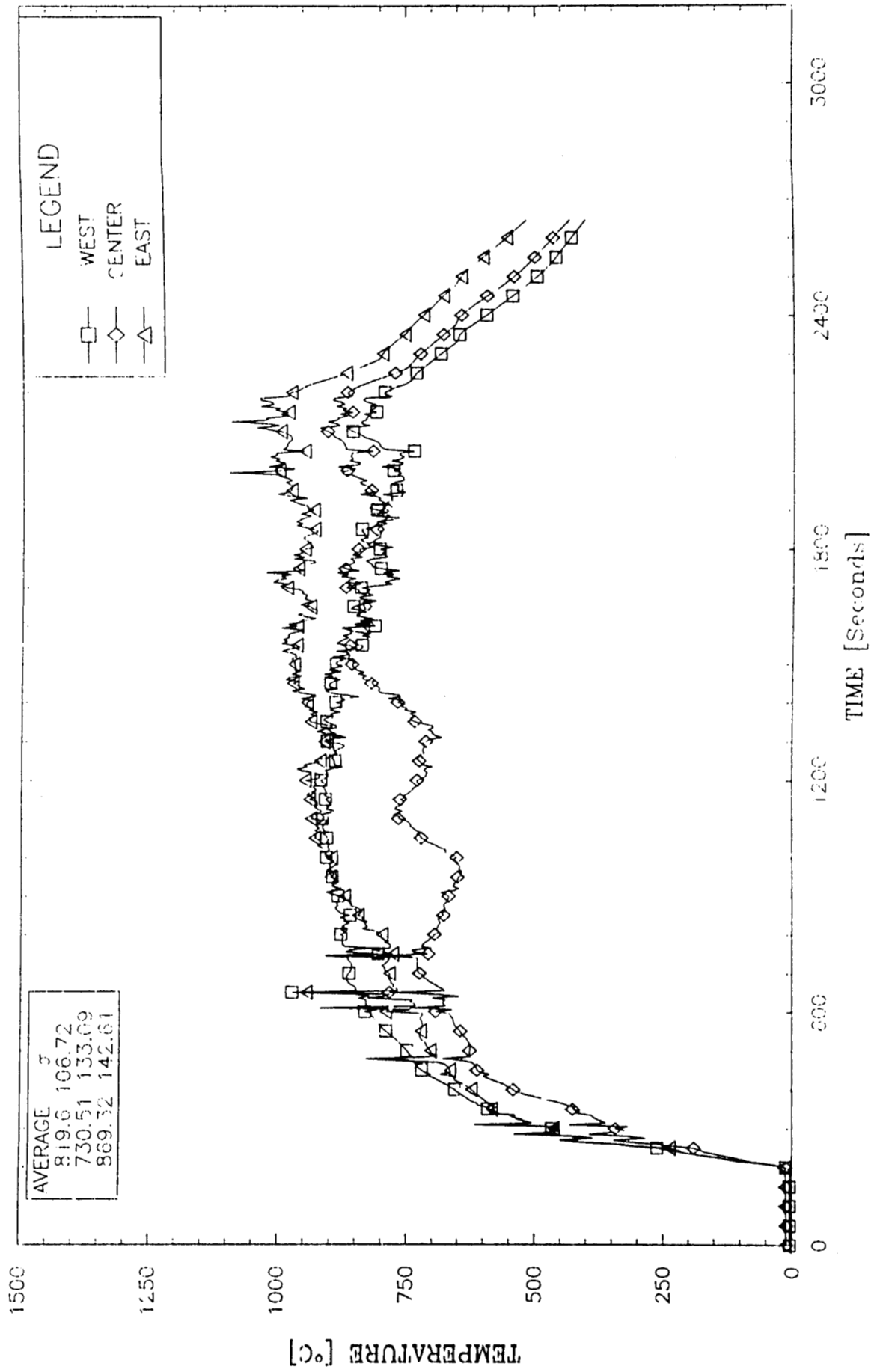


Figure 8.3 Backface Temperature Histories for Slug Calorimeters at Fuel Surface

NUCLEAR WINTER FIRE TEST POOL SURFACE CALORIMETERS

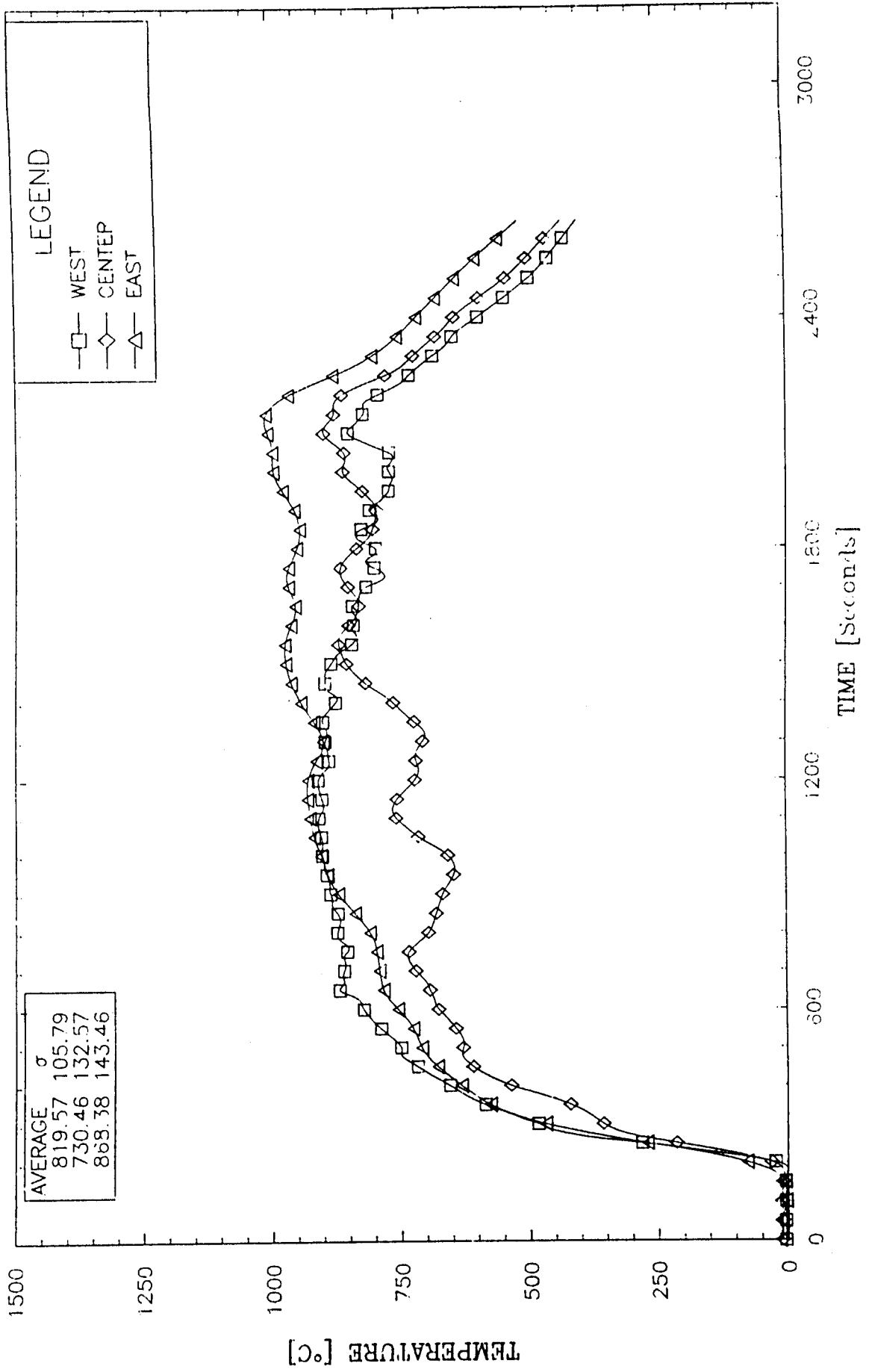


Figure 8.4 Smoothed Temperature Histories for Slug Calorimeters

NUCLEAR WINTER FIRE TEST
HEAT FLUX - FUEL SURFACE CALORIMETERS

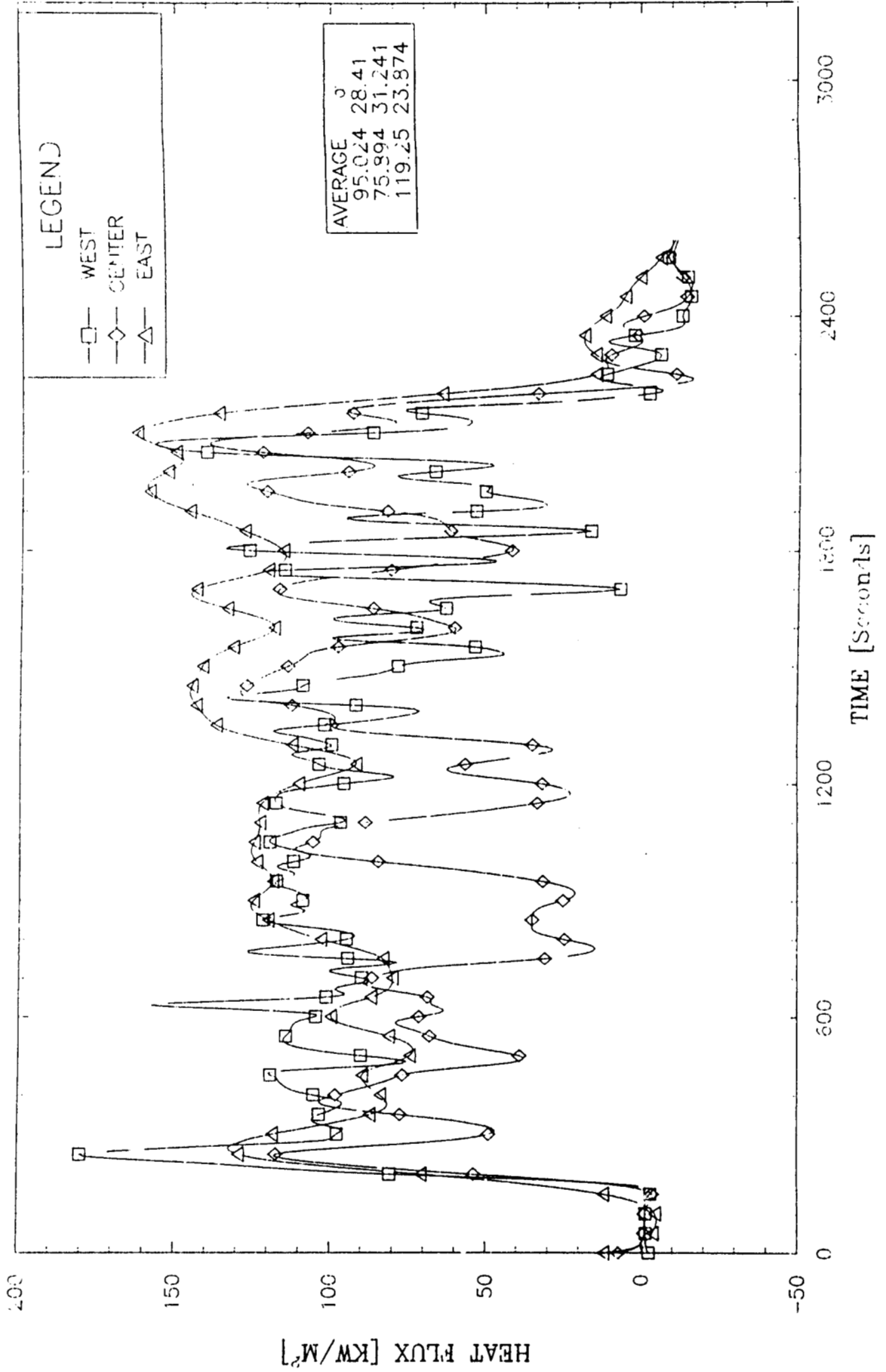


Figure 8.5 Heat Flux to Pool Surface From Slug Calorimeters

NUCLEAR WINTER FIRE TEST
POOL SURFACE RADIOMETER OUTPUT

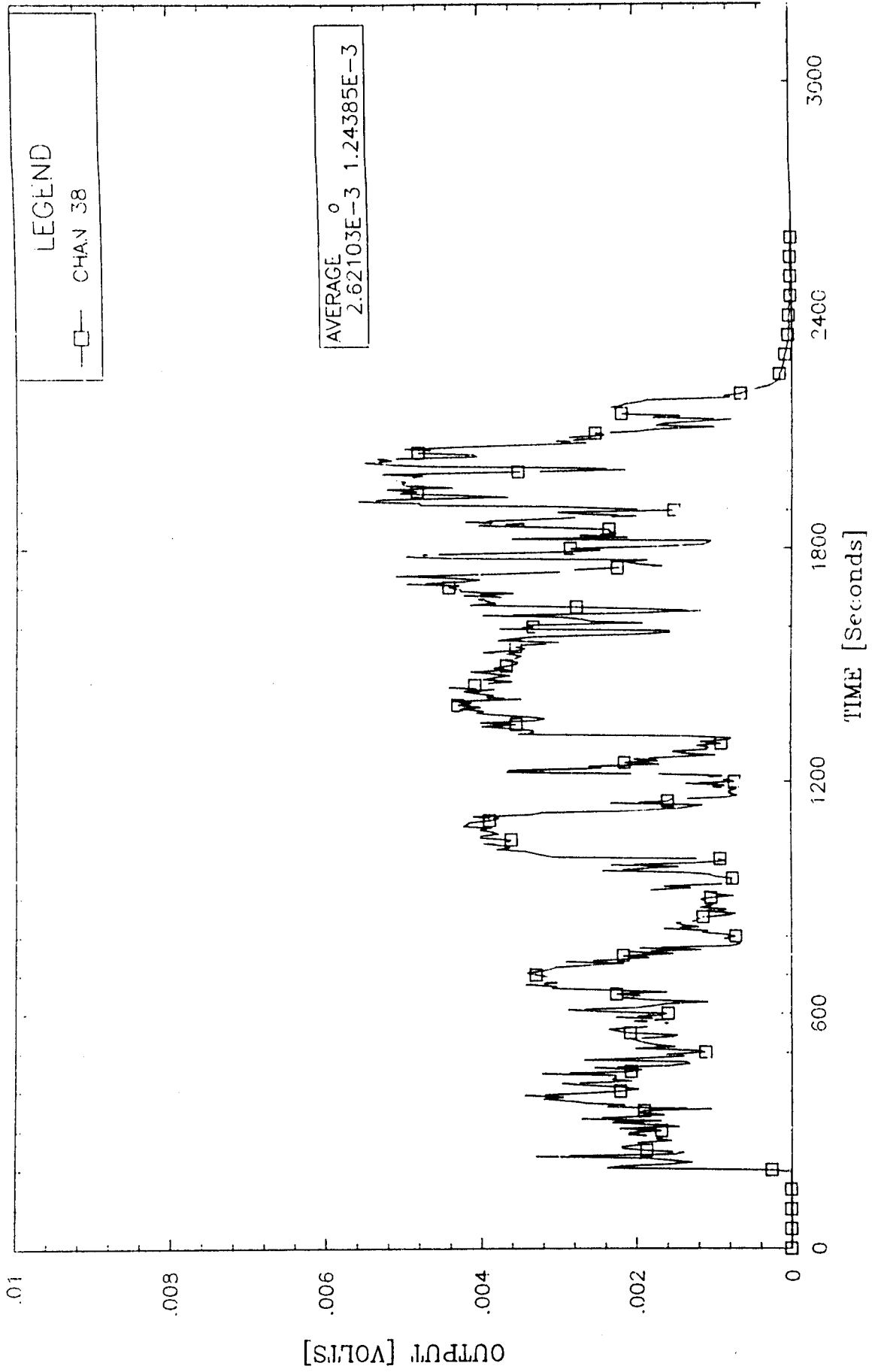


Figure 8.6 Fuel Surface Radiometer Output

NUCLEAR WINTER FIRE TEST POOL SURFACE RADIOMETER TEMPERATURE

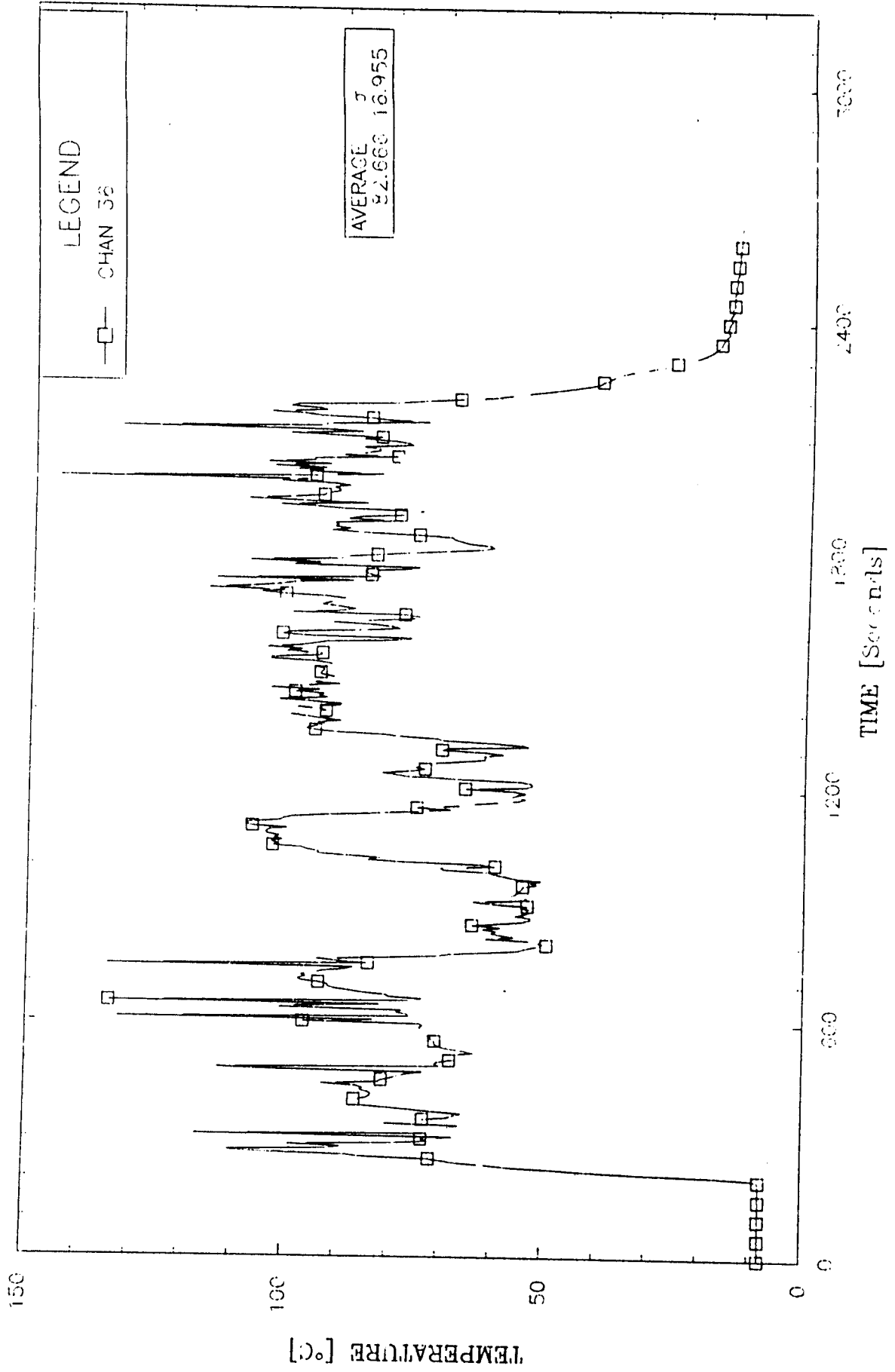


Figure 8.7 Fuel Surface Radiometer Temperature

IX. WEATHER CONDITIONS DURING THE TEST

The weather condition which most affects open pool fire testing is the wind. Four plots of wind speed for the test have been included in this report. Figure 9.1 is a plot of the magnitude of the wind speed during the time of the test. The mean velocity over the time of the burn was 2.76 meters per second. The standard deviation from the mean value was 0.94 meters per second. The wind speed was seen to increase as the test progressed with the maximum value of 6.31 meters per second occurring ~ 25 minutes into the test. The velocity components of the wind in the east/west, and the north/south directions were also computed and are shown in Figures 9.3 and 9.4. It can be seen that the wind toward the end of the test was moderately strong and primarily from the west.

For comparison, the wind data from a number of other tests is included below :

Test	Average Wind	Std Dev	Maximum Wind
PNC	<1.2 m/sec		---
DOT-A	2.0 m/sec	0.90 m/sec	---
DOT-B	1.2 m/sec	0.8 m/sec	---
DOT-C	1.5 m/sec	0.8 m/sec	---
Trupact-I-Test 1	1.24 m/sec	0.69 m/sec	3.69 m/sec
Trupact-I-Test 0	1.68 m/sec	0.95 m/sec	4.21 m/sec
Current	2.76 m/sec	0.94 m/sec	6.31 m/sec

It should be noted that the winds during this test were too strong to have met the regulatory requirements for open pool fire testing of transportation containers. The barometric pressure was 0.800 bar measured with a Wallace & Tiernan model FA129 altimeter and 0.789 bar measured with a Wallace & Tiernan model FA233 barometer. The ambient temperature averaged 7.8 °C over the test duration.

NUCLEAR WINTER FIRE TEST
WIND SPEED

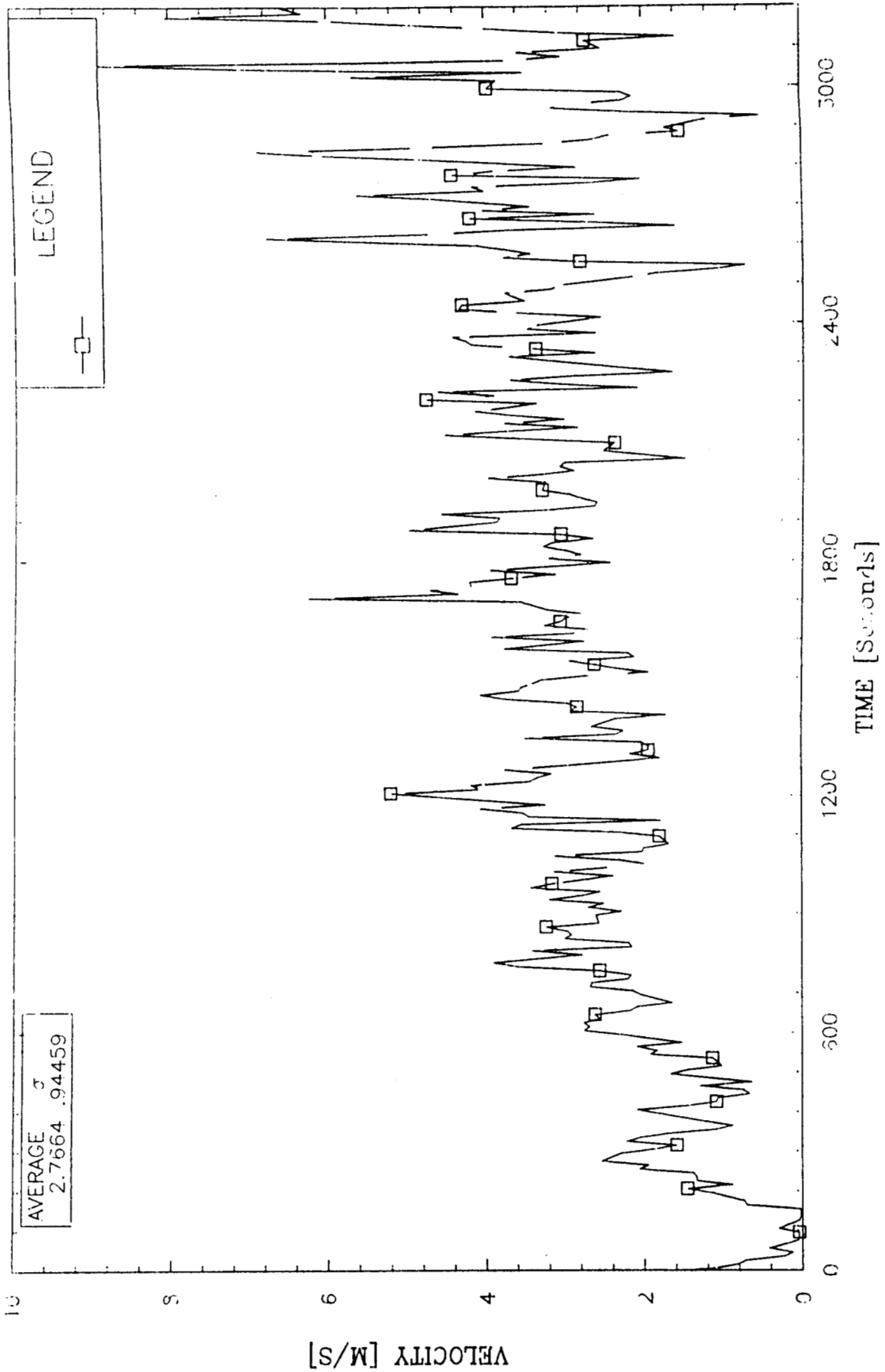


Figure 9.1 Wind Speed During Test

NUCLEAR WINTER FIRE TEST WIND DIRECTION

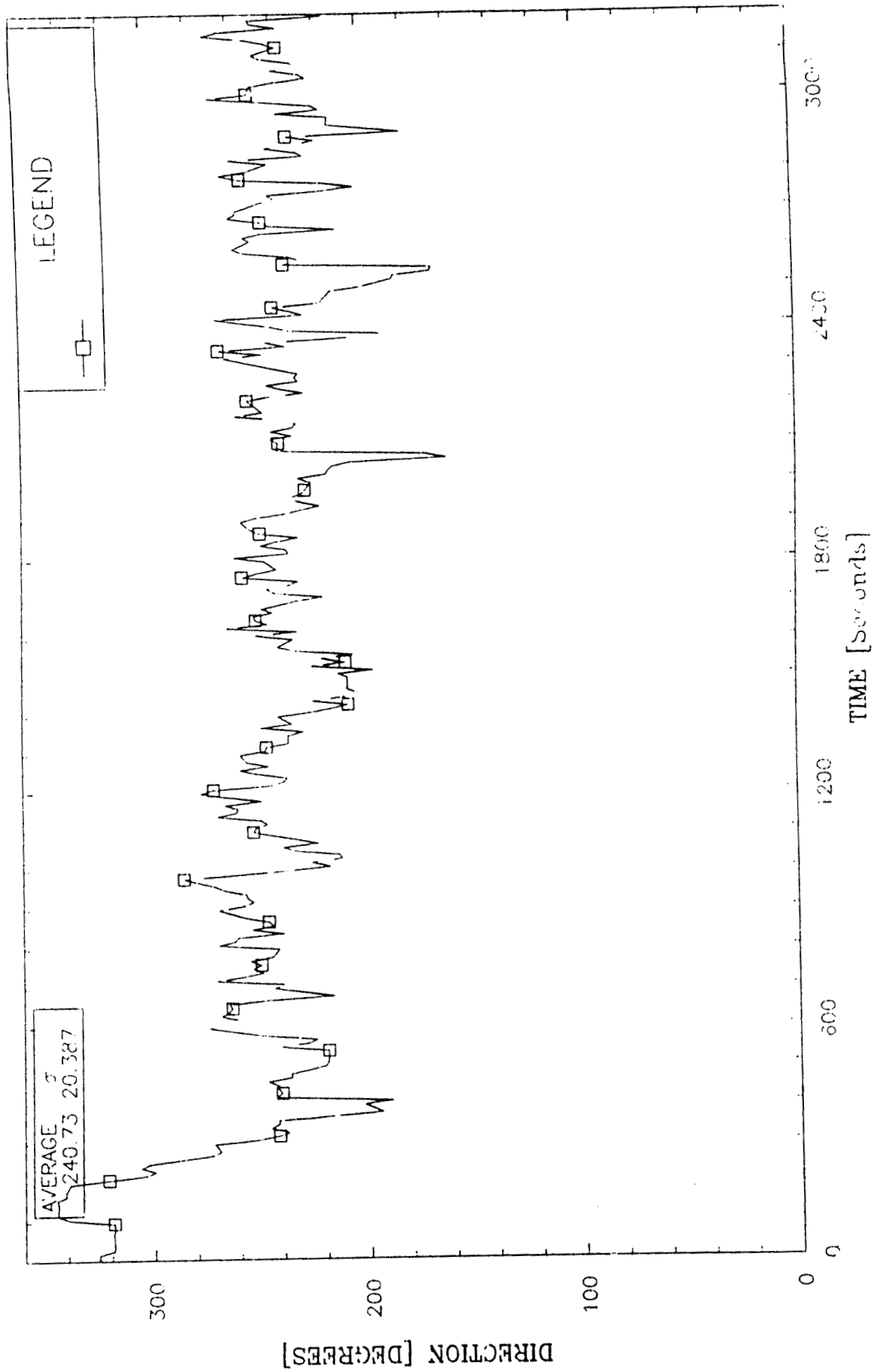


Figure 9.2 Wind Direction During Test

NUCLEAR WINTER FIRE TEST
COMPONENT OF WIND FROM WEST

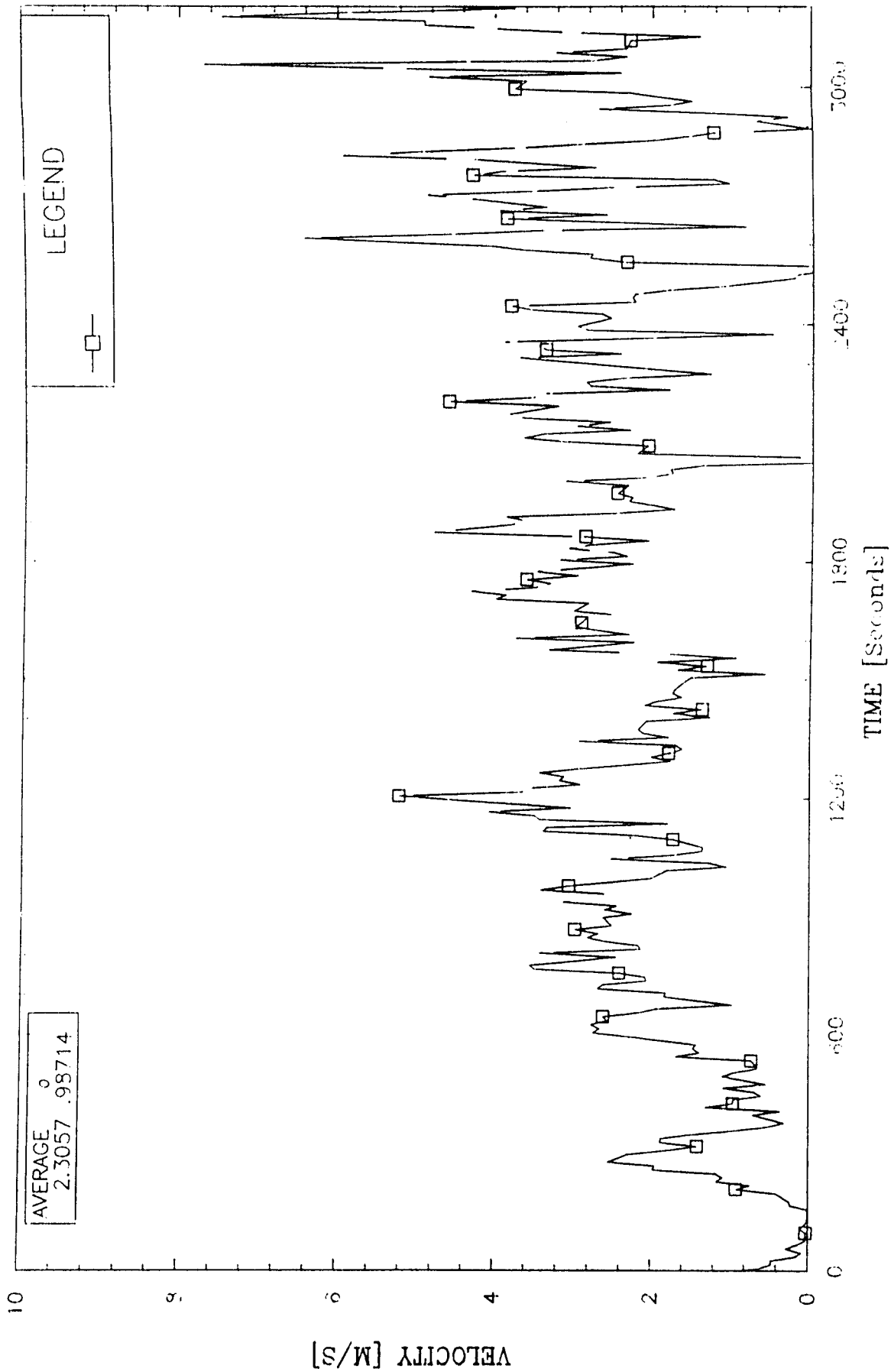


Figure 9.3 East Wind Velocity Component

NUCLEAR WINTER FIRE TEST
COMPONENT OF WIND FROM SOUTH

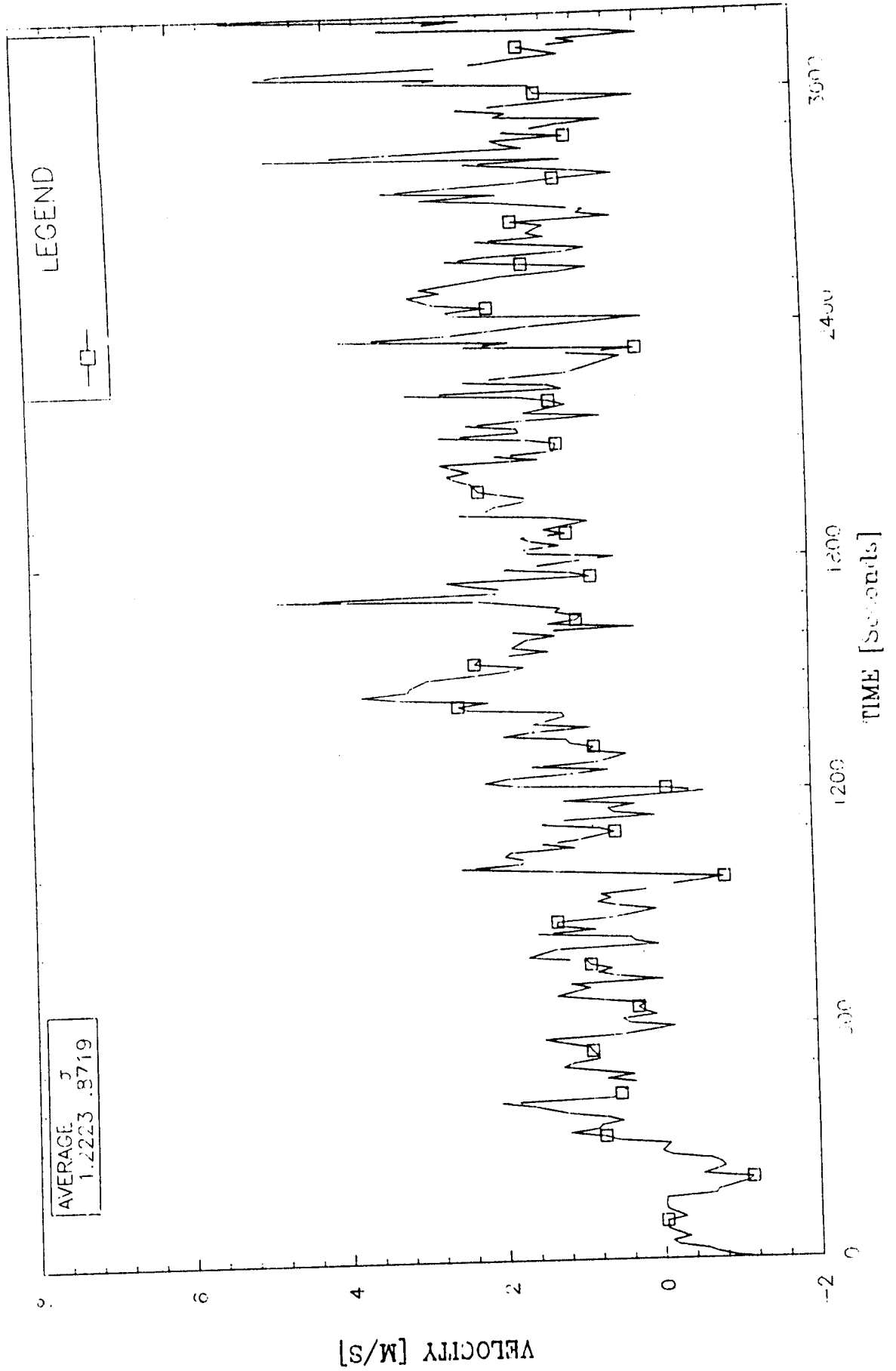


Figure 9.4 North Wind Velocity Component

NUCLEAR WINTER FIRE TEST AMBIENT TEMPERATURE

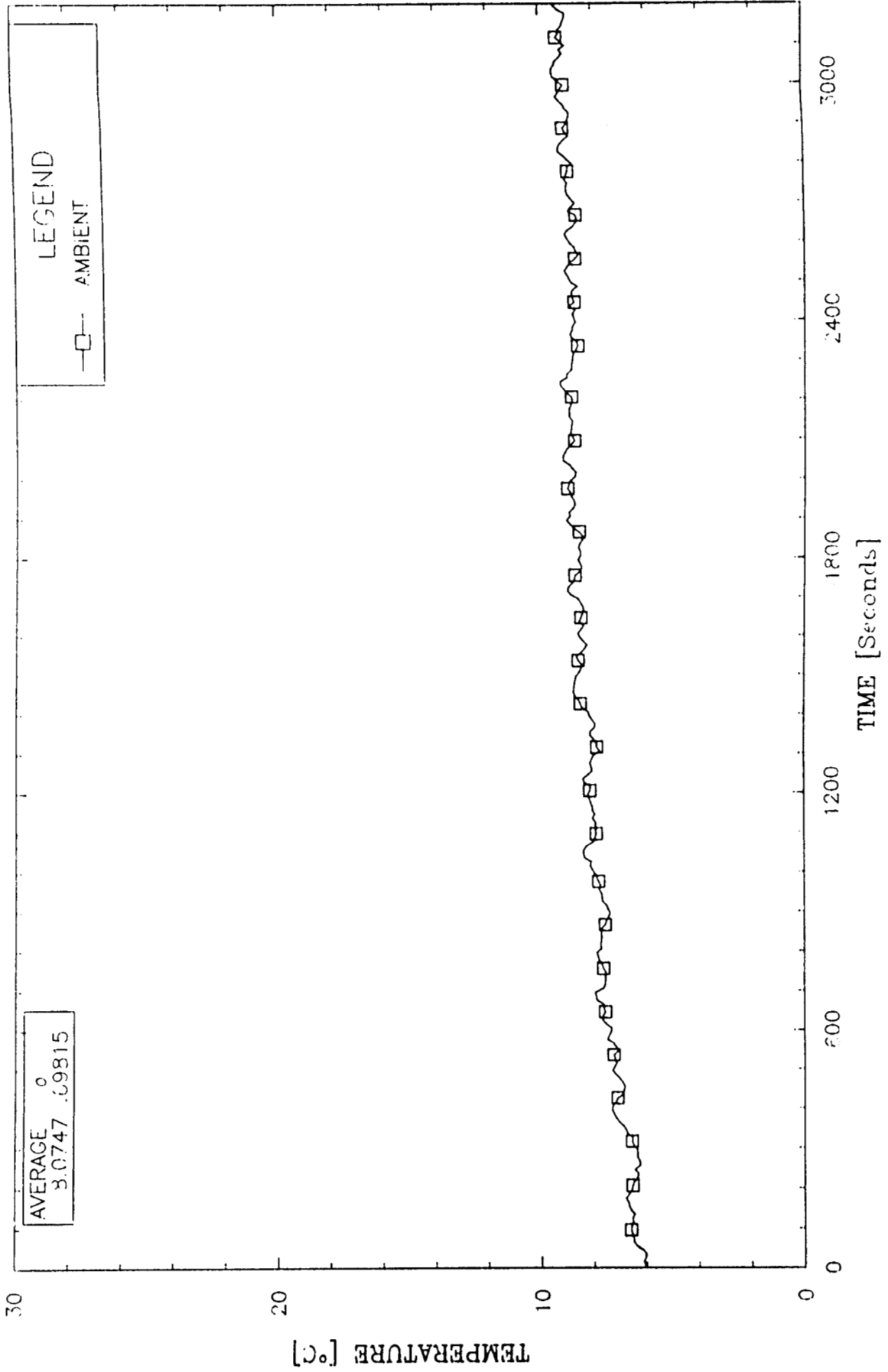


Figure 9.5 Ambient Temperature

REFERENCES

- 1.) Einfeld W., Mokler, B. V., Zak, B. D., and Morrison, D. J., "A Characterization of Smoke Properties From Small, Medium and Large Scale Hydrocarbon Pool Fires," Aerosols '87, 1987 Annual Meeting of the American Association for Aerosol Research, Seattle, WA, September, 1987.
- 2.) Gregory, J.J., Mata, R., Keltner, N.R., "Thermal Measurements in a Series of Large Open Pool Fires", SAND 85-0196, Sandia National Laboratories, Albuquerque, NM, 1986.
- 3.) Gregory, J.J., Keltner, N.R., and Mata, R. Jr., "Thermal Measurements in Large Pool Fires," Heat and Mass Transfer in Fire, ASME-HTD-VOL. 73, pp 27-36, 1987. (To be published in the Journal of Heat Transfer)
- 4.) Schneider, M.E., and Kent, L.A., "Measurements of Gas Velocities and Temperatures in a Large Open Pool Fire," Heat and Mass Transfer in Fire, ASME-HTD-VOL. 73, pp. 37-47, 1987. (To be published in Fire Technology)
- 5.) Keltner, N.R., Mata, R., Gregory, J.J., Kent, L.A., Schneider, M.E., "Diagnostics from an open pool fire test of TRUPACT-I", Sandia National Laboratories Internal Memo, RS7537/87/1.
- 6.) Kent, L.A., and Schneider, M.E., "The Design and Application of Bi-directional Velocity Probes for Measurements in Large Pool Fires," ISA Transactions, 26, #4, pp. 25-32, 1987. (also as ISA Paper # 87-0203).
- 7.) Drysdale, Dougal, Fire Dynamics, John Wiley & Sons, 1985, pp-141-142.
- 8.) McCaffrey, B.J., and Heskestad, G., "A Robust Low-Velocity Probe for Flame and Fire Application", Combustion and Flame, 26, 125-127, (1976).
- 9.) McCaffrey, B.J., "Purely Bouyant Diffusion Flames: Some Experimental Results", NBSIR 79-1910, National Bureau of Standards, 1979.
- 10.) Blackwell, B.F., Douglas, R.W., "A User's Manual for the Sandia One-Dimensional Direct and Inverse Thermal (SODDIT) Code", SAND 85-2478, Sandia National Laboratories, Albuquerque, NM, 1986.
- 11.) Beck, J.V., Blackwell, B.F., and St. Clair, Jr., C.R., Inverse Heat Conduction, John Wiley & Sons, 1985.
- 12.) Sparrow, E.M., and Cess, R.D., Radiation Heat Transfer, Hemisphere Publishing, 1978.
- 13.) Matthews, L., Longenbaugh, R., and Mata, R., "Transpiration Radiometer in Fire Characterization," InTech, Vol. 33, No. 8, pp 55-60, 1986.

APPENDIX A : Radiative Flux Enhancement Due to Fluctuating Temperatures

The heat flux to a cold wall at temperature T_o from a thick grey gas at temperature T_f , is mostly due to radiative transport if the flow velocity is low, and the gas temperature T_f is high. In this discussion we examine only the radiative heat transfer from the gas to the wall. The assumption is made that the cold wall and the surrounding gas can both be treated as blackbodies.

If the flame temperature fluctuates with time, the flux to the wall is given by:

$$Q = \sigma (T_f^4 - T_o^4) \quad \text{A.1}$$

The fluctuations in T_f will result in the average of Eqn. A.1 over time to be greater than the flux calculated from average values eg.

$$Q = \sigma (T_{ave}^4 - T_o^4) \quad \text{A.2}$$

If a periodic form of variation is chosen for T_f , the general form of the calculated average flux was found to be:

$$Q = \sigma [T_f^4 (1+\alpha) - T_o^4] \quad \text{A.3}$$

where α ranges from 0 to on the order of one depending on the exact form of the fluctuating flame temperature. More specifically the value of α is a function of ψ and ζ where :

ψ is the ratio of total fluctuation amplitude to mean temperature.

ζ is the fraction of time that the temperature exceeds the mean value.

Results are shown in Figure A.1 for sine, triangle, and square waves. Only in the square wave case was ζ modified. In general, as the amplitude of fluctuation increases the enhancement of radiative flux over the average calculation (eqn A.2) increases. Secondly, as the kurtosis in the flame temperatures increases, the enhancement increases slightly. In real data at least three parameters should be measured to estimate the radiative heat transfer; the mean flame temperature, the standard deviation in flame temperature, and the kurtosis in the flame temperature.

For the sine wave, $T_f = T_{ave} + A/2 (\sin(\omega t))$ the value of ψ is defined as $\psi = A/T_{ave}$. The result for flux is : $\alpha = 0.75 \psi^2 + 3/128 \psi^4$.

For the triangle wave if the maximum flame temperature minus the minimum temperature is defined as A, and ψ is defined as before, the enhancement parameter α is given by $\alpha = 1/2 \psi^2 + 1/80 \psi^4$.

For the square wave, again, A is defined as the swing in flame temperature, and ψ as A/T_{ave} . In this case the fraction of time during which the temperature is above the mean value can easily be varied and this fraction is defined as ζ . The result for α is now more complex, as it is a function of both ψ and ζ .

$$\alpha = \zeta \psi^2 (6 + 4\psi + \psi^2 - 6\zeta - 12\psi\zeta - 4\psi^2\zeta + 8\psi\zeta^2 + 6\psi^2\zeta^2 - 3\psi^2\zeta^3)$$

Radiation Enhancement

due to Fluctuating Temperatures

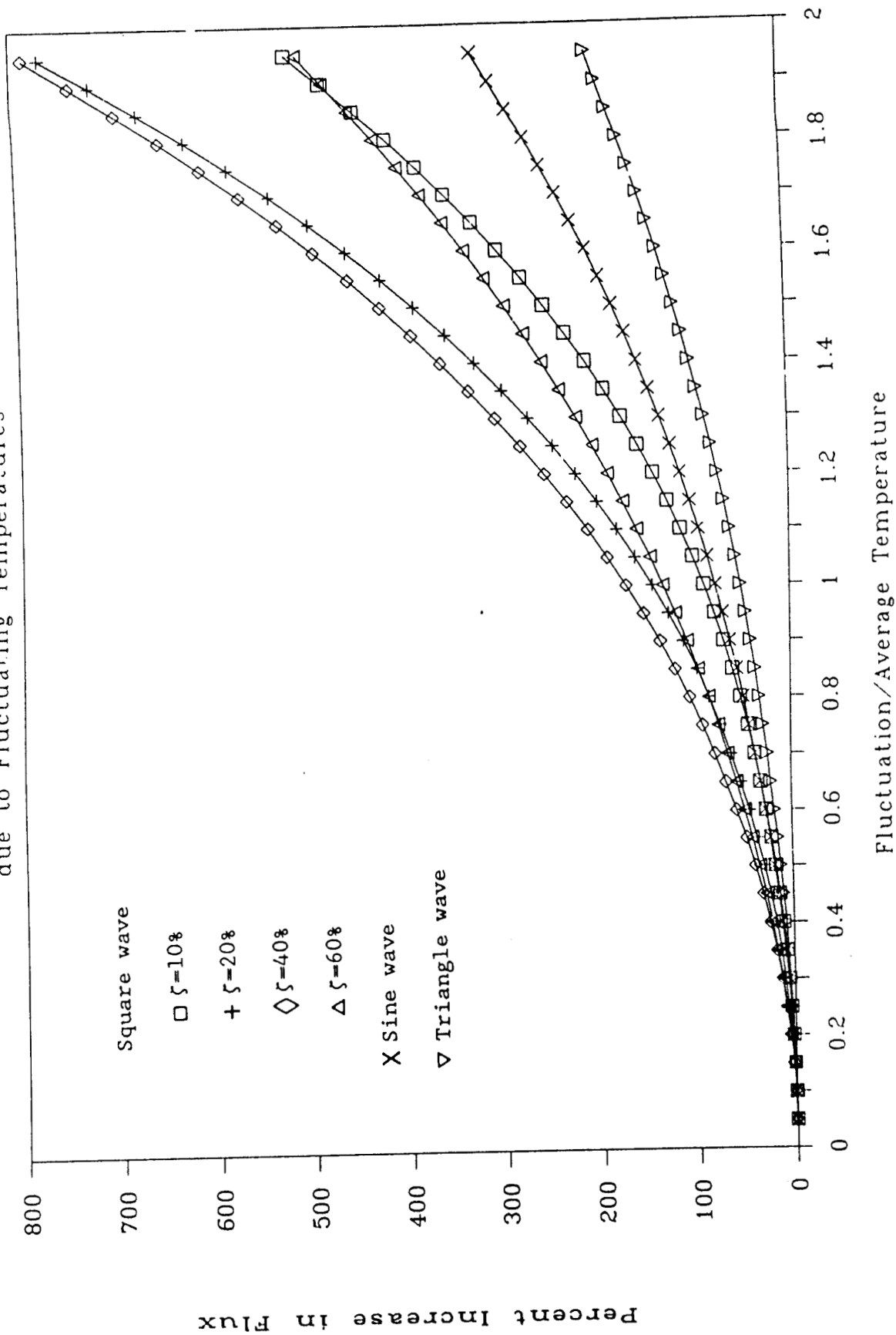


Figure A.1 Radiation Enhancement Due to Intermittency

APPENDIX B : Curvefits - Net Fluxes to Plate Calorimeters

An attempt was made to estimate the convective and radiative flux terms by examination of the results from the non-shrouded sides of plate calorimeters. The equation:

$$Q_{net} = \sigma \epsilon (T_f^4 - T_p^4) + h (T_f - T_p)$$

was used to represent the relationship between flame temperature, plate surface temperature, and net hot wall flux to the plate. At any particular station measured values exist for the temperatures and flux involved as a function of time. The values of ϵ and h were estimated for a given station by minimizing the residual between the estimates of Q_{net} from temperatures and the measured values of Q_{net} in the least squares sense. Results for the two plates of differing thicknesses in the current test are listed below, along with values for a 6.35 mm thick plate calorimeter used in the Trupact-I-Test 1.

Current Test

Location [m]	<u>6.35 mm Plate</u>		<u>19 mm Plate</u>	
	ϵ	h [W/m ² -°C]	ϵ	h [W/m ² -°C]
4.11	0.384	35.0	0.644	20.0
3.30	0.427	37.5	0.669	27.7
2.49	0.374	52.4	0.610	45.7
1.68	0.138	100.7	0.357	97.6

Trupact-I-Test 1 - 6.35 mm plate

Location	ϵ	h [W/m ² -°C]
4.93	0.462	39.1
4.62	0.310	75.8
4.01	0.266	78.4
3.10	0.187	111.9
2.49	0.178	111.8

Examining the curves of Q_{net} and the predicted values seem to indicate that the initial heat-up period is not predicted by equation A.2.1 as well as the time histories after heat up has occurred. The values of ϵ and h seem to give too much significance to the convective term. The reasons for this may be:

- The heat transfer mechanism may vary with time. This procedure forces a single constant value of ϵ and h to be assigned which may not make physical sense. At the least, we know that the effective flame emissivity varies dramatically with time.

- During the latter part of the fire, the plate temperatures are close to the flame temperatures. As a result, the radiative flux can be approximated by a linear function. Because the estimates cover the total test duration, the linear term in the Q_{net} equation would incorporate the effects of the linearized radiative flux. As a result, the value for h will be too high.

- There may be non-linear terms due to gas property or velocity variations. Very simple analysis shows velocity to be proportional to the square root of temperature in this region of the flames. The heat transfer coefficient from classical experiments is related to the Reynolds and Prandtl numbers.

$$h = 0.0288 \rho C_p U Re_x^{-1/5} Pr^{-2/3}$$

Analysis of the variations in density, thermal conductivity and viscosity with temperature were inserted into this classical equation for local turbulent heat transfer to a plate. This analysis seems to indicate that most of the anticipated convective flux enhancement due to velocity increases are ameliorated by changes in the gas properties. Results ranged from 8 to 26 W/m²-K, depending on the downstream location and the assumed plate and flame temperatures. This analysis makes a number of assumptions, including the application of steady state classical heat transfer solutions to an extremely transient problem.

DISTRIBUTION:

DOE/TIC-4500, Rev 74, UC-71 (187)

US Department of Energy (3)

Attn: T. Hindman
F. Falci
L. Harmon

Routing DP 123
Washington, DC 20545

US Department of Energy
Albuquerque Operations Office

Attn: K. Gollhofer
P.O. Box 5400
Albuquerque, NM 87115

US Department of Energy

Idaho Operations Office
Attn: C. Dwight
550 Second Street
Idaho Falls, ID 83401

US Department of Energy

Routing RW-33
Attn: C. Kouts
1000 Independence, SW
Washington, DC 20585

U.S. Department of Agriculture

Forest Products Laboratory
Attn: R. H. White
1 Gifford Pinchot Drive
Madison, WI 53705-2398

US Air Force Engineering and
Services Center (3)

Attn: Col. L. D. Hokanson - RD
J. Walker - RDCF
C. W. Risinger - RDCF
Tyndall AFB, FL 32403-6001

Air Force Weapons Laboratories (2)

Kirtland AFB
Attn: Capt. S. Sumner
Capt. G. James
Albuquerque, NM 87117-6008

Atmospheric Sciences Laboratory (3)

Attn: K. White SLCAS-AS-D
R. Pinnick SLCAS-AS-A
R. Sutherland SLCAS-AS-M
White Sands Missile Range, NM 88002

US Coast Guard (4)

Marine Fire and Safety
Research Staff

Attn: D. Beene (3)
R. Richards

Avery Point
Groton, CT 06340

US Coast Guard Headquarters

Attn: A. L. Schneider (G-MTH-4/13)
Washington, DC 20593

Defense Nuclear Agency (3)

RARP

Attn: D. Auton
Maj. R. Hartley
Maj. V. Oxford

6801 Telegraph Road
Alexandria, VA 22310-3398

Environmental Evaluation Group

Attn: D. L. Shomaker, Librarian
P.O. Box 968
Santa Fe, NM 87503

Federal Railroad Administration, DOT
Equipment and Operating Practices Safety
Research Division

Attn: M. C. Gannett, Chief
400 7th Street, SW
Washington, DC 20590

Federal Railroad Administration (2)
Office of Research and Development

Attn: C. Orth, Research Manager
D. Dancer

400 Seventh Street, SW
Washington, DC 20590

DISTRIBUTION (continued):

Lawrence Livermore National Laboratory (2)
Attn: H. K. Hasegawa
K. F. Foote
P.O. Box 5505 L-442
Livermore, CA 94550

National Institute of Standards
and Technology (9)
Center for Fire Research
Attn: V. Babrauskas
H. Baum
L. Y. Cooper
R. Levine
H. Mitler
G. Mulholland
J. Quintiere
K. Steckler
W. D. Walton
Gaithersburg, MD 20899

NASA Johnson Space Center (2)
Attn: L. Linley
M. V. Gunaji
P.O. Drawer MM
Las Cruces, NM 88004

Naval Air Systems Command (3)
Department of Navy
Attn: P. Campbell
Washington, DC 20361

Naval Research Laboratory
Attn: W. M. Tolles
4555 Overlook Avenue
Washington, DC 20375

Naval Research Laboratory (2)
Combustion Section
Chemical Dynamics Branch
Attn: P. A. Tatem
F. W. Williams
Washington, DC 20375

Naval Research Laboratory
Code 6183
Attn: J. Leonard
Washington, DC 20375

Naval Sea System Command (3)
Attn: W. Boyce
CODE-SEA 56Y52
Washington, DC 20362-5101

Naval Surface Weapons Center,
Code R402 (2)
Attn: M. Lacey
F. Williams
Bldg. 4-176
Silver Spring, MD 20903-500

Office of Security Evaluations (2)
Attn: J. L. Torres, Director
C. Mauck
Defense Programs - DP-4, GTN
Washington, DC 20545

Transportation Systems Center
Attn: W. Hathaway
Kendall Square
Mail Stop DTS-43
Cambridge, MA 02142

Transportation Test Center
Attn: W. G. Larson
P.O. Box 11130
Pueblo, CO 81001

The University of Akron
Dept. of Mechanical Engineering
Attn: B. T. F. Chung
Akron, OH 44325

Karman Laboratory of Fluid Mechanics
and Jet Propulsion (2)
California Institute of Technology
Attn: E. E. Zukoski
T. Kubota
Pasadena, CA 91125

University of California
Fire Research Laboratory
Attn: B. G. MacCracken
Berkeley, CA 94720

DISTRIBUTION (continued):

University of California (5)
Dept. of Mechanical Engineering
Attn: A. C. Fernandez-Pello
R. Greif
J. Pagni
C. L. Tien
R. B. Williamson
6175 Etcheverry Hall
Berkeley, CA 94720

University of California
Mechanical, Aerospace and
Nuclear Engineering Dept.
Attn: A. Lavine
5532 Boelter Hall
Los Angeles, CA 90024

Kansas State University
Dept. of Mechanical Engineering
Attn: D. L. Fenton
Manhattan, KS 66506

University of Kentucky
College of Engineering
Dept. of Mechanical Engineering
Attn: K. Saito
242 Anderson Hall
Lexington, KY 40506-0046

Railroad Technology Center
IIT Research Center
Attn: M. Johnson
Senior Engineering Advisor
10 West 35th Street
Chicago, IL 60616

University of Maryland
Dept. of Fire Protection Engineering
Attn: J. A. Milke
College Park, MD 20742

University of Maryland
Dept. of Mechanical Engineering
Attn: B. J. McCaffrey
Baltimore, MD 21228

The University of Maryland
Dept. of Mechanical Engineering
Attn: J. P. Gore
College Park, MD 20742

M.I.T.
Dept. of Chemical Engineering
Attn: A. F. Sarofin
Cambridge, MA 02139

Michigan State University (3)
Department of Mechanical Engineering
Attn: A. Atreya
J. R. Lloyd
M. Koochesfahani
E. Lansing, MI 48824-1226

University of Michigan (2)
College of Engineering
Attn: G. M. Faeth
V. S. Arpaci
217 Aerospace Engineering Bldg.
Ann Arbor, MI 48109-2140

New Mexico State University (2)
Dept. of Mechanical Engineering
Attn: L. Mathews
E. Hensel
Box 3450
Las Cruces, NM 88003

University of New Mexico (3)
NMERI
Attn: R. E. Tapscott
T. Stepetic
D. Zalen
Box 25
Albuquerque, NM 87131

University of Notre Dame
Aerospace and Mechanical Engineering
Attn: K. T. Yang
Notre Dame, IN 46556

DISTRIBUTION (continued):

Purdue University
School of Mechanical Engineering
Attn: R. Viskanta
West Lafayette, IN 47096

Rutgers University
Mechanical Engineering Dept.
Attn: Y. Jaluria
P.O. Box 909
Piscataway, NJ 08855

Stanford University
Dept. of Mechanical Engineering
Attn: R. Moffat
Stanford, CA 94305

Virginia Polytechnic Institute and
State University
Attn: T. Diller
114 Randolph Hall
Blacksburg, VA 24061

Washington State University
Dept. of Mechanical Engineering
Attn: W. Grosshandler
Pullman, WA 99164-2920

University of Washington
Dept. of Mechanical Engineering
Attn: R. C. Corlett
Seattle, WA 98105

Worcester Polytechnic Institute
Center for Firesafety Studies
Attn: J. R. Barnett
Worcester, MA 01609

N. J. Alvares
3628 Oak Knoll Drive
Redwood City, CA 94062

Accident Modeling & Simulation
Attn: R. D. Peak
Apt. A
99 North Wavery Place
Kennewick, WA 99336

American Vamag Company
Attn: V. Radovic
1061 Linden Avenue
Ridgefield, NJ 07657

Applied Research Associates, Inc.
Attn: Michael J. Wilson
P.O. Box 40128
Tyndall AFB FL 32403

Battelle, Columbus Division
Attn: R. J. Burian
505 King Avenue
Columbus, OH 43201-2693

BDM
Attn: C. Tappan
1820 Randolph Road, SE
Albuquerque, NM 87106

BFGoodrich
Attn: M. M. Hirschler
Geon Vinyl Division
P.O. Box 122
Avon Lake, OH 44012

Ceramic Materials Dept./3M
Attn: R. R. Licht
2007-1S-12 EM Center
St. Paul, MN 55144-1000

Chevron Corporation
Attn: D. L. Blomquist
P.O. Box 7924
San Francisco, CA 94120-7924

Construction Technology Laboratories
Attn: R. G. Burg
5420 Old Orchard Road
Skokie, IL 60077-1030

EG&G, Idaho, Inc.
Attn: W. Walters
P.O. Box 1625
Idaho Falls, ID 83415

DISTRIBUTION (continued):

EXXON Research and Engineering Company
Materials Technology Division
Attn: P. E. Schlett
P.O. Box 101
Florham Park, NY 07932

Fire Science Technologies
Attn: C. L. Beyler
3215 Donnybrook Lane
Cincinnati, OH 45239

Factory Mutual Research (6)
Attn: R. Alpert
M. Delichatsios
J. De Ris
G. Heskestad
J. Newman
A. Tewarson
1151 Boston-Providence Turnpike
Norwood, MA 02062

Hughes Associates, Inc. (2)
Attn: P. J. DiNenno
R. G. Gewain
Suite 902
2730 University Blvd. West
Weaton, MD 20902

Mobil Research and Development Corp.
Attn: G. C Hoff
P.O. Box 819047
Dallas, TX 75381-9047

Nuclear Packaging Inc.
Attn: Charles J. Temus
1010 South 336th Street
Federal Way, WA 98003

PABCO
Pabco Insulation Division
Attn: F. B. Hutto, Jr.
1110 - 16 Road
Fruita, CO 81521

Raychem Corp. (2)
Attn: David Vatcher
R. O. Bremner
300 Constitution Drive
Menlo Park, CA 94025-1164

RPM Carboline Company
Attn: C. Magdalin
1401 S. Hanley Road
St. Louis, MO 63144-2985

Southwest Research Institute (3)
Attn: J. J. Beitel
N. Stamp
A. Wenzel
6220 Culebra Road
San Antonio, TX 78284

SRI International
Physical Sciences Division
Attn: R. S. Alger
333 Ravenswood Avenue
Menlo Park, CA 94025

StanChem Inc.
Attn: W. A. Rains
656 Berlin Street
East Berlin, CT 06023

Standard Oil
Engineered Materials Company
Attn: E. J. Peters
P.O. Box 808
Niagara Falls, NY 14302-0808

Textron Specialty Materials
Attn: M. Blake
2 Industrial Avenue
Lowell, MA 01851

TRW Space and Technology Group
Applied Technology Div. (R1/1132)
Attn: F. E. Fendell
1 Space Park
Redondo Beach, CA 90278

DISTRIBUTION (continued):

Underwriters Laboratories
Attn: R. Berhinig
333 Pfingsten Road
Northbrook, IL 60062

VTEC Laboratories Inc.
Attn: N. Schultz
540 Faile Street
Bronx, NY 10474

GECHEM
Service Recherche
Avenue de Broqueville 12
B1150 Bruxelles
BELGIUM

Queen's University
Dept. of Mechanical Engineering
Attn: A. M. Birk
Kingston, Ontario K7L 3N6
CANADA

National Research Council of Canada (3)
Fire Research Section
Division of Building Research
Attn: T. Z. Harmathy
G. Loughheed
I. Oleszkiewicz
Ottawa, Ontario K1A-OR6
CANADA

University of New Brunswick (2)
Fire Science Center
Attn: F. R. Steward
J. E. S. Venart
Fredericton, NB E3B-5A3
CANADA

University of Western Ontario
Dept. of Mechanical Engineering
Attn: E. J. Weckman
London, Ontario, N6A 5B9
CANADA

Technical University of Denmark
Attn: B. Bohm
Building 402
2800 Lyngby
DENMARK

GERPy - D.C.A.N. Toulon
Attn: A. Artaud
Chief Engineer, Armaments
83800 Toulon Naval
TOULON, FRANCE

University of Stuttgart
Institute for Technical Chemistry
Attn: A. Schonbucher
Pfaffenwaldring 55
D-7000 Stuttgart 80
GERMAN FEDERAL REPUBLIC

Power Reactor and Nuclear Fuel
Development Corp.
Attn: M. Kubo
9-13, 1-Chome, Akasaka
Minato-Ku, Tokyo, T107
JAPAN

University of Tokyo
Dept. of Mechanical Engineering
Attn: Masaru Hirata, Professor
Bunyko-Ku
TOKYO 113
JAPAN

E. Odgaard
OSEBERG-2 Project
c/o Kvaerner Engineering A/S
Johan Drengsruds vei 52
N-1370 Asker
NORWAY

Lund University
Dept. of Fire Safety Engineering
Attn: S. E. Magnusson
Box 118
S-221 00 LUND
SWEDEN

DISTRIBUTION (continued):

National Testing Institute
Attn: U. Wickstrom
P.O. Box 857, S-501-15
Boras
SWEDEN

Fire Research Station (2)
Attn: G. Cox
M. Shipp
Borehamwood
Herts WD6-2BL
UNITED KINGDOM

1512 M. R. Baer
1512 J. C. Cummings
1513 D. W. Larson
1513 A. C. Ratzel
1553 B. F. Blackwell
5121 D. F. McVey
5128 B. E. Bader
6300 R. W. Lynch
6320 J. E. Stiegler
Attn: TTC Master File
6320 TTC Library
6321 R. E. Luna
6321 B. D. Zak
6321 W. Einfeld
6322 J. M. Freedman
6322 N. N. Brown
6322 L. E. Romesberg
6322 M. M. Warrant
6323 G. C. Allen, Jr.
6323 J. L. Moya
6323 J. D. Pierce
6323 H. R. Yoshimura
6413 J. J. Gregory
6511 R. S. Longenbaugh
6511 W. H. McCulloch
7525 R. Mata
7530 T. L. Workman
7537 B. L. Bainbridge
7537 N. R. Keltner (20)
7537 L. A. Kent
7537 J. T. Nakos
7537 K. B. Sobolik
8244 C. M. Hartwig
8351 W. L. Flower
8524 J. A. Wackerly
9114 L. A. Boye
3141 S. A. Landenberger (5)
3151 W. I. Klein (3)
3154-1 C. L. Ward (8)
For DOE/OSTI